MASTER THESIS

University of Stavanger

UNIVERSITY OF STAVANGER

EXPERIMENTAL STUDY AND OPTIMIZATION OF EXPANDING PIN TECHNOLOGY FOR HEAVY DUTY MACHINE JOINT APPLICATION

DATE

JUNE, 2021

Soheil Salahshour Langeroodi

University Supervisor: Hirpa G. Lemu

External Supervisor: Øyvind Karlsen

PROPOSED BY

BONDURA TECHNOLOGY AS

bondura® technology

University of Stavanger

FACULTY OF SCIENCE AND TECHNOLOGY

MASTER'S THESIS

Study programme/specialization : Engineering Structures and Materials with Specialization in Mechanical Engineering	Spring semester, 2021. Open/~~Confidential~~
Author : Soheil Salahshour Langeroodi	**Signature** 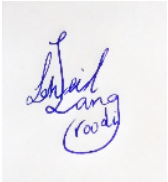

Faculty Supervisor : Prof. Hirpa G. Lemu

External Supervisor : Øyvind Karlsen (Bondura Technology AS)

Title of master's thesis : Experimental Study and Optimization of Expanding Pin Technology for Heavy Duty Machine Joint Application

Credits (ECTS) : 30

Keywords : Expanding Pin System, Stress Analysis, Experimental Study, Finite Element Analysis, Abaqus, Shape Optimization	Number of pages: ……91…… + supplemental material/other: …… Stavanger, ……14/06/2021…… date/year

Preface

The research reported in this thesis is carried out as part of the study in order to fulfill master of science programme in Structural and Material Engineering with specialization in Mechanical systems at University of Stavanger, Department of Mechanical and Structural Engineering and Materials Science. The subject was proposed by Bondura Technology AS, a specialized company in design and manufacturing of pin solutions. The thesis was done during spring semester, 2021.

I would like to express my gratitude to my supervisor Professor Hirpa G. Lemu for all the useful comments, remarks and supports through the learning process of this master thesis and for giving me the opportunity to work on this interesting topic. I would like to thank CTO Bondura Technology AS and industrial PhD candidate Øyvind Karlsen for his cooperation and help all along the way. Sharing his knowledge through many valuable comments and in-depth discussions specially for experimental part of the study was a great help.

During the experimentation, Yaaseen Ahmad Amith, Emil Surnevik Kristiansen and Swen Roemer, engineers of IMBM laboratory at UiS did a great assistance and their knowledge and experience about methods and using tools facilitated the experimental part of this research. Thank you for this important contribution.

I would like to thank my friends and fellow students for keeping a very pleasant and motivating environment, especially my dear friends Ahmed Ali, Kari, Ankit, Helga, Johannes, Majid and Reza who made my stay in Stavanger a great life experience. The biggest thanks go to my father and mother, Ghasem Salahshour and Afsaneh Aghazadeh and my brother Saeid for supporting me through the entire master programme, keeping me motivated and to make it possible for me to just concentrate on my studies. Thank you for believing in me even in the most difficult moments and to helping me to always do my best.

Soheil Salahshour Langeroodi
Stavanger, June 2021

Abstract

In this thesis, a type of pin joint, namely Bondura Expanding Pin System (EPS) is subject of study which has ability to create a rigid and reliable connection. This joint system is specially designed for heavy duty machines where excessive loading to the pin can cause damage to the joint components and create slack in the connection that often leads to malfunctioning in the machine.

This research concentrates on two concepts; stress analysis of the EPS and optimization of it. To achieve these goals, combination of analytical, experimental and Finite Element Analysis (FEA) are carried out. The available formulas for different parts of EPS are investigated. For assessing validity of formulas available in literature for interaction between conical pin-sleeve, a FEA is performed using Abaqus/CAE software. Bondura sleeve which is an expanding (split) sleeve has four cuts that one of them is a complete cut (cut-through). The comparison of the results show that existing formulas can be used for initial prediction of stresses and pressure in EPS with good precision.

The experimental job is conducted in order to find out stress level and distribution in the equipment support. For this purpose, a thick cylinder was manufactured as test boss and in several locations along its outer surface, induced strains were measured while EPS joint was subjected to fastening torque of screws. Comparison of results of the conducted FEA and experimental values for stress state in the test boss are in good agreement. The effect of friction and expansion of sleeve on stress state of test boss is analysed comprehensively in the experimental part of this study. Moreover, a FEA is implemented for parametric study of friction. A relationship between maximum von Mises in the test boss and friction coefficient is extracted regarding the fastening torque of 200 Nm.

After carrying out stress analysis on EPS and verification of the FE model, the optimization process was implemented in order to find a shape which creates a lower stress state in the joint components while preserving enough pressure or radial stress to ensure suitable clamping force in the joint. The optimization result provided a profile for tapered section of pin-sleeve mating surface. The optimised profile needed some modifications to make it applicable in joint assembly. FE results show that for the new optimised shape, applying lower amount of fastening torque to EPS can provide the same radial pressure and clamping force in the test boss.

Finally, a FE parametric study was carried out on angle of taper of pin-sleeve mating section to quantify the best angle. The obtained results show that the current angle of taper of Bondura EPS which is 12° is the most suitable angle since it creates considerable amount of radial stress and consequently clamping force in the equipment support.

Contents

List of Figures

List of Tables

List of Symbols

a	Internal radius of cylinder
A	Cross-sectional area
A_s	Surface area
A_t	Tensile area
b	External radius of cylinder
d	Nominal diameter of a screw thread
d_c	Collar diameter
d_r	Root diameter of a screw thread
d_m	Mean diameter of a screw thread
D	External diameter of pin
E	Modulus of elasticity or Young's modulus
F	Applied force
F_i	Preload
F_p	Proof load
k	Gauge factor (k-factor) of the strain gauge
K	Torque coefficient
ΔL	Change of length
L	Original length
N	Normal force
P_l	Lowering load
P_r	Rising load
p	Internal pressure in cylinder i.e. contact pressure
P	Inserted load to pin-sleeve from screws i.e. preload
r	Mean radius of cylinder
R	Relative resistance
S_p	Proof strength
S_y	Yield strength
t	Thickness of cylinder
T	Applied torque
T_c	Collar torque
T_l	Lowering torque
T_r	Rising torque
u	displacement
u_1	Axial displacement

2α	Thread angle
β	Angle of taper
ΔR	Change of resistance
λ	Lead angle
ν	Poisson's ratio
ϵ	Strain
ϵ_θ	Strain in hoop (circumferential) direction
ϵ_r	Strain in radial direction
ϵ_z	Strain in axial direction
ϵ_f	Strain of failure
μ	Friction coefficient
μ_c	Friction coefficient of collar
ρ	Resistivity
ψ	Helix angle
σ	Stress
σ_θ	Stress in hoop (circumferential) direction
σ_r	Stress in radial direction
σ_z	Stress in axial direction
σ_{1x}	Axial stress in pin
σ_{2x}	Axial stress in sleeve
σ'_{1x}	Derivative of axial stress in pin
σ_{1r}	Radial stress in pin
σ_{2r}	Radial stress in sleeve
σ'	von Mises stress
τ_{max}	Maximum shear stress

Abbreviations

ATOM	Abaqus Topology Optimization Module
BC	Boundary Conditions
CAE	Computer Aided Engineering
CDF	Computational Fluid Dynamic
CMM	Coordinate Measuring Machine
CPU	Central processing Unit
DCM	Ductile Coulomb-Mohr
DE	Distortion Energy
EPS	Expanding Pin System
FC	Friction Coefficient
FE	Finite Element
FEA	Finite Element Analysis
FEM	Finite Element Method
HBM	Hottinger Baldwin Messtechnik Company
MSS	Maximum Shear Stress
RAM	Random Access Memory
SG	Strain Gauge

1

Introduction and Background

1.1. Background on Expanding Pin System

A pin joint is a type of connection between two objects that provides only relative rotation about a single axis. All translations as well as rotations about other axis are prevented and it is considered a 1 Degree of Freedom (DoF) system. In kinematics a pin joint is formally called a revolute joint and when analyzing motion in two dimensions may also be referred to as a pivot point or as a hinge. A pin joint has many applications in oil and gas, lifting, heavy machinery and other industries.

A pin joint is always susceptible to wear and tear due to slip of bare metals on each other regardless of greasing time intervals. When wearing happens in support holes it requires restoring the holes to their original diameter and tolerance. The pivot joint has direct impact on the functioning of the machine and when it wears out the machine no longer performs properly and results in need for repair to avoid failure. A pivot point is manufactured to be inserted through support holes with a bushing or bearing housing. The support holes are usually just a little bit larger than the pin diameter to prevent slack, because increased diameter difference increases slack and movements of the pin. After inserting the pin, it is secured in place on one side to prevent from falling out.

The contact surface area between the pin and the support hole is a narrow rectangle where the width of this rectangular contact surface depends on the support thickness, on the diameter tolerances of the pin and the support bore, and the loading of the pin. Reduced tolerances result in a wider contact surface which means for a definite loading the stress will decrease. As a rule, for installation and retrieval purposes, bigger tolerance is an advantage, but for operational purposes a smaller tolerance is needed. Most often the material of the pin is a harder material than the support, so the support hole will begin to wear out by enlarging the diameter of the support holes where the pivot is no longer stable and it leads to malfunction and danger in working environment. One of the traditional solutions in industry is installing a liner which is expensive and time consuming.

The expanding pin system (EPS) shown in Figure 1.1 is a pivot pin assembly with a high superiority for substitution of old pivots.EPS is a perfect solution for pin-support slack problem. In the EPS both ends of the pin are tapered and a pair of expansion sleeves are fitted at both ends of the pin followed by washers or securing element. In the EPS as the elements are tightened the expansion sleeves are forced over the tapered ends of the pin creating a wedge pressure between the pin and the support holes which locks the EPS into the pivot. This system eliminates the wearing process. Since expanding pin is secured from both sides it provides greater safety. The joint components of Bondura® EPS is shown in Figure 1.2.

Figure 1.1: Bondura® EPS [1]

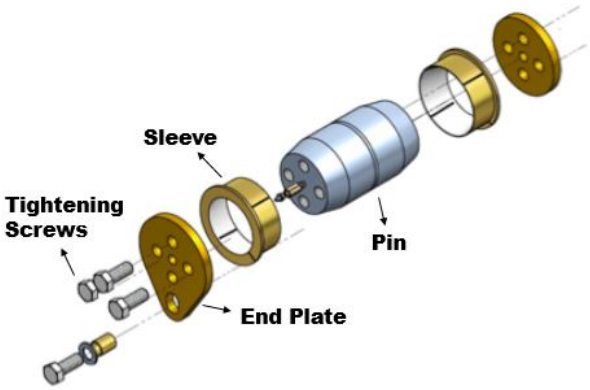

Figure 1.2: Bondura® EPS joint components

EPS locks the pin assembly to the equipment supports and hence prevents any relative movement between these two and it a big advantage comparing with “normal” cylindrical bolts. When torque is applied to the pin assembly, the sleeve expands radially until it locks to the support of the equipment. By preventing the relative movement consequently any tear, wear or ovality problems is prevented in the equipment supports which means avoiding repair expenditures.

Another advantage of EPS is providing larger contact area which means reduction of local stress experienced by supports. When torque is applied to the EPS and it is locked inside the support hole the contact area will be 360^o while this does not occur for standard bolts. The stress distribution around Bondura EPS and a conventional pin is shown in Figure 1.3. When external loading is applied to joint, the contact area will be 180^o in pulling or pushing sequences which is in total a greater contact area. For heavy machinery the contact pressure between the PIN assembly and the support wall can cause design limitations more than the shear or combined stresses in the PIN itself which means by having a larger contact area, the local stress distribution would become more uniform.

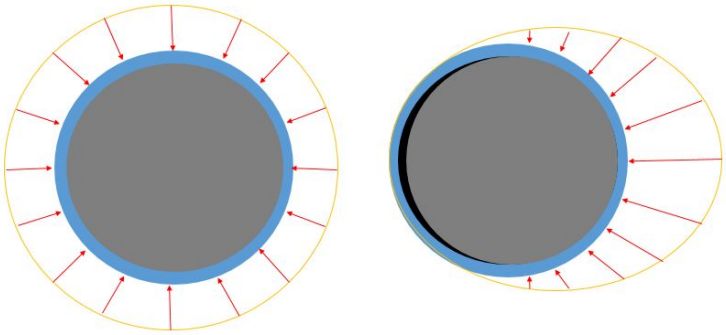

Figure 1.3: Stress distribution around (left) Bondura pin with zero tolerance after tightening, (right) standard pin

Expanding Pin System has the advantages of simple structure, good centering and providing more uniform stress distribution on support lugs and hence is perfectly fitted for various types of machinery and equipment. By applying torque to the fastening screws of the system, the sleeve expands and applies a compression force between surfaces including sleeve-pin, sleeve-support bore and sleeve-end plate. The locking principle works based on friction between these surfaces and the amount of compression stress created in these parts after tightening the fastening screws. A similar concept is found in transmission shafts where an expansion pin is used in mechanical press and hot die forging press [6]. One of the important aspects of EPS is the amount of preload applied to the screws. If tightening or even retightening force is too large, the corresponding contact

surfaces would experience permanent plastic deformation to the expansion sleeve and the ends of the pin, the result is not only make the component hard to be disassembled, even makes the stress distribution nonuniform. Therefore in the process of the EPS design, special consideration should be dedicated to the sleeve thickness and slit width, but also the optimum contact length and contact stress for different rated torque are crucially important.

1.2. Recent Studies on Expanding Pin System

The subject of stress analysis of an expanding pin assembly has not attracted so much attention and previous master theses of Berkani [7] and Akhtar [8] will be used as main sources for this study.

Berkani in his master thesis, studied the stress applied to the support both experimentally and numerically. His experimental work was performed with the use of a *test boss* that acted as the host support. By installing strain gauges on four different points on circumferential of the test boss, he manged to read the strains created during tightening of the assemblies' screws. He did the expeiment on two Bondura 6.6 assemblies with 88.9 and 120 mm diameters. Catman software coupled with reading and registering the strain gauges provided him radial stresses in his experiment. He performed the stress measuring in normal and temperatures up to 60^oC. For numerical analysis, Berkani used Ansys software to analyse stress distributions and magnitude in steps defined for inserting preload on screws. He carry out the FEA from low temperatures -40^oC up to 60^oC. He also considered the model of test boss both with a free (similar to experimental test) and a fixed boundary conditions. His FEM results show that in the case the test boss is fixed, a better stress distribution is observed.

Akhtar [8] in his thesis analyzed the related factors to maximum possible preloads of the bondura EPS and the relationship between applied torque level and preload. He also did a comparison between bondura EPS and standard bolts in terms of preload capability and to some extent investigated the loss of preload due to plastic deformation (microasperities).

Based on the previous studies it could be concluded that there is still need for more study and investigation on stress distributions and interaction between different parts of the EPS assembly specially for stress created after applying torque on fastening screws and the effect of movement or better to say slip of the sleeve on the conical part of the pin. By applying torque to the screws of the end plate, the expanding sleeve will move forward on the pin and at the same time it will expand. Obviously, existence of slits allow more expansion of the sleeve. Since the sleeve is embedded between pin and the support hole, its expansion is restricted and part of its energy will be dissipated. A similar study has been done by Andrzejuk et. al. [2] where they analysed a conical sleeve with pivot joint under axial loading. In their study, they evaluated energy dissipation between cooperating surfaces of a friction pair theoretically and also they included structural friction, elastic and frictional effects by taking into account the Lame's problem. An illustration of their conical sleeve with pivot and the experimental layout are shown in Figure 1.4.

It is necessary to have a clear understanding about stress state in the expanding joint system to conduct the optimization process precisely and correctly. When the fastening screws are tightened and the pin is locked, a type of residual stress is created in cut sleeve, pin and internal part of the support lug. This residual stress will affect the strain response and stress distribution of engaged parts when they undergo machine loading.

1.3. Objectives

One of the objectives of this thesis is to setup an experiment to measure and obtain strains and stresses between the equipment support and Bondura EPS Φ88.9. These stresses are created due to fastening torque of the screws and loads on the conical ends of the pin. The evaluation of validity of the mathematical model of Ref. [2] for a cut sleeve is another question since these formulas are applicable for a perfect sleeve, but the sleeve in Bondura EPS is not perfect and has four cuts which

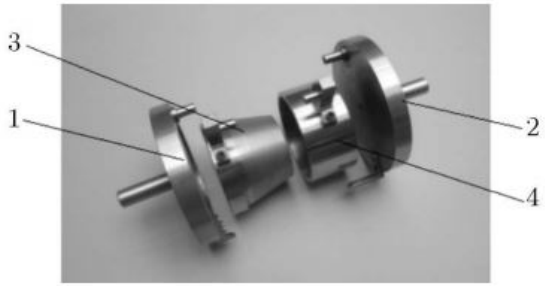

(a) Design of the experimental model of a sleeve-pivot friction joint (decomposed system): 1 – lower pressure plate grip, 2 – upper grip, 3 – pivot, 4 – sleeve

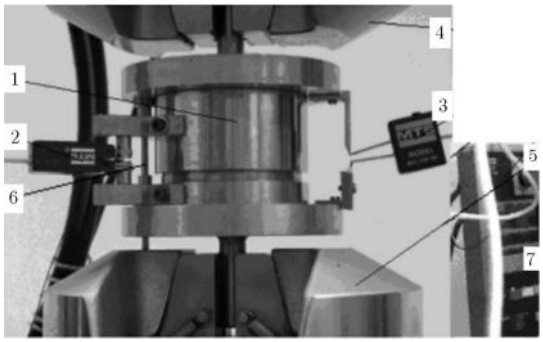

(b) Fastening of the tested model and an overview of its components: 1 – sleeve-pivot, 2 – extensometer type Ext 26, 3 – extensometer type Ext COD; 4, 5 – upper and lower gripping jaws of the MTS testing machine, 6 – steady pin, 7 – programmer

Figure 1.4: Conical Sleeve and pivot pin [2]

one of them is a complete cut (cut-through). Moreover, developing a finite element (FE) model for finding strains and stress distributions of the EPS components is another goal of this thesis.

The final objective of the thesis is optimizing Bondura EPS Φ88.9. The results of FEA are useful tool for implementing structural optimization process.

Briefly, this thesis is focused on stress analysis of EPS and in addition, establishing a methodology for structural optimization of the joint assembly.

1.4. Thesis Structure

The remaining part of the thesis is structured as follows:

Chapter 2 Theoretical Analysis - gives a detailed view referred to different mechanisms that exist in EPS including screw threads, interaction of conical pin-sleeve and thick cylindrical shells related to sleeve-support interaction.

Chapter 3 Experimental Study - gives an explanation of the test setup and steps carried out to obtain strains in a test boss resembling the equipment support. The effects of friction and expansion of sleeve are studied in detail. The findings of the experimentation are discussed.

Chapter 4 Finite Element Analysis - explains the FE procedure adopted in this thesis to model Bondura EPS in the FE software Abaqus. Modelling procedure, assumptions, simplifications and limitations for FEM are mentioned in this chapter.

Chapter 5 Comparison of the Results - provides a comprehensive comparison between numerical results with FE results for conical pin-sleeve interaction and comparison between experimental results with FE results for test boss. In addition, the results of a parametric study on the effect of friction coefficient is explained.

Chapter 6 Optimization - explains the methodology for shape optimization of the pin, particularly the angle of taper at the ends of the pin.

Chapter 7 Conclusion and Recommendations - provides a summary about subjects studied in this thesis and findings. In addition, some issues which require more research and investigation are suggested for future works.

2

Theoretical Analysis

In this chapter, concepts and basics for theoretical analysis of an Expanding Pin System (EPS) are subjects of study. Bondura EPS can be divided into three different parts, threaded part of joint which consists of fastening screws, expanding part which includes the interaction between conical sleeve and pivot pin and interaction between sleeve and support bore. These three different mechanisms are described in the following sections separately.

2.1. Threaded Part- Screws

There has been tremendous number of innovations in the fastener field over time. Designers can benefit from an overwhelming variety of fasteners available for selection. Screw threads are one of the most familiar mechanisms in the world with different applications and they are used practically in every machine in some way or another.

Basically, a screw thread is a long wedge with a triangle shape cross section which is wrapped tightly around a cylinder or in the case of tapered threads around a cone with each wrap of the wedge snug against the previous wrap. The wedge follows a path in the shape of a helix.

A wedge uses the mechanism of an inclined plane to convert the force at its blunt end to force perpendicular to its inclined surface which makes it very useful in different applications like lifting of heavy objects. Screw threads work based on wedge mechanism with this difference that they convert rotational force into linear force along the longitudinal axis of the cylinder. This mechanism in screw threads is used to assemble components by driving an external thread into an internal thread and then wedging between them. Before going through analysis of this mechanism, it is necessary to indicate the terminology of screw threads which is illustrated in Figure 2.1 whose dimensional parameters are explained as follows [3];

Pitch is the distance between adjacent thread forms measured parallel to the thread axis.

Major diameter d is the largest diameter of a screw thread.

Minor or root diameter d_r is the smallest diameter of a screw thread.

Pitch or mean diameter d_m is the theoretical diameter between the major and minor diameters.

Lead l, not shown in figure, is the distance the nut moves parallel to the screw axis when the nut is given one turn. For a single thread, the lead is the same as the pitch.

Thread angle 2α is the angle between the thread flanks.

Crest is the top most point or surface of a thread.

Root is the bottom of the groove.

In Bondura EPS, screws are used to fasten the end plate to the joint assembly. When the screws are tightened, they create an axial load applied to the conical sleeve resulting in pushing and expanding the sleeve and it locks the joint. The mechanism of applied torque and preload or axial load in the joint will be described at the rest of this section.

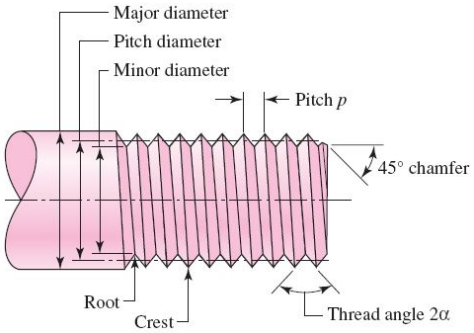

Figure 2.1: Terminology of screw threads [3]

The shape of threads in a screw is different and it can be square, ACME or v-shape. In Figure 2.2a, a square-threaded power screw is subjected to axial load F. λ and ψ are the lead and helix angles, respectively. The force required to raise load F is defined as P_R (Figure 2.2b) and the required force for lowering this load is defined as P_L (Figure 2.2c). Both of these forces can be determined by writing equilibrium equations regarding this fact that friction force acts to oppose motion. The equilibrium equations for raising the load are:

$$\begin{aligned} \sum F_H &= P_R - N sin\lambda - \mu N cos\lambda = 0 \\ \sum F_V &= F + \mu N sin\lambda - N cos\lambda = 0 \end{aligned} \tag{2.1}$$

In a similar way, for lowering the load, there are,

$$\begin{aligned} \sum F_H &= -P_L - N sin\lambda + \mu N cos\lambda = 0 \\ \sum F_V &= F - \mu N sin\lambda - N cos\lambda = 0 \end{aligned} \tag{2.2}$$

where N is the normal force and it is in fact the force that surfaces exert to prevent solid objects from passing through each other. f is friction coefficient. By eliminating N from first equation, the amount of force for raising the load is obtained as,

$$P_R = \frac{F(sin\lambda + \mu cos\lambda)}{cos\lambda - \mu sin\lambda} \tag{2.3}$$

and for lowering the load,

$$P_L = \frac{F(\mu cos\lambda - sin\lambda)}{cos\lambda + \mu sin\lambda} \tag{2.4}$$

By dividing the numerator and the denominator of these equations by cosλ and using relation tan$\lambda = l/\pi\, d_m$ the following equations are resulted,

$$P_R = \frac{F[(l/\pi d_m) + \mu]}{1 - \mu l/\pi d_m} \tag{2.5}$$

$$P_L = \frac{F[\mu - (l/\pi d_m)]}{1 + \mu l/\pi d_m} \tag{2.6}$$

Now, considering that the torque is the product of the force (whether it is for raising force, P_R, or lowering force, P_L) and the mean radius $d_m/2$, the torque for raising and lowering the load is obtained as,

$$T_R = \frac{F d_m}{2}\left(\frac{l + \pi\mu d_m}{\pi d_m - \mu l}\right) \tag{2.7}$$

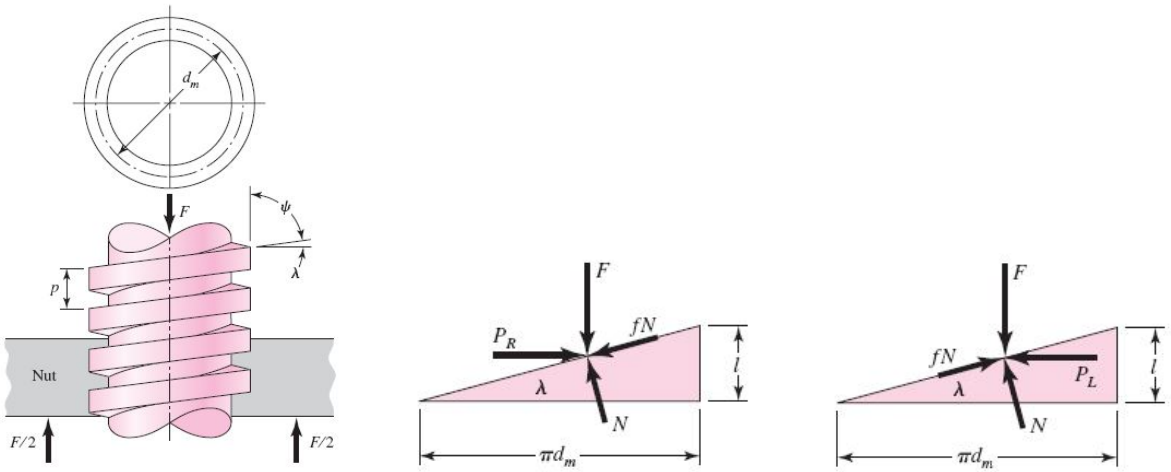

(a) Schematic of a power screw (b) Raising the load (c) Lowering the load

Figure 2.2: Load mechanism in threads [3]

$$T_L = \frac{F d_m}{2}\left(\frac{\pi \mu d_m - l}{\pi d_m + \mu l}\right) \tag{2.8}$$

These derived equations are valid for square threads where the normal thread load is parallel to the axis of the screw. In the case of other type of threads like the V-shape thread shown in Figure 2.1, the normal thread load is inclined to the axis due to the thread angle 2α and the lead angle λ. Lead angles are very small and hence the inclination due to lead angle can be neglected. Using this assumption, only the effect of the thread angle is considered in the rest of the calculations. Angle α which is half of the thread angle increases the frictional force by the wedging action of the threads. It means the frictional terms in Eq. (2-7) should be divided by $\cos\alpha$. For raising the load i.e. tightening a screw, this yields

$$T_R = \frac{F d_m}{2}\left(\frac{l + \pi \mu d_m sec\alpha}{\pi d_m - \mu l sec\alpha}\right) \tag{2.9}$$

Eq. (2-9) gives an approximation for raising torque since the effect of the lead angle has been neglected.

In power screws, a third component is needed to carry the axial component and it is called thrust or collar bearing. In case of screws used in EPS, screw head acts like the collar and helps to create more axial load to end plates. If we consider the mean diameter of collar as d_c and its friction coefficient as μ_c, then the required torque for creation of axial load F is

$$T_c = \frac{F \mu_c d_c}{2} \tag{2.10}$$

The amount of preload in joints is very important and it is directly related to torque applied to the screws. If the preload of a screw is beyond its strength, it can cause plastic deformation in the screw or in a worse case, the screw would be cut. For a bolt, its elongation due to the preload F_i can be computed based on the formula $\delta = F_i\ l / A\ E$. When the nut is tightened, the value of bolt elongation can be measured by a micrometer or a caliper and tightening will be continued until the respective value of preload is achieved. Usually measuring the elongation of a screw is not possible, because the threaded end is inside a blind hole. There are some methods which provide opportunity for this measurement like using a wrench torque, pneumatic-impact wrenching, or the turn-of-the-nut method.

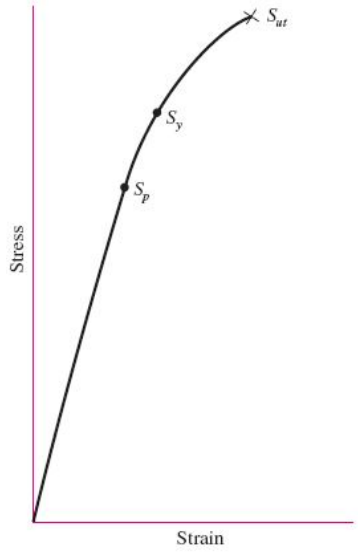

Figure 2.3: Typical stress-strain diagram for bolt materials [3]

Even though the coefficients of friction may vary widely for contact surfaces between screw threads and threads of joint component, we can obtain a good estimate of the torque required for a specified preload by combining Eqs. (2.9) and (2.10):

$$T = \frac{F_i d_m}{2}\left(\frac{l + \pi\mu d_m sec\alpha}{\pi d_m - \mu l sec\alpha}\right) + \frac{F_i \mu_c d_c}{2} \tag{2.11}$$

Eq. (2.11) can be rewritten based on angle of wedge of the screw λ, then it gets the following form,

$$T = \frac{F_i d_m}{2}\left(\frac{tan\lambda + \mu sec\alpha}{l - \mu tan\lambda sec\alpha}\right) + \frac{F_i \mu_c d_c}{2} \tag{2.12}$$

The diameter of the screw head is approximately 1.5 times the nominal size of it. Therefore the mean collar diameter $d_c = (d + 1.5d)/2 = 1.25d$. Thus, Eq. (2.12) can now be arranged to

$$T = [\frac{d_m}{2d}\left(\frac{tan\lambda + \mu sec\alpha}{l - \mu tan\lambda sec\alpha}\right) + 0.625\mu_c]F_i d \tag{2.13}$$

The term in brackets can be defined as *torque coefficient* **K** and so

$$K = \frac{d_m}{2d}\left(\frac{tan\lambda + \mu sec\alpha}{l - \mu tan\lambda sec\alpha}\right) + 0.625\mu_c \tag{2.14}$$

Eq. (2.13) can be written as

$$T = KF_i d \tag{2.15}$$

The coefficient of friction depends upon the surface smoothness, accuracy of roughness measurement, and degree of lubrication. On the average, both μ and μ_c are about 0.15. The interesting fact about Eq. (2.14) is that $K = 0.20$ for $\mu = \mu_c = 0.15$ and it is independent of screw size and whether the screw threads are coarse or fine.

In order to be able to use a screw for several times, it is required to specify the the amount of pretension before the screw experiences plastic deformations. There are several guidelines about how much pretension is probably appropriate to apply to a screw. One of the guidelines is related to the strength of the screw. Figure 2.3 shows the stress-strain diagram of a good-quality bolt material

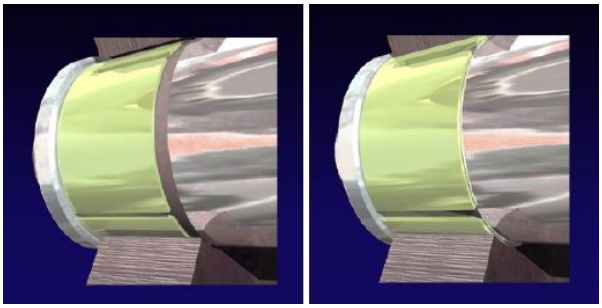

Figure 2.4: Interaction of conical pin-sleeve

which is applicable for screws. The shape of the diagram is different with conventional stress-strain diagram for steels, because the bolt has been exposed to cold working or other similar strengthening processes and therefore the region of plastic deformation has become smaller. Also there is no clearly defined yield point and the diagram progresses smoothly up to fracture corresponding to the tensile strength. This means the bolt or screw will retain its load-carrying capacity regardless of how much preload is given to it. This is what keeps the screw tight and determines strength of the joint. The pre-tension can be considered as the "muscle" of the joint and its magnitude is determined by the screw strength. It is recommended for both static and fatigue loading that the amount of preload be around $0.75F_p$ [3] where F_p is the proof load and can be obtained from the relation $F_p = A_t S_p$. This preload is valid for non-permanent connections and reused fasteners. A_t is called the tensile area and it is in fact the cross sectional area of the screw with diameter equal to root diameter, d_r, and S_p is the proof strength and a good approximate for its value is $S_P = 0.85S_y$ where S_y is the yield strength of the screw material. There are other recommendations for applying torque to the screws as a control value of the fastener tension which can be selected to be 0.60 of the fastener proof load [9] that ensures safe elastic region for functioning of the screws.

2.2. Expansion Part

In this section, stress analysis related to interaction of conical sleeve and pivot pin is studied. The ends of the pivot pin is tapered as the inside part of the conical sleeve. When the screws of the Bondura EPS is tightened, the end plate pushes the sleeve and makes it advance and expand simultaneously. A 3D schematic of sleeve-pin is shown in Figure 2.4. Bodura conical sleeve is actually an expanding sleeve type and its four slits gives it better capability to expand and advance which makes the locking operation happen with lower axial force. The stress analysis of sleeve-pin provided in this section is limited to a sleeve without slits.

Generally the static analysis of different types of interacting joints can be carried out by investigation of displacements in an external loading function. A simplified model of sleeve-pin assembly loaded by axial force αP is shown in Figure 2.5. αP is a representation of preload of screws where $0 < \alpha < \alpha_1$ and an assumption has been made that α_1=1.

In order to derive stress relationships, a section with height δx is set for analysis. Theoretical considerations have been taken for both the conical sleeve and pivot pin. The mathematical modeling is developed by Andrzejuk et.al [2] and here the case realted to loading of the sleeve-pin section is provided. The external radius r_0 of the joint section shown in Figure 2.5b can be written as

$$r_0 = R - x tan\beta \tag{2.16}$$

In the section of the investigation of sleeve-pin joint, the equation of force equilibrium is

$$\Delta\sigma_{1x}F_1 = \Delta\sigma_{2x}F_2 \rightarrow \Delta\sigma_{2x} = \frac{r_0^2}{r_{z0}^2 - r_0^2}\Delta\sigma_{1x} \tag{2.17}$$

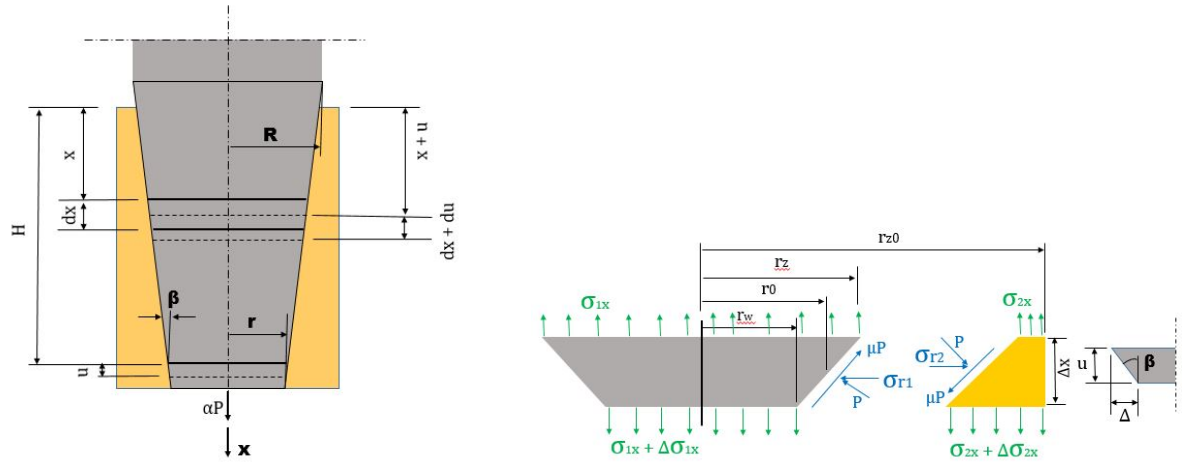

(a) Sleeve-pivot joint

(b) Section of sleeve, pivot pin and displacement scheme

Figure 2.5: Physical model of sleeve-pin

where F_1 and F_2 are the related to the fields of the cross sectional area of the sleeve-pin section and $\Delta\sigma_{1x}$ and $\Delta\sigma_{2x}$ are the amounts of increase in normal stresses in the considered section of sleeve-pin joint. The equations of axial and radial stresses will be derived separately for pivot pin and sleeve. Thus subscripts 1 and 2 are assigned to pivot pin and sleeve, respectively.

2.2.1. Considerations for the pivot section

The equation of equilibrium in the x-axial direction can be written as follows regarding projection of forces,

$$-\sigma_{1x}\pi r_0^2 - \mu p cos\beta 2\pi r_0 \frac{\Delta x}{cos\beta} - p sin\beta 2\pi r_0 \frac{\Delta x}{cos\beta} + (\sigma_{1x} + \Delta\sigma_{1x})\pi r_0^2 = 0 \tag{2.18}$$

where μ is the coefficient of friction between contact surfaces of the sleeve-pin joint. By solving Eq. (2.18) for p, the pressure for the contact surface joint can be obtained which is dependent on increase of stress in pivot pin due to axial load,

$$p = \frac{\Delta\sigma_{1x}}{\Delta x}\frac{r_0}{2(tan\beta + \mu)} \tag{2.19}$$

The equilibrium equation acting in the pivot pin section in the radial or y-direction is

$$(-\sigma_{1r} + \mu p sin\beta - p cos\beta)2\pi r_0 \frac{\Delta x}{cos\beta} = 0 \tag{2.20}$$

By substituting p from Eq. (2-19) in Eq. (2-20), the radial stress in pivot pin section gets the form of following equation

$$\sigma_{1r} = \frac{-r_0 cos\beta(1 - \mu tan\beta)}{2(\mu + tan\beta)}\frac{\Delta\sigma_{1x}}{\Delta x} \tag{2.21}$$

Since the sleeve-pin system is symmetric in the different directions of x, y and z, and in accordance to Hook's law, the following strain and stress relations are valid

$$\sigma_{1z} = \sigma_{1y} = \sigma_{1r} \qquad \epsilon_{1z} = \epsilon_{1y} = \epsilon_{1r} \qquad \epsilon_{1z} = \frac{1}{E_1}[\sigma_{1z} - \nu_1(\sigma_{1x} + \sigma_{1y})] \tag{2.22}$$

Taking into account the above equation, pin radial strain takes the form

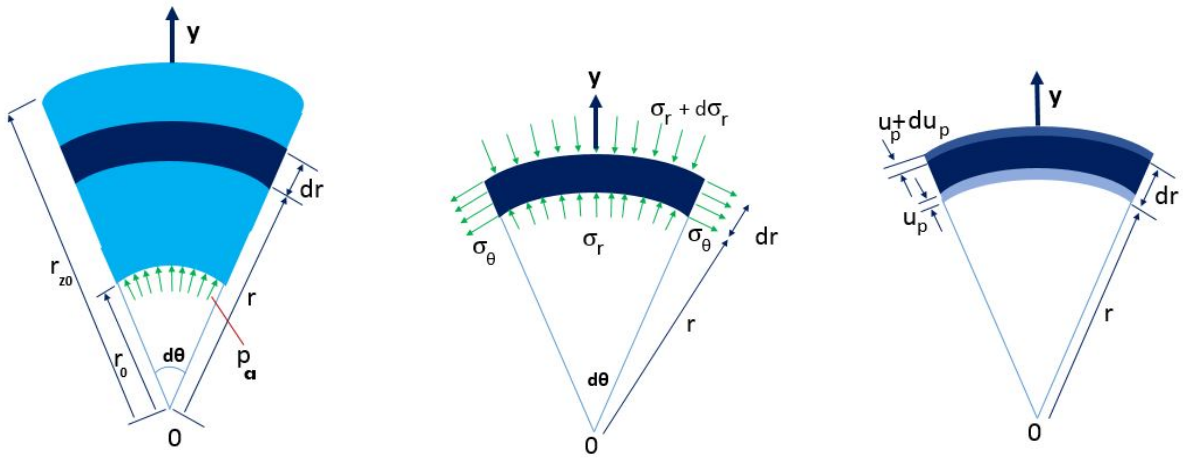

(a) A section of sleeve (b) Stresses in a section of sleeve (c) Radial expansion in sleeve

Figure 2.6: Radial stress and displacement in the sleeve section

$$\epsilon_{1r} = \frac{\sigma_{1r}(1-\nu_1)}{E_1} - \frac{\nu_1\sigma_{1x}}{E_1} \tag{2.23}$$

where ν_1, E_1 are Poisson's ratio and Young's modulus of the pivot section. As a result of the interaction of sleeve-pin, the pin section experiences a radial deformation and consequently its radius changes. The absolute value of the radial displacement can be described after substituting formula (2.21) into equation (2.23) and this substitution yields

$$\Delta r_{01} = \epsilon_{1r} r_0 = \frac{-r_0^2 cos\beta(1-\mu tan\beta)(1-\nu_1)}{2E_1(\mu+tan\beta)} \frac{\Delta\sigma_{1x}}{\Delta x} - \frac{\nu_1 r_0 \sigma_{1x}}{E_1} \tag{2.24}$$

2.2.2. Considerations for the sleeve section

By evaluating stresses acing on the respected section of the conical sleeve, the equilibrium equation in axial direction takes the following form

$$-\sigma_{2x}\pi(r_{z0}^2 - r_0^2) + \mu p cos\beta 2\pi r_0 \frac{\Delta x}{cos\beta} + p sin\beta 2\pi r_0 \frac{\Delta x}{cos\beta} + (\sigma_{2x} + \Delta\sigma_{2x})\pi(r_{z0}^2 - r_0^2) = 0 \tag{2.25}$$

By simplifying above equation, an equation equivalent to Eq. (2.19) can be obtained for pressure per unit at the contact surface joint. The equilibrium equation in y-radial direction is

$$(\sigma_{2r} - \mu p sin\beta + p cos\beta) 2\pi r_0 \frac{\Delta x}{cos\beta} = 0 \tag{2.26}$$

so the radial stress of sleeve appears as

$$\sigma_{2r} = -p cos\beta(1-\mu tan\beta) = p_a \tag{2.27}$$

As it is illustrated in Figure 2.6, the stress distribution of σ_{2r} and displacements u_p in the radial direction can be determined by using Lame's theorem, so

$$\sigma_{2r} = \frac{E_2}{1-\nu_2^2}(C_1(1+\nu_2) - \frac{C_2}{r^2}(1-\nu_2)) \qquad u_p = C_1 r + \frac{C_2}{r} \tag{2.28}$$

The integration constants in Eq. (2.28) can be determined with the help of boundary conditions as follows

$$\sigma_{2r} = \begin{cases} -p_a = pcos\beta(1-\mu tan\beta) & for \quad r = r_0 \\ 0 & for \quad r = r_{z0} \end{cases} \tag{2.29}$$

Then the constants are obtained as

$$C_1 = \frac{(1-\nu_2)r_0^2 cos\beta p(1-\mu tan\beta)}{E_2(r_0^2 - r_{z0}^2)} \qquad C_2 = \frac{(1+\nu_2)r_0^2 r_{z0}^2 cos\beta p(1-\mu tan\beta)}{E_2(r_0^2 - r_{z0}^2)} \tag{2.30}$$

By substituting Eq. (2.30) in radial stress function of the first formula of Eq. (2.28), a formula which describes the radial stress in a section of sleeve is derived in the following form

$$\sigma_{2r} = \frac{r_0^2 cos\beta p(1-\mu tan\beta)}{r_0^2 - r_{z0}^2}(1 - \frac{r_{z0}^2}{r^2}) \tag{2.31}$$

Similarly, the radial displacement u_p which is shown in Figure 2.6c can be determined from the second formula of Eq. (2.28),

$$\sigma_{2r} = \frac{r_0^2 cos\beta p(1-\mu tan\beta)}{E_2(r_0^2 - r_{z0}^2)}[(1-\nu_2)r + (1+\nu_2)\frac{r_{z0}^2}{r}] \tag{2.32}$$

For $r = r_0$ from Eq. (2.19), Eq. (2.32) is transformed to the following form

$$u_p|_{r=r_0} = \frac{-r_0^4 cos\beta(1-\mu tan\beta)}{2E_2(r_0^2 - r_{z0}^2)(tan\beta+\mu)}[(1-\nu_2) + (1+\nu_2)\frac{r_{z0}^2}{r_0^2}]\frac{\Delta\sigma_{1x}}{\Delta x} \tag{2.33}$$

The displacement Δ between the contact surface elements of sleeve-pin joint (Figure 2.5b) can be determined based on expansion of sleeve and deformation of pivot pin which is given by

$$\Delta = u_p|_{r=r_0} - \Delta r_{01} = \frac{\Delta\sigma_{1x}}{\Delta x} z_1 + \sigma_{1x}\frac{\nu_1 r_0}{E_1} \tag{2.34}$$

where in the above equation z_1 is

$$z_1 = \frac{r_0^2 cos\beta}{2}\frac{1-\mu tan\beta}{tan\beta+\mu}[\frac{-r_0^2}{E_2(r_0^2 - r_{z0}^2)}(1-\nu_2 + (1+\nu_2)\frac{r_{z0}^2}{r_0^2}) + \frac{1-\nu_1}{E_1}] \tag{2.35}$$

A mutual axial displacement of the conical sleeve and pivot pin joint is expressed as following formula

$$u = \frac{\Delta}{tan\beta} = \frac{\Delta\sigma_{1x}}{\Delta x}\frac{z_1}{tan\beta} + \sigma_{1x}\frac{\nu_1 r_0}{E_1 tan\beta} \tag{2.36}$$

By substituting z_1 from Eq. (2.35) to Eq. 2.36, the axial displacement gets the following form

$$u_1 = \eta_3(R - xtan\beta)^2\sigma'_{1x} + \eta_4(R - xtan\beta)\sigma_{1x} \tag{2.37}$$

where

$$\begin{gathered} \eta_1 = \frac{\chi}{E_2}(1-\nu_2 + (1+\nu_2)\frac{r_{z0}^2}{r^2}) + \frac{1-\nu_1}{E_1} \qquad \eta_2 = \frac{cos\beta(1-\mu tan\beta)}{2(tan\beta+\mu)tan\beta} \\ \eta_3 = \eta_1\eta_2 \qquad \eta_4 = \frac{\nu_1}{E_1 tan\beta} \qquad \chi = \frac{1}{\frac{r_{z0}^2}{r^2}} - 1 \end{gathered} \tag{2.38}$$

Based on definition of axial strain which is the derivative of axial displacement with respect to x, it can be derived using Eq. (2.37) as

$$\epsilon_{1x} = \frac{du_1}{dx} = \eta_3(R - xtan\beta)^2\sigma''_{1x} + (R - xtan\beta)(\eta_4 - 2\eta_3 tan\beta)\sigma'_{1x} - \eta_4 tan\beta\sigma_{1x} \tag{2.39}$$

According to Hook's law, the relationship between the stresses and axial strain is

$$\epsilon_{1x} = \frac{1}{E_1}[\sigma_{1x} - \nu_1(\sigma_{1z} + \sigma_{1y})] \tag{2.40}$$

Taking into account the symmetry condition of the system and using the first formula of Eq. (2.22), Eq. (2.40) can be rewritten as

$$\epsilon_{1x} = \frac{\sigma_{1x}}{E_1} - 2\sigma_{1r}\frac{\nu_1}{E_1} \tag{2.41}$$

After substituting Eq. (2.16) and (2.21) in Eq. (2.41), the axial strain takes the new form as

$$\epsilon_{1x} = \frac{\sigma_{1x}}{E_1} + \eta_5(R - xtan\beta)\sigma'_{1x} \qquad \eta_5 = \frac{\nu_1 cos\beta(1 - \mu tan\beta)}{E_1(tan\beta + \mu)} \tag{2.42}$$

by combining the Eqs. (2.39) and (2.42), it results in a homogeneous quadratic differential equation with variable coefficients which are designated as follows

$$\begin{gathered}\eta_3(R - xtan\beta)^2\sigma''_{1x} + \eta_6(R - xtan\beta)\sigma'_{1x} - \eta_7\sigma_{1x} = 0 \\ \eta_6 = \eta_4 - 2\eta_3 tan\beta - \eta_5 \qquad \eta_7 = \eta_4 tan\beta + \frac{1}{E_1}\end{gathered} \tag{2.43}$$

By defining a function for axial stress in the form of $\sigma_{1x} = (R - xtan\beta)^\lambda$ and substituting it in Eq. (2.43), the characteristic equation can be obtained as

$$\lambda^2 - B_4\lambda - C_{12} = 0 \qquad B_4 = 1 + \frac{\eta_6}{\eta_3 tan\beta} \qquad C_{12} = \frac{\eta_7}{\eta_3}tan^2\beta \tag{2.44}$$

The roots of the characteristic Eq. (2.44) are obtained using the following equation

$$\Delta_{41} = B_4^2 + 4C_{12} > 0 \qquad \lambda_{9,10} = \frac{B_4 \pm \sqrt{\Delta_{41}}}{2} \tag{2.45}$$

the general solution to the differential equation $(2.43)_1$ may be written in the form of

$$\sigma_{1x} = C_{13}(R - xtan\beta)^{\lambda_9} + C_{14}(R - xtan\beta)^{\lambda_{10}} \tag{2.46}$$

The integration constants C_{13} and C_{14} are determined based on the boundary conditions, therefore

$$\sigma_{1x} = \begin{cases} 0 & for \quad x = 0 \\ \frac{\alpha P}{\pi r^2} & for \quad x = H \end{cases} \tag{2.47}$$

The above boundary conditions result in the following relationships for the integration constants

$$C_{13} = -C_{14}R^{\lambda_{10}-\lambda_9} \qquad C_{14} = \frac{\alpha P}{\pi r^2(r^{\lambda_{10}} - R^{\lambda_{10}-\lambda_9}r^{\lambda_9})} \qquad r = R - Htan\beta \tag{2.48}$$

The axial stress gets the form of

$$\sigma_{1x} = C_{14}[(R - xtan\beta)^{\lambda_{10}} + (R - xtan\beta)^{\lambda_9}R^{\lambda_{10}-\lambda_9}] \tag{2.49}$$

subsequently, the stress derivative is

$$\sigma'_{1x} = C_{14} tan\beta[\lambda_9 R^{\lambda_{10}-\lambda_9}(R - xtan\beta)^{\lambda_9-1} - \lambda_{10}(R - xtan\beta)^{\lambda_{10}-1}] \tag{2.50}$$

For $x = H$, the stress derivative becomes as follows

$$\sigma'_{1x}(x = H) = C_{14} tan\beta(\lambda_9 R^{\lambda_{10}-\lambda_9} r^{\lambda_9-1} - \lambda_{10} r^{\lambda_{10}-1}) \tag{2.51}$$

Now, based on the obtained results for axial stress and its derivative, it is possible to determine the axial displacement of the extreme cross section at $x = H$ to the following form dependent on the external force which was defined as αP

$$u_1(x = H) = \frac{\alpha P}{\pi r}(\eta_4 + \frac{\eta_3 tan\beta(\lambda_9 R^{\lambda_{10}-\lambda_9} r^{\lambda_9} - \lambda_{10} r^{\lambda_{10}}}{r^{\lambda_{10}} - R^{\lambda_{10}-\lambda_9} r^{\lambda_9}}) \tag{2.52}$$

Eq. (2.52) describes the load-axial displacement of the conical sleeve- pivot pin joint. It is necessary to highlight that the sleeve used in Bondura EPS has four slits which are not considered in the obtained formulas, but it is obvious that due to existence of these slits, the sleeve can expand and advance more. This matter will be investigated in Chapter of results.

2.3. Sleeve-Support Bore Interaction

In this section the interaction between conical sleeve and inner surface or bore of the equipment support will be investigated. In this study, the support is replaced with a test boss and the numerical and experimental studies will be carried out on the test boss which is shown in Figure 2.7a. Due to expansion action of the sleeve, a radial stress will be induced to the bore of the test boss. Moreover, axial advancement of sleeve is opposed by friction force between contact surface of the sleeve and test boss. The friction force has two components including friction coefficient and the force perpendicular to the longitudinal axis of the test boss which is actually resulted from the radial stress of sleeve.

The test boss can be considered as a thick cylindrical shell. A thick cylinder with inner radius a and outer radius b exposed to internal pressure p_1 and external pressure p_2 is illustrated in Figure 2.7b. A cylindrical coordinate can be defined by r for radial, θ for circumferential and z for axial directions. For analysis purposes, a thin cut of thickness dz from the cylinder is considered. The cylindrical volume element is $dr(rd\theta)dz$. Because of radial symmetry there are no shear stresses act on the volume element and normal stresses are functions of r only. The nonzero stress components are principal stresses σ_r, σ_θ and σ_z. The distributions of these stresses through the wall thickness are determined by the equations of equilibrium, compatibility relations, and stress-strain relations [10].

Equation of Equilibrium

By neglecting body force components, the equilibrium equations for cylindrical coordinates is simplified to

$$r\frac{d\sigma_r}{dr} = \sigma_\theta - \sigma_r \quad or \quad \frac{d}{dr}(r\sigma_r) = \sigma_\theta \tag{2.53}$$

Strain-Displacement Relations and Compatibility Condition

The relationships of strain displacement for the thick-walled cylinder are

$$\epsilon_r = \frac{\partial u}{\partial r} \quad \epsilon_\theta = \frac{u}{r} \quad \epsilon_z = \frac{\partial w}{\partial z} \tag{2.54}$$

where $u = u(r, z)$ and $w = w(r, z)$ are displacement components in r and z directions, respectively. Since the test boss is a thick-walled cylinder without end caps, the shear strain components are zero because of radial symmetry. In addition, it is assumed that ϵ_z is constant. Eliminating

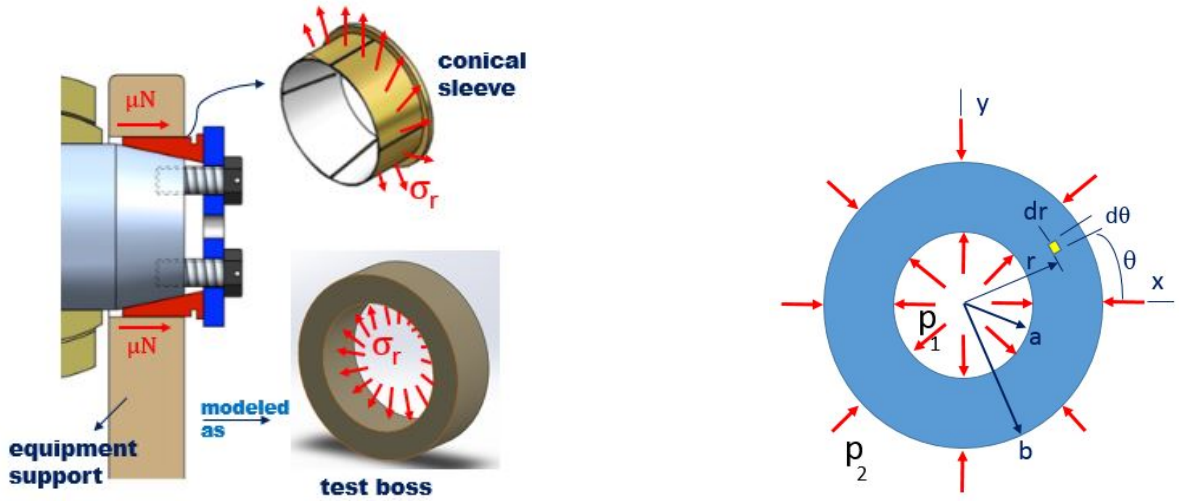

(a) Stress interaction between sleeve-test boss

(b) Cross section of thick cylindrical shell

Figure 2.7: Sleeve-test

the displacement $u = u(r)$ from the first two equations of Eq. (2.54) results in strain compatibility condition for the thick-walled cylinder as follows

$$r\frac{d\epsilon_\theta}{dr} = \epsilon_r - \epsilon_\theta \quad or \quad \frac{d}{dr}(r\epsilon_\theta) = \epsilon_r \tag{2.55}$$

Stress-Strain Relations

The material of the test boss is isotropic and linearly elastic, thus the stress-strain relations can be written as

$$\begin{aligned} \epsilon_r &= \frac{1}{E}[\sigma_r - \nu(\sigma_\theta + \sigma_z)] \\ \epsilon_\theta &= \frac{1}{E}[\sigma_\theta - \nu(\sigma_r + \sigma_z)] \\ \epsilon_z &= \frac{1}{E}[\sigma_z - \nu(\sigma_r + \sigma_\theta)] = constant \end{aligned} \tag{2.56}$$

where E and ν denote the modulus of elasticity and Poisson's ratio of the test boss, respectively. By substituting the first two equations of Eq. (2.56) in Eq. (2.55), a relationship between σ_r, σ_θ σ_z and their derivatives are found. Using the assumption that ϵ_z is constant, the last formula of Eq. (2.56) can be used to indicate the derivative of $d\sigma_z/dr$ in terms of the derivatives of σ_r and σ_θ. This expression helps to eliminate $d\sigma_z/dr$ from Eq. (2.55) and makes this equation dependent on σ_r, σ_θ and their derivatives. Eq. (2.53) can be used to eliminate σ_r-σ_θ, because the undifferentiated terms in σ_r and σ_θ occur in the form of σ_r-σ_θ. Thus, the following differential expression can be extracted

$$\frac{d}{dr}(\sigma_r + \sigma_\theta) = 0 \tag{2.57}$$

Integration of Eq. (2.57) yields the following result

$$\sigma_r + \sigma_\theta = 2C_1 \tag{2.58}$$

where $2C_1$ is integration constant and for simplicity of form in subsequent expressions, the factor is considered in the equation. Elimination of σ_θ from Eqs. (2.53) and (2.58) leads to the following expression based on σ_r

$$\frac{d}{dr}(r^2\sigma_r) = 2C_1 r \tag{2.59}$$

Integration of Eq. (2.59) results in

$$\sigma_r = (1 - \frac{a^2}{r^2})C_1 + \frac{C_2}{r^2} \tag{2.60}$$

where the integration is carried out from the inner radius a to the radius r. C_2 is a second integration constant. Substituting Eq. (2.60) into Eq. (2.58) gives the expression for σ_θ as

$$\sigma_\theta = (1 + \frac{a^2}{r^2})C_1 - \frac{C_2}{r^2} \tag{2.61}$$

The integration constants C_1 and C_2 can be determined based on the boundary conditions. Considering the loading of the test boss, it is subjected to internal pressure of σ_r = -p at its inner surface, r=a, and since there is no external pressure acting on its outer surface, it means σ_r = 0 at r=b which results in the following values for the constants

$$C_1 = \frac{pa^2}{b^2 - a^2} \qquad C_2 = -pa^2 \tag{2.62}$$

By substituting the constants of Eq. (2.62) in Eqs. (2.60) and (2.61), the stress components in radial and hoop directions are obtained as

$$\sigma_r = \frac{pa^2}{b^2 - a^2}(1 - \frac{b^2}{r^2}) \tag{2.63}$$

$$\sigma_\theta = \frac{pa^2}{b^2 - a^2}(1 + \frac{b^2}{r^2}) \tag{2.64}$$

The test boss does not have any movement in axial or z-direction. The outer surface of the test boss experiences no force, but its inner surface is exposed to friction force created by outer surface of the conical sleeve. Overall equilibrium of forces in the axial direction requires

$$\int_a^b \sigma_z 2\pi r\, dr = \mu N \tag{2.65}$$

In Eq. (2.65), N is the force perpendicular to the inner surface of the test boss and it is created by expansion of the conical sleeve. Therefore, the stress component in axial direction for inner surface of the test boss takes the form of

$$\sigma_z = \frac{\mu N}{\pi(b^2 - a^2)} \tag{2.66}$$

By setting up an experiment and measuring the hoop strain on the outer surface of the test boss, it is simple to obtain all stress components on the inner and outer surfaces of the test boss. It is very useful to know the stress components on the inner surface of the test boss, because it resembles the inner surface of the equipment support and this can provide useful information about existing stresses in the bore of the support which act as the residual stresses. This matter can have effect on lifetime of the equipment support and knowing this can improve evaluations on equipment structural response. By having the hoop strain on the outer surface of the test boss and using the second formula in Eq. (2.56) and also considering that both σ_r and σ_z are zero at r=b, the hoop stress can be found by the following equation

$$\sigma_{\theta(ext)} = E\epsilon_{\theta(ext)} \tag{2.67}$$

After finding the hoop stress, Eq. (2.64) can be used to find the magnitude of internal pressure (for r=b)

$$\sigma_{\theta(ext)} = \frac{2a^2}{(b^2 - a^2)} p \tag{2.68}$$

Finally, by having the internal pressure, all stress components which act on the internal surface of the test boss can be calculated (for r=a)

$$\sigma_{r(int)} = -p \qquad \sigma_{\theta(int)} = \frac{b^2 + a^2}{(b^2 - a^2)} p \qquad \sigma_{z(int)} = \frac{\mu N}{\pi(b^2 - a^2)} \tag{2.69}$$

In Eq. (2.69), N is actually the radial force created by expansion of the sleeve and it can be calculated by considering internal pressure multiplied in internal surface of the test boss as

$$N = \sigma_{r(int)} A = \sigma_{r(int)} (2\pi aL) \tag{2.70}$$

where L is the length of the test boss. By substituting Eq. (2.70) in the third formula of Eq. (2.69), the internal axial stress of the test boss is found in the following form

$$\sigma_{z(int)} = \frac{2\mu aL}{b^2 - a^2} \sigma_{r(int)} \quad or \quad \sigma_{z(int)} = -\frac{2\mu aL}{b^2 - a^2} p \tag{2.71}$$

The internal axial stress is negative since it is in negative direction of z-axis and it has a compressive characteristic.

2.4. Evaluation of Failure

There are several theories which have been formulated and tested and provide today's accepted practices for investigation of failure of material. These theories are categorized into two different classes including ductile and brittle materials. This classification is based on material strain range before failure i.e. defined by ϵ_f. If $\epsilon_f > 0.05$, the material is considered as ductile, otherwise the material with $\epsilon_f < 0.05$ feature is classified as brittle [3].

Since the materials of the joint system are ductile, this section is limited to failure theories for this class of material. The accepted theories for ductile materials which are generally known as *yield criteria* are [3]:

- Maximum shear stress (MSS)
- Distortion energy (DE)
- Ductile Coulomb-Mohr (DCM)

At the rest of this section, MSS and DE are investigated.

2.4.1. Maximum Shear Stress

The Maximum-Shear-Stress theory sets the *yield limit* of the material as a criteria and compares the maximum shear stress in any element of the material with it. Exceeding this criteria means beginning of the yielding. The MSS theory is also reffered to as **Tresca** Theory [3].

The MSS is a conservative theory and it indicates that the maximum shear stress occurs on a surface 45^o from the tensile surface with a magnitude of $\tau_{max} = \sigma/2$. The maximum shear stress at yield could be defined as $\tau_{max} = S_y/2$. For a general state of stress with principle stresses ordered as $\sigma_1 \geq \sigma_2 \geq \sigma_3$, the maximum shear stress is τ_{max} = (σ_1-σ_3)/2. Thus, the MSS is violated or the yielding happens when the following condition dominates

$$\tau_{max} = \frac{\sigma_1 - \sigma_3}{2} \geq \frac{S_y}{2} \quad or \quad \sigma_1 - \sigma_3 \geq S_y \tag{2.72}$$

Eq. (2-72) helps to find the maximum shear stress and compares it with yield stress to evaluate the failure condition of the materials. Based on the stress state in the test boss which is $\sigma_{\theta(int)} \geq \sigma_{z(int)} \geq \sigma_{r(int)}$, then the MSS is the determined by

$$\tau_{max} = \frac{\sigma_{\theta(int)} - \sigma_{r(int)}}{2} \tag{2.73}$$

In the literature, 2 τ_{max} is known as $Tresca$ stress.

2.4.2. Distorsion Energy

The Distortion-Energy theory considers the yielding at a state where the distortion strain energy per unit volume reaches or exceeds the distortion strain energy for yield [3]. The distortion-energy (DE) theory is developed based on observation of ductile material under hydrostatic stress where it exhibits yield strengths more than values given by the simple tensile test. Thus it was suggested and accepted that yielding is not a simple tensile or compressive phenomenon and basically it is related somehow to the angular distortion of the stressed element. The criteria for DE which is derived from strain energy of the elements of a part and is known as **von Mises** stress takes the following form for a three-dimensional stress state

$$\sigma_{vonMises} = [\frac{(\sigma_1 - \sigma_2)^2 + (\sigma_2 - \sigma_3)^2 + (\sigma_3 - \sigma_1)^2}{2}]^{1/2} \tag{2.74}$$

Therefore, the von Mises stress, σ', for the test boss is calculated similar to above equation

$$\sigma_{vonMises} = [\frac{(\sigma_{\theta(int)} - \sigma_{z(int)})^2 + (\sigma_{z(int)} - \sigma_{r(int)})^2 + (\sigma_{r(int)} - \sigma_{\theta(int)})^2}{2}]^{1/2} \tag{2.75}$$

In this theory yielding happens when the von Mises stress becomes larger than the material yield stress. Both MSS and DE criteria will be used in order to evaluate whether the test boss exceeds the yield limit or not.

2.5. Summary

In this chapter, the EPS has been divided into three different categories including *threaded part* for attaching the end plate and squeezing the sleeve, *expansion part* related to interaction of conical sleeve-pin and *sleeve-support bore interaction* which is considered as internal loading of a thick cylinder. The governing equations for each category have been provided. The equations for thick cylinder will be used for obtaining stress magnitudes based on measured strains on test boss in $Chapter3$. Further analysis for equations of sleeve-support interaction (in this study, sleeve-test boss) will be done in $Chapter4$ and the results of the related formulas will be compared with Finite Element Modeling results to evaluate the feasibility of application of these formulas for a sleeve with slits. In addition, two failure theories for ductile materials have been introduced and they will be used to investigate the stress state in the test boss.

3

Experimental Study

In order to investigate and analyse the contact stresses between conical sleeve, pin and the inner surface of the equipment support, an experimental test has been carried out. Bondura Expanding Pin System (EPS) is applicable to different heavy machinery, so to evaluate the stress state inside the equipment support bore, a test boss is designed and built for this experiment. Recording of test boss external hoop strains created by torquing the fastening screws of the system have been measured step-wise. HBM strain gauges type LY4-1-5/120 have been used in this experimental study. An image and also the clarification of each designation in gauge code name are shown in Figures 3.1a and 3.1b. The test is conducted in room temperature and registration of temperature shows a range of 21.7°C to 23°C. Even though the temperature difference is very low and that may not have significant effect on reading of strains while running the test according to information in SG catalogue (which is provided in Appendix A.1), a compensation method has been applied to test setup to omit the effect of temperature variations. This method is known as dummy gauge and it is useful when the strain gauge alloy metal is different with the test object material. In this technique, a dummy gauge which is identical to the active one is installed on an unstrained sample of the same material as the test specimen [11]. The sample with the dummy gauge is placed in thermal contact with the test specimen, adjacent to the active gauge as it is illustrated in Figures 3.1c. In this experiment, the dummy gauges are wired into a half-Wheatstone bridge and they are placed near to the active gauges so that the temperature effects on the active and dummy gauges cancel each other. The dummy gauges were selected and installed on a similar test ring with the same material considering the following items recommended by [12];

a) The same gauge type as the active strain gauge is used,

b) They are applied in a spot where they are subjected to the same interference effect as the active gauges,

c) They are only subjected to the interference effect and never to the quantity to be measured ϵ_M or its side effects.

A strain gauge basically works on the principle of a simple metal conductor wire that tends to have an impact on its length, cross-sectional area and resistance due to applied stress. In fact, the resistance of the wire is directly proportional to the length of the wire and inversely proportional to its cross-sectional area, according to the following equation [4],

$$R = \rho \frac{L}{A} \tag{3.1}$$

where R = resistance of the wire, ρ = resistivity, L = length of the wire and A = area of the cross-section of the wire. When a force is exerted to an object, it will result in change of dimensions of the object and this creates strain. This strain causes change in resistance of the gauge which is

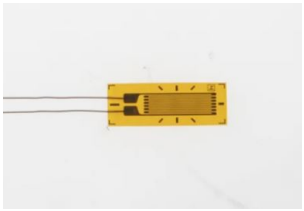

(a) HBM strain gauge type LY4-1-5/120

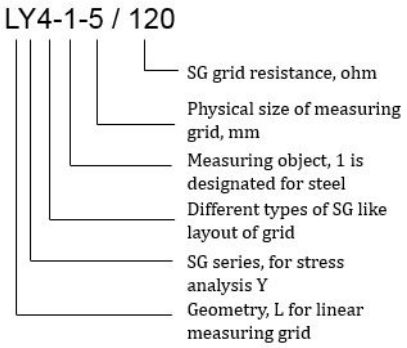

(b) Clarification of code name [13]

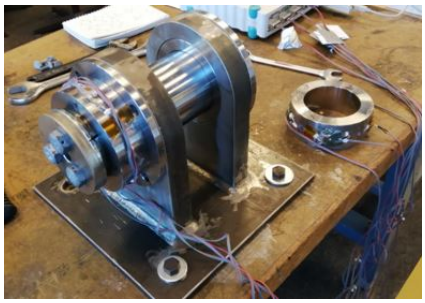

(c) Active-dummy gauge technique

Figure 3.1: Strain gauge types, classification codes and gauging techniques

attached to the object. The relationship between the strain ϵ ($\epsilon = \Delta L / L_0$) and the relative change of the resistance of a strain gauge is described by [12]

$$\frac{\Delta R}{R_0} = k\epsilon \tag{3.2}$$

The factor k which is known as the gauge factor is a characteristic of the strain gauge. The exact value is specified for each strain gauge by the manufacturer. The gauge factor for gauges used in this experiment is "2". Therefore, by measuring the resistance change of the strain gauge, the strain and consequently the created stress in the object can be determined by stress-strain constitutive equations. The magnitude of change in resistance is quite small when compared to the resistance of the strain gauge. Thus it is important to measure it accurately to determine the strain precisely. Wheatstone Bridge Circuit is a competent method o measure this small changes in resistance.

The wiring method used for connecting the wires of gauges to the amplifier can have different configurations and in this experiment a half-Wheatstone bridge is used. Charles Wheatstone developed this method to measure unknown resistance values and as a means of calibrating measuring instruments, voltmeters, ammeters, etc, by the use of a long resistive slide wire. The Wheatstone Bridge is used to measure very low values of resistances down in the milli-Ohms range.

In the Wheatstone full-bridge shown in Figure 3.2a, two resistors R_1 and R_2 have the same known resistance, R_3 is the variable resistor and R_4 is the unknown resistance [14]. When there is no force applied to the strain gauge, rheostat is varied and finally positioned in such that the voltmeter will indicate zero deflection. This condition is called bridge balancing and it represents that there is no strain on the gauge. On the other hand, If the strain gauge is either tensed or compressed, then the resistance can increase or decrease. Therefore, this causes unbalancing of the bridge. This produces a voltage indication on voltmeter corresponding to the strain change. If the strain applied on a strain gauge is more, then the voltage difference across the meter terminals is more. If the strain is zero, then the bridge reaches to balance and voltmeter shows zero reading. In bridge balancing condition the following relation is valid and by changing the value of variable resistor R_3, the unknown resistance (R_4) could be found

$$\frac{R_1}{R_4} = \frac{R_2}{R_3} \tag{3.3}$$

When two strain gauges are mounted on a measuring object, a half-bridge Wheatstone configuration is achieved as shown in Figure 3.2b. The reason is that now half of the four resistors in the circuit are strain gauges. One of the strain gauges is active and the other one is dummy and this arrangement compensates strain changes due to temperature changes as the two parts experience the same temperature.

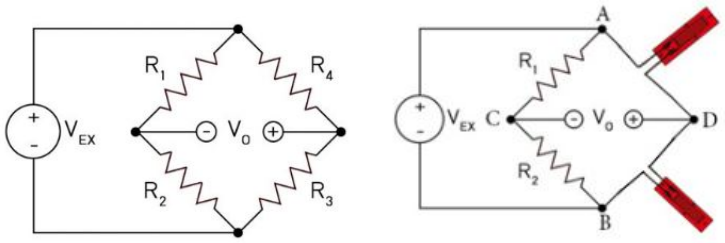

(a) Wheatstone bridge (b) Wheatstone half-bridge

Figure 3.2: Circuit configurations [4]

In the test setup of this study, the half-Wheatstone bridge configuration have been applied to 3 pairs of active-dummy gauges and all of them were plugged in to the HBM's amplifier QuantumX and then Catman 4.5 software was used for measuring of strains throughout the tests. Based on half-Wheatstone bridge configuration, the corresponding bridge factor was selected and assigned to each gauge via Catman 4.5 software.

3.1. Test Procedure

In order to investigate the stress state of Bondura EPS, three different test layouts have been performed, namely 1) non-lubricated sleeve, 2) lubricated sleeve (on both inner and outer surfaces of the sleeve) and 3) cut-lubricated sleeve. The purpose of doing a test with lubricated sleeve is to evaluate the effect of friction and to analyse how much of applied torque would be dissipated by friction. In addition, the point of interest for performing tests on cut-lubricated sleeve is to analyse how much of the applied torque to the joint system is merely used to expand the sleeve elastically.

A test jig was used in order to resemble the equipment supports and the assembly of the pin system has been done on this test jig. The test boss was used as one of the supports and the strain measurements were carried out on the outer surface of it. A schematic of test assembly is shown in Appendix A.2. In Bondura pin assembly, normally the ends of the pin should be in line with the outer edges of the supports. Thus, a longer pin was used throughout this experiment to provide this condition for the test boss. The test boss was restricted to move axially which simulates the real situation in practice and this was one of the main purposes of conducting this experimentation. The material of the pin is steel with yield stress of 962 MPa and ultimate tensile strength of 1074 MPa. The material of the sleeve is S355J2+N steel with yield stress of 403 MPa and ultimate tensile strength of 547 MPa. The sleeve has surface treatment with yellow chromatic-zinc passivation coating. The end plate is made of S355 with similar mechanical characteristics as sleeve, but without any coating. The test boss is S355J2 steel with yield strength of 420 MPa and tensile strength of 583 MPa. The list of alloying elements of the different materials of the EPS are available in Table 3.1. An illustration of these components are provided in Appendices A.3, A.4 and A.5.

Table 3.1: Alloying elements of EPS material

Element	C %	Si %	Mn %	P %	S %	Cr %	Ni %	Mo %	Al %	V %	CU %	CA %	CEV
Pin	0.39	0.40	0.80	0.035	0.035	1.7	1.7	0.30	0.012				
Sleeve	0.14	0.39	1.23	0.010	0.032	0.21	0.13	0.03		0.05	0.24	0.0049	0.43
Boss	0.13	0.33	1.26	0.008	0.031	0.22	0.18	0.04		0.06	0.2		0.43

Bondura 6.6 Ø88.9 pin system has three M16 screws and by tightening them, the locking mechanism of the system is triggered. The recommended torque for this pin system is 160 Nm. In order

to provide a wider view of the joint performance, a torque range between 40 Nm up to 200 Nm was applied to the system considering the fact that the screws do not experience plastic deformation for the highest applied torque. In order to reduce the effect of friction force of screws, installation manual recommends to lubricate the screws while installing them. The reason for lubrication is that in many threaded fastener applications, around 90% of the torque is consumed to overcome the underhead and the thread friction and only 10% of the actual work is usefully translated into screw tightness [15]. The lubrication was performed using Bondura lubrication paste with the trade name of MOLYKOTE(R) P-74 PASTE.

As mentioned before, the torque was applied step-wise, beginning from 40 Nm with adding 20 Nm at each step until it reached to 200 Nm. During each test, the screws were hand-tightened at first. In order to do torquing operation precisely, a torque wrench was used which is shown in Figure 3.3a. The torque increase was applied to each screw at each step and a time interval was dedicated after for settlement of strains and stresses, because when the torque is applied to the system, the friction would be in dynamic state and it will take a while to change to static state. After domination of static state of friction in the system, there was no strain change visible on the strain monitoring screen.

For each test after reaching to 200 Nm torque and recording the strains, it was necessary to dismantle the EPS completely and start the next test. This dismantling was required to start each test from zero strain state in test boss. For removing the conical sleeve gently, Bondura Multi-Tool was used. This instrument is shown in Figure 3.3b and by clamping it to sleeve and applying torque to its central screw, it removes the sleeve from the pin.

(a) Torque Wrench (b) Bondura Multi-Tool

Figure 3.3: Test equipment

3.2. Test Results

In this section, the test results for the three different test layouts are provided separately.

3.2.1. Non-lubricated Sleeve

The first test layout which has been studied experimentally is non-lubricated sleeve which resembles the real case application of Bondura EPS. The cleanliness of the contact surfaces of all joint components is very important on locking mechanism of the assembly, because the existence of oil, grease or any other substance can affect the functioning of the mechanism in practice and in this study can lead to fault data acquisition.

Three strain gauges were installed on the outer surface of the test boss with an angular distance of 90 ° between them. In order to obtain a more general recording of strains, the test boss was rotated and placed in different positions around the pin. The strain measurements are shown in Figures 3.4- 3.6. In the presented graphs, the vertical axis shows the measured strains and the horizontal axis is time. Eqs. (2.67) and (2.68) are used to calculate the external hoop stress and consequently the internal pressure of the test boss. Afterwards, the value of internal pressure is substituted in the first two equations of Eq. (2.69) to find the values of internal radial and hoop stresses, respectively. To provide a better presentation of test results, a simple visualization of the magnitude of radial and hoop stresses at each measured point is provided beside the strain graphs. All visualizations are related to torque amount of 200 Nm which leads to the highest value of the measured strains.

In the assembly manual of the Bondura EPS, it is recommended to use a rubber or plastic hammer and tap all around the end plate after applying a definite amount of torque to the screws and then resume the tightening them operation. The purpose of this task is to release uneven accumulated stresses due to existence of the static friction and provide the opportunity for a better stress distribution. This step had to be skipped while tightening the screws in this test layout, because this could affect the connectivity and accuracy of the strain gauges and lead to damage to the them. But this step was followed and applied while doing the tests for lubricated condition of sleeve (both perfect and cut sleeves). The reason is that lubrication provides a slipping condition that even a weak tapping can have effect on displacements of sleeve and so that it can create a better stress distribution state by releasing the accumulated stresses. This matter will be discussed in the next two sections.

As mentioned before, the conical sleeve of the Bondura EPS has four slits. One of the slits is a complete cut or cut-through which gives the sleeve possibility to expand more and easily. In this test layout, this cut-through is placed at position of 90° (by taking into account the standard polar coordinate with zero coordinate at position of 3 O'clock). From the radial and hoop stresses shown in Figures 3.4- 3.6, it is obvious that the stress distribution inside the test boss is not uniform. These stresses are considered as residual contact pressure [16] and since the test boss does not have end caps, the longitudinal stress is smaller than hoop and radial stresses. Hence, it is not shown in the visualizations. One of the main reasons for this uneven stress distribution is friction. The compressive force between the contact surface of the conical sleeve and pin creates friction which prevents the relative slippage. In addition, the region of the test boss around the cut-through experiences more stresses. So other reason for nonuniform stress distribution is due to the cut-through where the sleeve expands more in this region and as a result more stress is induced into the test boss.

Another region where the amounts of radial and hoop stresses are high is the region in opposite side of the cut-through which is located at 270°. This matter could be related to this fact that a point at this region acts like a hinge point and provides the possibility of two (right and left) sections of the sleeve to expand or in other words rotate around this point. This matter could be used as a guide for assembly of the sleeve in different equipment regarding the dominant loads affecting on the joint.

In order to better evaluate the effect of positioning the sleeve opening, a series of tests have been carried out by placing it at different locations. The respected strain graphs and stress visualizations are available in Appendix A.6. The same principle about the location of the opening has been observed when the sleeve was rotated to 45°, 315° and 225° positions. By comparing the resulted stresses based on position of the cut-through, it can be concluded that when the cut-through is placed at top position (90°), a lower level of stress is produced in the test boss.

It is worth noting that by applying an optimum torque on the joint, the bore of the equipment will find wider distribution of the load over its perimeter and the effect of the concentration of the stress will decrease to some extent. This can improve the fatigue life because it is attributed to the residual compressive stress surrounding the equipment bore. Nevertheless, the tightening torque should be strong enough to prevent slipping [17] between sleeve and equipment support.

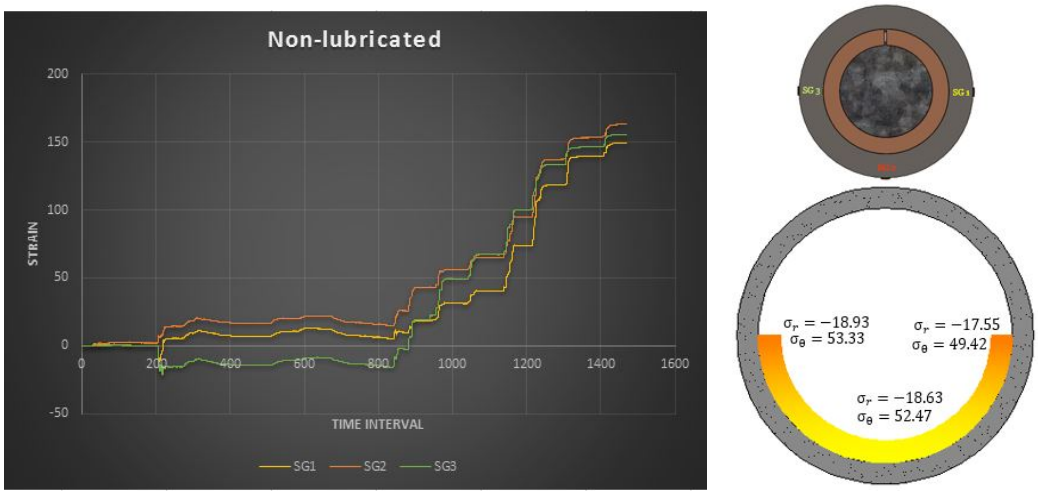

Figure 3.4: Non-lubricated sleeve with sleeve cut-through at top and SGs at 0°, 270° and 180°

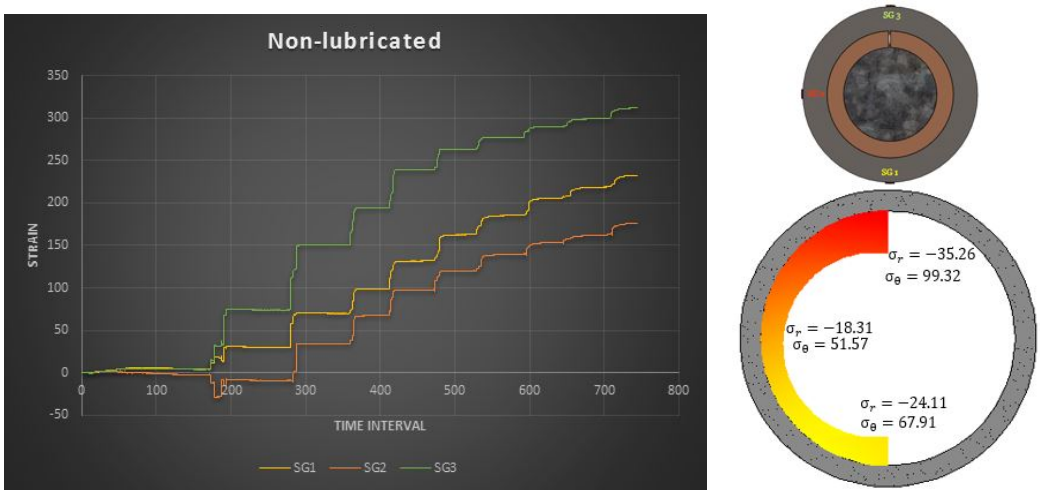

Figure 3.5: Non-lubricated sleeve with sleeve cut-through at top and SGs at 270°, 180° and 90°

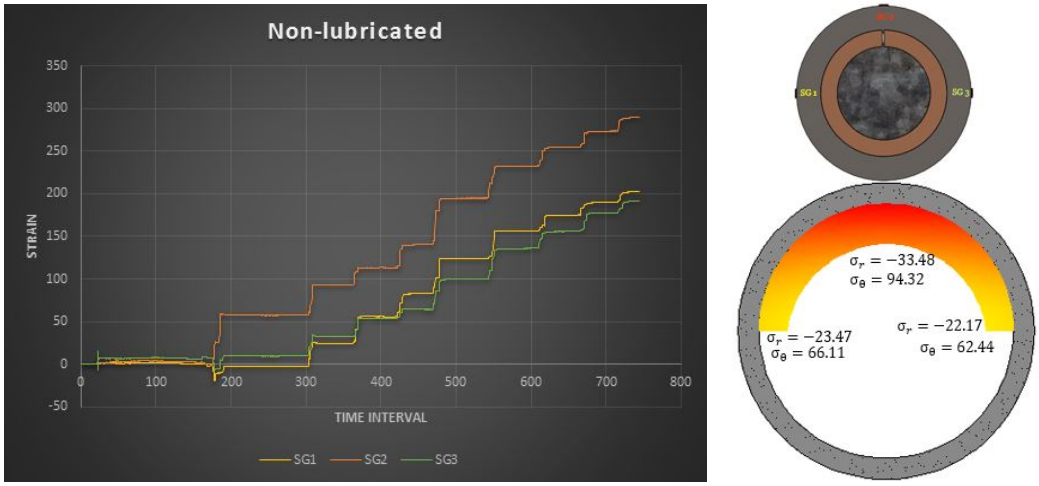

Figure 3.6: Non-lubricated sleeve with sleeve cut-through at top and SGs at 180°, 90° and 0°

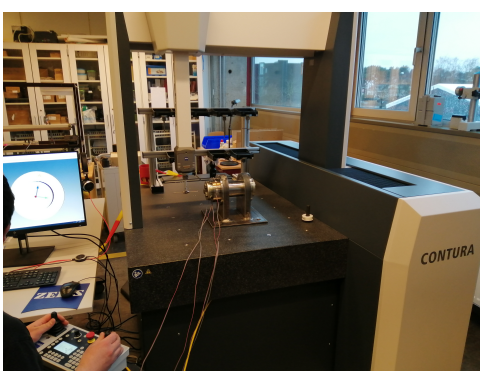

(a) ZEISS coordinate measuring machine

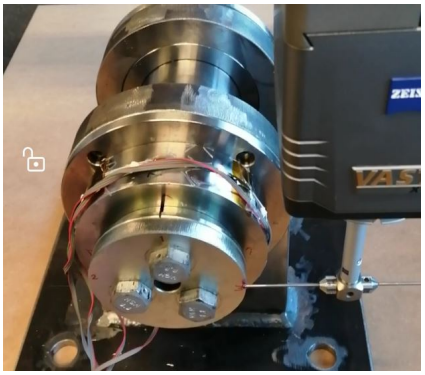

(b) Measuring operation of the machine

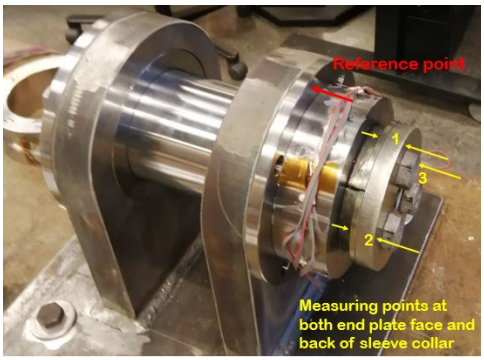

(c) Locations of the reference and measuring points

Figure 3.7: Measurement of conical sleeve axial movement

The tightening of screws squeezes the sleeve axially and due to wedge effect of the tapered end of the pin, the sleeve expands. To evaluate the relationship between axial movement and resulted stresses in the test boss, a series of measurements were implemented by a high precision Coordinate Measuring Machine (CMM). The related arrangements are shown in Figures 3.7. The reference point was set at top face of the flange and 6 measuring points at 90°, 180° and 0° including points on face of the end plate and on the backside of the sleeve collar were considered for determination of sleeve axial movement.

In Table 3.2, distances between the front face of the end plate and the reference point are listed which are accurately measured by CMM for each step of torquing. By looking at this table and evaluating the measured distances, it is clear that by increasing the torque which means higher axial load, the distance between the two mentioned components decreases up to torque value of 80 Nm. This is in fact something obvious that by increasing the compression force, the contraction will happen. But after this value of torque, the distance between the end plate and the reference point on top of the flange has increased. This was an unexpected issue during the tests. The reason for this matter can be justified by considering the elongation of the pin. It means that by increasing the applied torque, the sleeve starts to slip and advance along the tapered end of the pin. But up to a level, the friction force opposes the advancement of the sleeve and since the magnitude of the force is significant, the axial force resulted from screws pulls the pin and enforces it to elongate.

In order to evaluate this matter in more detail, a comparison between theoretical formulas of Sections 2.1 and 2.2 and the experimental results is performed.

From measurement results of the Table 3.2, it could be calculated that, first the sleeve moves approximately 0.009 mm towards the flange and then it moves about 0.031 mm away from it. Thus, it is concluded that practically, the sleeve is totally 0.040 mm displaced.

By considering the final applied torque of 160 Nm and using Eq. (2.15), the amount of preload

Table 3.2: Distance between face of the end plate and reference point

Torque	**(Nm)**	**40**	**60**	**80**	**100**	**120**	**140**	**160**
Distance	point 1	63.958	63.948	63.947	63.954	63.960	63.964	63.977
(mm)	point 2	63.955	63.944	63.947	63.957	63.962	63.965	63.976
	point 3	63.954	63.945	63.947	63.958	63.964	63.969	63.982

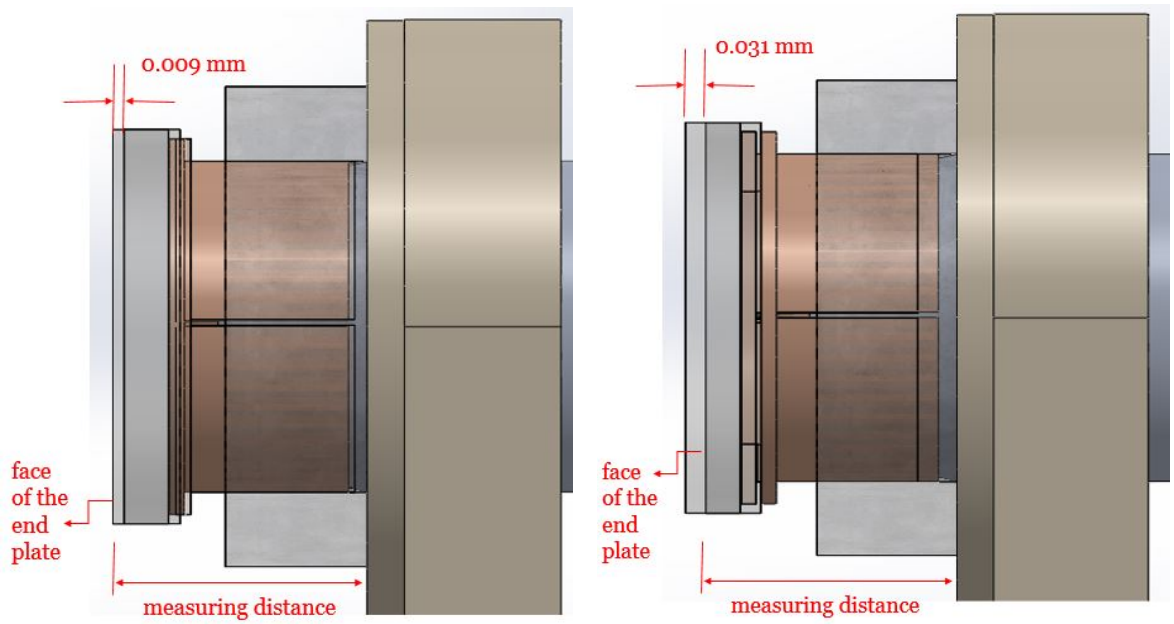

(a) Sleeve approaching the test boss (b) Sleeve moving away from the test boss due to pin elongation

Figure 3.8: Sleeve movements while torquing the fastening screws

created by fastening the screws could be calculated. As it is mentioned before, K can be considered equal to 0.2. Then, the preload for M16 screw which has the nominal diameter of 16 mm would be 50 kN. Since the joint system has three screws, the amount of total preload or i.e. axial load is 150 kN. Afterwards, by considering the material and geometrical characteristics of the sleeve and the pin and also by using Eq. (2.52), the theoretical amount of sleeve axial displacement is calculated equal to 0.040 mm. This theoretical value is for a sleeve without slits. The theoretical value is in a good agreement with the experimental value. But it is necessary to consider that the amount of sleeve advancement in experimental measurements from hand tightened state until applied torque of 40 Nm is not taken into account. So it means, the sleeve advancement in reality is more that 0.040 mm which is acceptable due to existence of the four slits on the sleeve.

This matter can be investigated further. Eq. (2.49) gives the longitudinal stress distribution along the pin axis. For applied torque equal to 160 Nm, the corresponding stress distribution is illustrated in Figure 3.9. The contact length of sleeve-pin is around 35 mm. The figure shows that at the end of the taper of the pin, the amount of longitudinal stress is σ_{1x}= 37.11 MPa. Dividing this stress by Young's modulus of elasticity of the pin (E = 210 GPa) yields the strain created inside the pin which is ϵ_x= 177 $\mu m/m$. The length of the pin is 210 mm, but the end of the pin which has a length of 30 mm is clamped in order to hold the pin in a fixed constraint. So by considering the effective length equal to 180 mm, the elongation of the pin is obtained as follows

$$\Delta L = \epsilon_x * L = 177 \mu m/m * 0.18 m = 31.79 \mu m \tag{3.4}$$

The calculated value for pin elongation is in good agreement with the measured value of 0.031

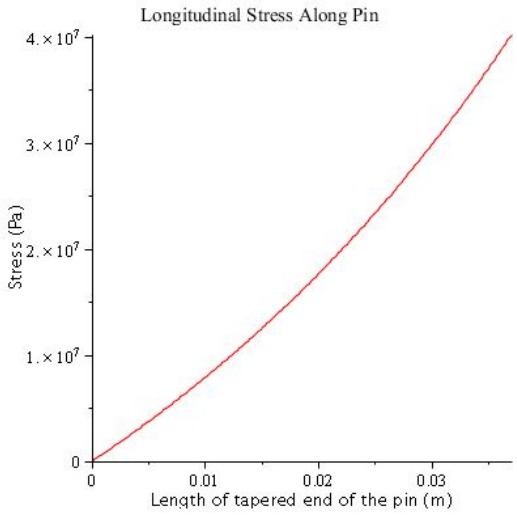

Figure 3.9: Longitudinal stress along tapered section of the pin according to Eq. (2.49)

mm (or 31 μm) by CMM shown in Figure 3.8b.

Another matter that can be mentioned here and has effect on the lifetime of the EPS joint is $frettingwear$. Fretting is defined as contact between surfaces subjected to reciprocating motion of low amplitude and it is quite different with reciprocating wear which occurs at much higher amplitudes. Fretting wear leads to surface degradation when the amplitude of the displacement is within the range from 1 to 100 μm [18].

Fretting wear involves various wear mechanisms such as adhesion, abrasion, oxidation and fatigue and at least two of these mechanisms should occur simultaneously to trigger this type of wear [18]. For EPS, abrasion and fatigue are two probable mechanisms which can occur due to movements of the equipment. Fretting wear produces oxidized wear debris and this can influence the rigidity of a joint. As mentioned in the section of test procedure, the conical sleeve of Bondura EPS is covered with yellow chromatic-zinc passivation coating. This can effectively hinder production of oxidation in the contact surface of the sleeve-support bore.

3.2.2. Lubricated Sleeve

Lubrication is a useful method mostly employed in fretting contacts to reduce wear associated with high friction. There are many factors affecting the fretting damage, including contact pressure, tangential force, sliding amplitude, vibration frequency, surface roughness, temperature,surface hardness and so on [19] which by selecting an appropriate lubricating agent, this type of failure could be significantly decreased.

In EPS, it is necessary to have entirely clean surface for each joint component to achieve the best locking force, otherwise it can result in slack joint due to slippage of joint components. Hence, for evaluation of the effect of friction between contact surfaces of sleeve-pin-test boss, lubrication was applied to the sleeve. In this test layout, both the inner and the outer surfaces of the conical sleeve was lubricated with Bondura lubrication paste with the trade name of MOLYKOTE(R) P-74 PASTE. The purpose of these tests are to investigate how much of the applied torque dissipates in the form of hysteresis deformation along contact surfaces of the sleeve. Figures 3.10-3.12 show the strains created in the hoop direction of the outer surface of the test boss and visualization of radial and hoop stresses inside it.

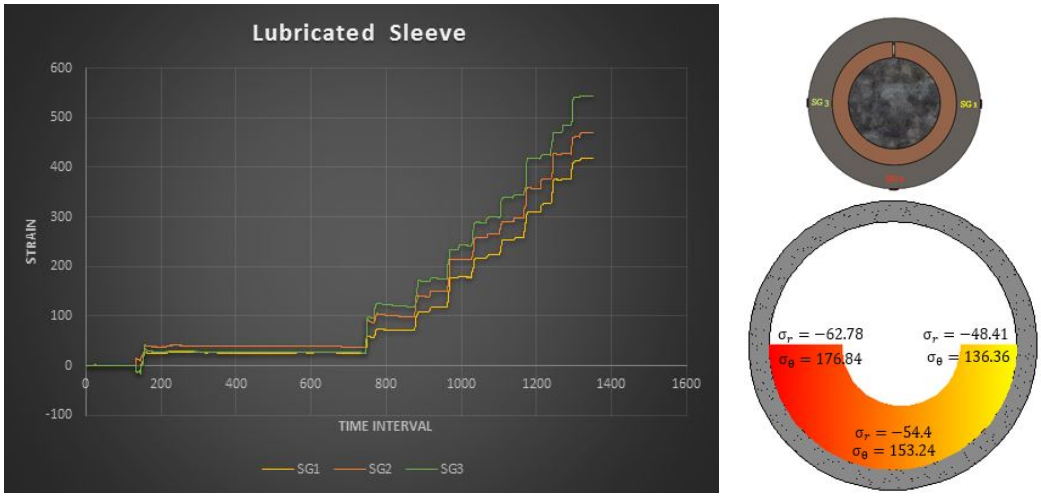

Figure 3.10: Lubricated sleeve with sleeve cut-through at top and SGs at 0°, 270° and 180°

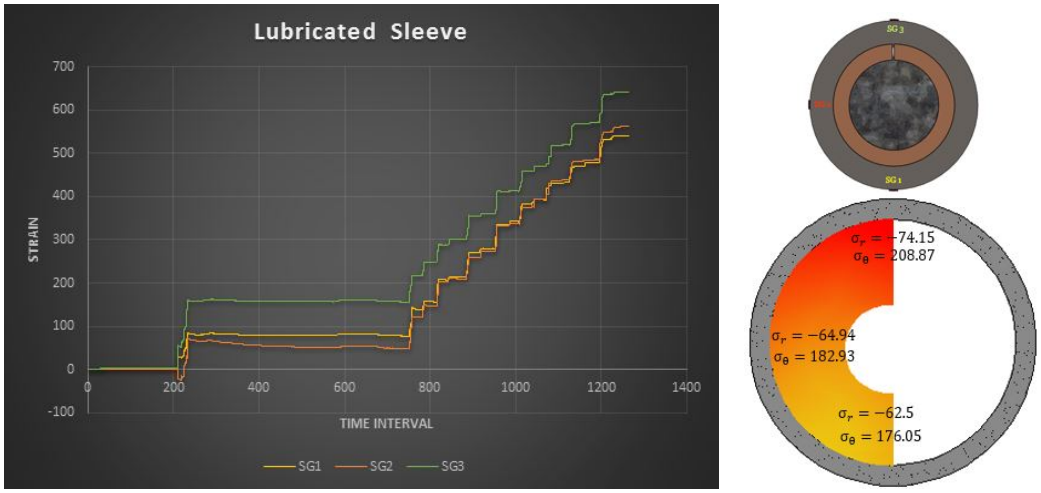

Figure 3.11: Lubricated sleeve with sleeve cut-through at top and SGs at 270°, 180°and 90°

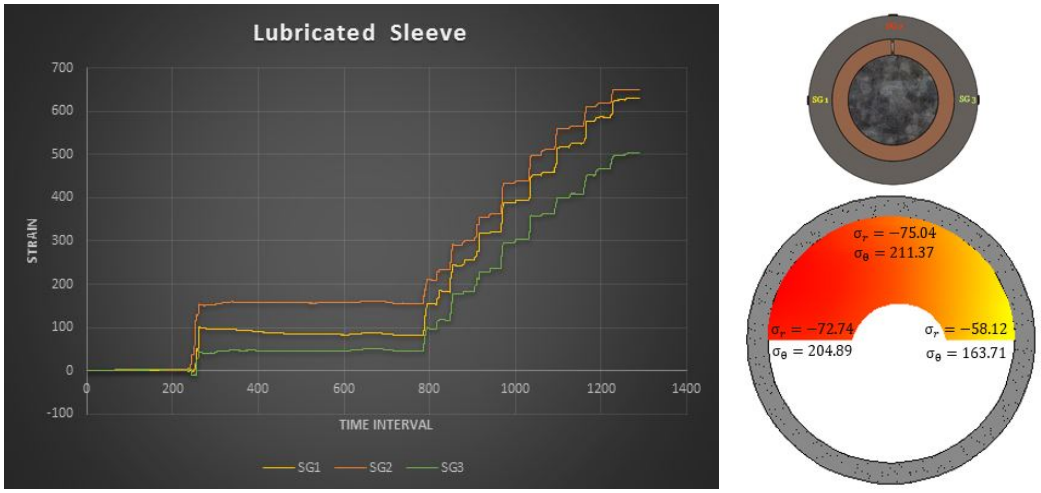

Figure 3.12: Lubricated sleeve with sleeve cut-through at top and SGs at 180°, 90° and 0°

The strain graphs show that the amount of stress inside the test boss has increased significantly. The stress distribution in lubricated condition is not uniform and it is to some extent similar to non-lubricated condition with this difference that the magnitude of increase in stresses in the region between 90° and 180° has been higher than other regions. This could be related to this fact that since the friction has decreased, the joint system tries to find a location where it can release stresses and this may happen locally in a location where the friction is lower, i.e. more slippage can occur there. This leads to accumulation of the stresses in a particular region. By comparing the change of stresses with non-lubricated condition, it is concluded that generally the stresses are distributed more uniformly as friction decreased. This fact is observed in other researches related to loading of a cylinder like [20]

In this test layout, the regions around the placement of the sleeve cut-through experience higher stresses than other regions which is similar to non-lubricated condition. A series of tests were performed for investigation the effect of position of sleeve cut-through. The results of these tests are available in Appendix A.7.

Among conducted tests, the case related to the sleeve complete notch at angular position of 315° results in lower stresses in the test boss. Moreover, in these series of tests it is observed that changing the location of the sleeve cut-through can lead to a more uniform stress distribution.

By comparing the strains and stresses of the lubricated condition with the non-lubricated, it is found out that both radial and hoop stresses at positions of 0°, 90°, 180° and 270° are increased with ratios of 2.68, 2.17, 3.3 and 2.74 times, respectively. It is possible to indicate that the average increase is equal to 2.72 times compared with non-lubricated condition. This means that in non-lubricated condition which is the form of application of the EPS in practice, around 63.24% of the applied torque is dissipated. This dissipation of energy is used to overcome the *friction force* and *deforming the sleeve elastically*. The dissipated energy due to friction is wasted in the form of elastic hysteresis deformations of sleeve, pin and bore of the test boss. The rest of the torque which is about 36.76% is used to expand the test boss and it will remain in the form of residual contact stress.

Elastic Hysteresis is defined as the difference between the strain energy required to generate a given stress in a material, and the material's elastic energy at that stress [21]. This energy is actually dissipated through internal friction or heat in a material during loading and unloading.

Basically, hard metals don't show elastic hysteresis under a moderate loading [22], but as it is observable in Figures 3.10-3.12, the magnitude of stresses inside the test boss is noticeable and makes this phenomenon to happen.

As it was mentioned in the previous section, a plastic hammer was used to tap the end plate of the joint assembly in order to release static frictions and provide a uniform fastening with lower stress accumulation in a specific region. After applying a definite torque to all the three screws, tapping was implemented gently around the front face of the end-plate and the the tightening with the same amount of torque was applied again. By looking at Figures 3.10-3.12, it is clear that the small jumps between each step of torquing is related to this matter.

Another interesting finding of this test layout is in association with small drop of strains that occurred between steps of the torquing. The reason of this happening is due to freedom of the slippage which is created by the lubrication. This drop of strains is more considerable for lower magnitudes of torque than the higher torques. It means at lower torques, the expanded lubricated sleeve finds the opportunity to find a stable situation by taking benefit from slippage.

3.2.3. Lubricated Cut Sleeve

Another test layout which was investigated in this experiment was using a cut sleeve. In clamping mechanism of the EPS, a part of the applied torque is used to deform the sleeve in an elastic range. In Bondura EPS, the sleeve slits make the expansion of it easier, but still a part of the applied torque is used to deform the sleeve. Thus, by cutting the sleeve to several parts, the need for elastic deforming

of sleeve would be omitted. The aim of these tests is to evaluate how much of torque is spent for this action. The sleeve is cut in four identical parts.

The results of these series of tests are exhibited through Figures 3.13-3.15. The strains and stresses are increased significantly in comparison with previous non-lubricated and lubricated sleeve test layouts and it is obvious that the stress state is to a great extent uniform along the whole inner surface of the test boss.

By evaluating the amount of growth in stresses, it is deduced that radial and hoop stresses at positions of 0°, 90°, 180° and 270° are increased with ratios of 4.62, 2.70, 4.68 and 4.36 times, respectively. The average ratio for increase in stresses is 4.09 times compared with the non-lubricated condition.

As it was stated in previous section for lubricated sleeve condition, 36.76 % of the fastening torque was experienced by the test boss which basically will remain in the form of residual contact stresses. The rest of the torque or applied energy is spent to overcome friction and deform the sleeve elastically. By making a comparison between lubricated sleeve and lubricated cut sleeve test results, it is concluded that 33.5 % of the applied torque is used to deform the sleeve in elastic region of material and 29.74 % is spent in the form of friction i.e. elastic hysteresis.

In these series of tests, again reduction of strains happened after fastening the screws with the predetermined amount of torque. These strain reductions basically originate from the possibility of slippage in lubricated state and are more significant at lower stress levels. A closer look at Figures 3.13-3.15 reveals three small strain jumps between torquing intervals. These small steps are created while the torque is applied and are related to fastening of the three screws of the joint indicating that torque is applied in a step-wise manner.

As it is clear in stress visualization demonstrations, absence of friction yields in high stress values inside the test boss. Despite the existence of large stresses, disassembly of lubricated sleeve was performed much easier than non-lubricated state. This issue highlights the importance of friction. Large errors in determining friction coefficients can result in applying excessive stress to joint components and it can accelerate their wear and tear. Thus, surface roughness of the joint components is an important parameter in producing friction and it must receive greater attention. The conical sleeve, pin and test boss used in this experiment have similar surface roughness of 3.2 μmRa according to ISO 2768 standard. Ra is the arithmetic average of the absolute values of the profile height deviations from the mean line [23].

Figure 3.13: Lubricated cut sleeve with SGs at 270°, 180° and 90°

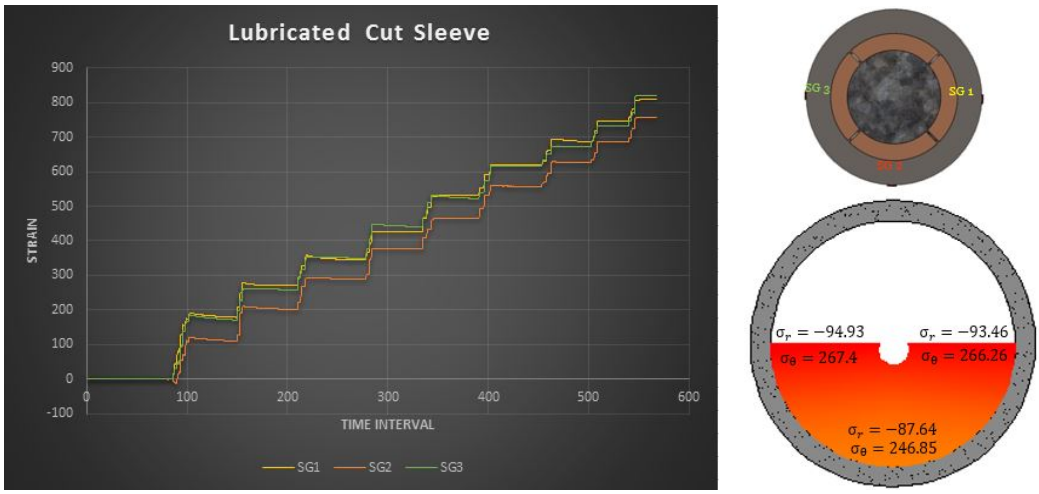

Figure 3.14: Lubricated cut sleeve with SGs at 0°, 270° and 180°

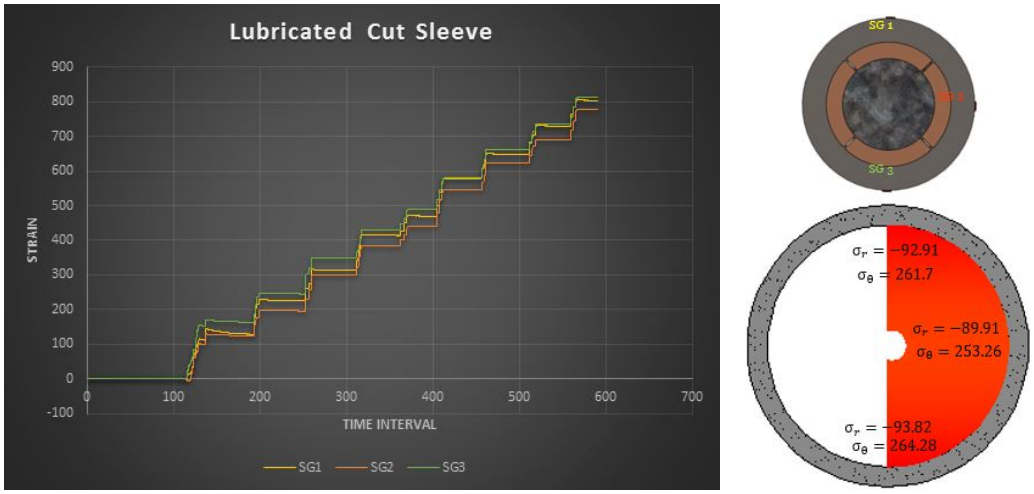

Figure 3.15: Lubricated cut sleeve with SGs at 90°, 0° and 270°

3.2.4. Comparing the Results from Different Tests

In order to make the results of the three test layouts more comparable and provide a better view about the stress distribution and residual contact stresses along the inner surface of the test boss, the average value of radial and hoop stresses have been calculated based on measurements of the conducted tests and they are shown in Figure 3.16. The graphs emphasize this fact that as friction decreases and also by cutting the sleeve, the amount of wasted torque or dissipated energy will decrease and actually this energy is consumed to expand the sleeve more and this induces more internal pressure in the intervention of sleeve/pin/test boss bore.

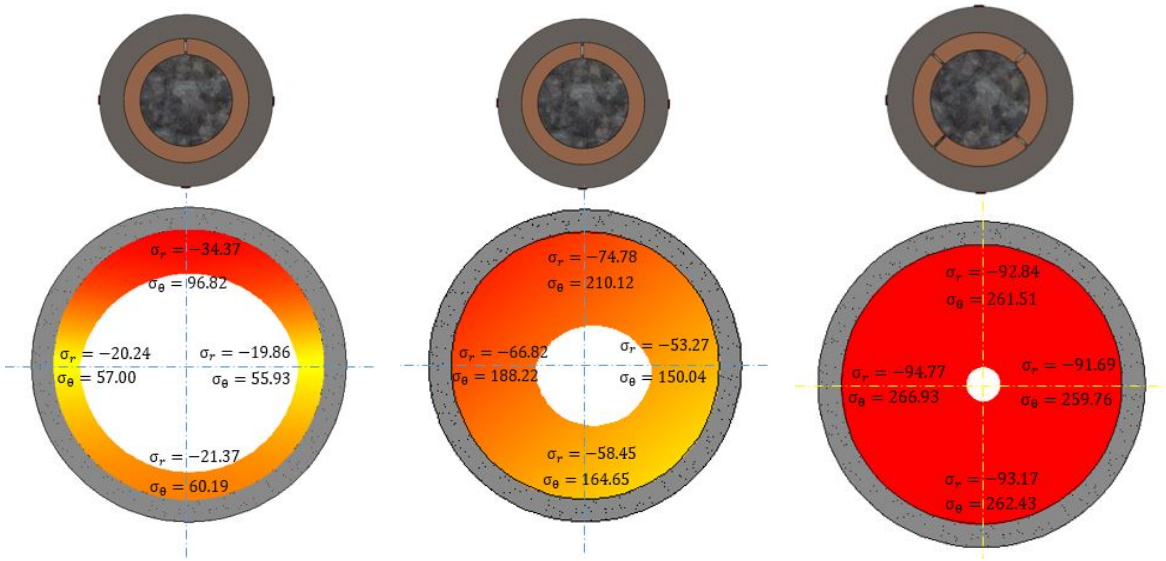

(a) Non-lubricated sleeve with sleeve opening at top

(b) Lubricated sleeve with sleeve opening at top

(c) Lubricated cut sleeve

Figure 3.16: Comparing stress distribution for the three test layouts

The characteristic of hoop stress inside the test boss is tensile while radial and axial stresses are compressive. For further analysis of the test boss stress level through different test layouts and to find out whether it has experienced yielding or not, MSS and DE theories are evaluated. The respective $Tresca$ and $vonMises$ stresses are calculated for each condition based on the highest values of stresses registered during measurements. The values are listed in Table 3.3. According to the calculated values for non-lubricated sleeve which resembles the real case application of EPS, both Tresca and von Mises stresses are much lower than the failure limits, but for lubricated cut sleeve, $vonMises$ and $Tresca$ stresses reach to 79 % and 86 % of material yield strength. MSS is a more conservative criteria than DE. Calculation of $Tresca$ and $vonMises$ stresses are provided below according to Eqs. (2.73) and (2.75), respectively. It is worth mentioning that σ_z which is given in Eq. (2.71) can be calculated based on the geometry of the test boss and also assuming a frction coefficient $\mu = 0.2$ as follows

$$\sigma_{z(int)} = \frac{2\mu aL}{b^2 - a^2}\sigma_{r(int)} = \frac{2 * 0.2 * 44.5 * 38}{64.5^2 - 44.5^2}\sigma_{r(int)} = 0.31\sigma_{r(int)} \tag{3.5}$$

For non-lubricated sleeve the calculations are;

$$\tau_{max} = \frac{\sigma_{\theta(int)} - \sigma_{r(int)}}{2} = \frac{96.82 - (-34.37)}{2} = 65.60MPa \longrightarrow \sigma_{Tresca} = 131.2MPa \tag{3.6}$$

$Tresca$ stress is two times of the value of τ_{max}.

$$\begin{aligned}\sigma' &= [\frac{(\sigma_{\theta(int)}-\sigma_{z(int)})^2+(\sigma_{z(int)}-\sigma_{r(int)})^2+(\sigma_{r(int)}-\sigma_{\theta(int)})^2}{2}]^{1/2}\\ &= [\frac{(\sigma_{\theta(int)}-0.31\sigma_{r(int)})^2+(0.31\sigma_{r(int)}-\sigma_{r(int)})^2+(\sigma_{r(int)}-\sigma_{\theta(int)})^2}{2}]^{1/2}\\ &= [\frac{(96.82-0.31*(-34.37))^2+(0.31*(-34.37)-(-34.37))^2+(-34.37-96.82)^2}{2}]^{1/2}\\ &= 124.07MPa\end{aligned} \tag{3.7}$$

Table 3.3: Evaluation of failure (yield criteria)

Test Layout	Tresca Stress	von Mises Stress	Yield Strength
Non-lubricated Sleeve	131.2	124.07	420
Lubricated Sleeve	284.9	262.93	420
Lubricated Cut Sleeve	361.7	333.84	420

As mentioned in section 3.1, the recommended torque for Bondura EPS Φ 88.9 mm is 160 Nm. The residual contact stresses resulted from tightening the screws of this system with the recommended torque is shown in Figure 3.17. The maximum residual hoop and radial stresses are located in position of 90° where the opening of the sleeve was placed. $Tresca$ and $vonMises$ stresses are calculated for this case base on maximum occured stresses and are presented in Table 3.4

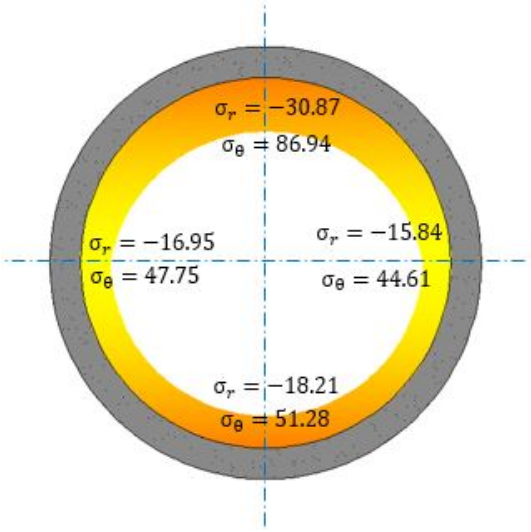

Figure 3.17: Stress distribution for recommended torque- non-lubricated sleeve

Table 3.4: Stress state for recommended torque

Test Layout	Tresca Stress	von Mises Stress	Yield Strength
Non-lubricated Sleeve	117.81	108.74	420

The interaction of hoop, radial and axial stresses creates the clamping force for EPS joint. In some other fields like clamping a work-piece, there are recommendations based on deformation of the work-piece due to clamping and cutting forces and it is intended to make these forces minimized and uniformed while preventing the movement of the work-piece during cutting or machining operations. There are a lot of researches that have studied this subject like [24], [25] and etc.

For EPS, there is no simple rule-of-thumb procedure for determining the clamping force and the magnitude of clamping force should be enough to hold the pin fixed during the operation of the equipment. The most important matter is to have a uniform clamping force whole along the bore circumference. Moreover, it is important to optimize this force to decrease the effect of wear and tear. On the other hand, since this clamping force is created by end-plate fastening screws, it is very important to maintain the initial clamping force, because this force gradually relaxes during prolonged exposure to the alternating external load [26]. This subject will be studied in more detail in Chapter 6, "$Optimization$".

3.3. Summary

In this chapter, the results of experimental study for investigation and analysis of stresses between conical sleeve-pin-equipment bore have been presented. The experimentation included three different test layouts including non-lubricated sleeve, lubricated sleeve and lubricated cut sleeve. According to obtained experimental results for Bondura Φ 88.9mm joint system, the following conclusions can be drawn:

- In non-lubricated condition, the stress distribution is not uniform.

- Stress concentrations happen in a region near sleeve cut-through and in region next to it (with 180° angular distance from sleeve cut-through).

- At the beginning of screw tightening, conical sleeve moves forward along the pin, but after reaching to a level of torque, pin undergoes tension and it elongates.

- Around 63% of the applied torque dissipates in the form of elastic hysteresis and expanding the sleeve and only 37% of it is effectively used to expand the test boss (result from lubricated sleeve tests).

- A part of dissipated torque which is around 33% is used to deform the sleeve elastically and about 30% of it is wasted in the form of elastic hysteresis deformation in different joint components to overcome friction (result from lubricated cut sleeve tests).

- Lubrication of the sleeve and also cutting the sleeve resulted in more uniform distribution of stresses along the bore of the test boss.

Further investigation about interaction between conical sleeve - pin and stresses which they experience will be provided in Chapter 5.

4

Finite Element Analysis

In this chapter, first a brief description on Abaqus/CAE is presented. Then the methodology adopted to model and analyse the Expanding Pin System (EPS) through FEA is provided. The details about material and geometrical considerations are described and mesh type and selection of suitable solving algorithm is thoroughly stated.

4.1. FE Software, Abaqus/CAE

All FE analyses of this study are performed using Abaqus/CAE 2017 software. This software has proven that it is a reliable software for various engineering problems.

Abaqus/CAE is an interactive environment used to create finite element models, submit Abaqus analyses, monitor and diagnose jobs, and evaluate results [27]. It has different modules like Standard, Explicit and CFD which each one has several add-on options to further extend its capabilities.

Abaqus/Standard and Abaqus/Explicit can be used to solve a large class of stress analysis problems. A fundamental division of such problems is into static or dynamic response where dynamic problems are those in which inertia effects are significant [28].

Stress analysis problems can be divided into two different categories including static and dynamic. A static stress analysis is used when inertia effects can be neglected. This type of analysis can be conducted in Abaqus/Standard either in a linear or non-linear way and in fact this method ignores time-dependent material effects (like creep, swelling, viscoelasticity), but it takes rate-dependent plasticity and hysteretic behavior for hyperelastic materials into account [28]. While linear static analysis involves the specification of load cases and appropriate boundary conditions, non-linearities can arise from material non-linearity, boundary conditions and large-displacement effects. Material non-linearity can be described in reference to the stress-strain diagram of metals shown in Figure 4.1.

In the first region before *yield point*, the stress-strain curve is linear and the behavior of material is elastic. Afterwards, the non-linear behavior of material starts and the material undergoes plastic deformations. It is worth mentioning that after *ultimate strength* damage to material is something unavoidable. The structural steel follows closely the presented curve. In the case of other type of materials like hyper-elastic or rubber type materials, the stress-strain curve is nonlinear from the beginning and this should be considered in simulations.

Non-linear boundary condition is a kind of boundary condition that varies with time. An example is contact phenomena where the parts which are not in touch come into contact with each other as the simulation proceeds.

Large displacements and deformation in parts of a simulation can lead to non-linearity of the problem. It is reasonable to always check for non-linear geometry condition. As a rule of thumb,

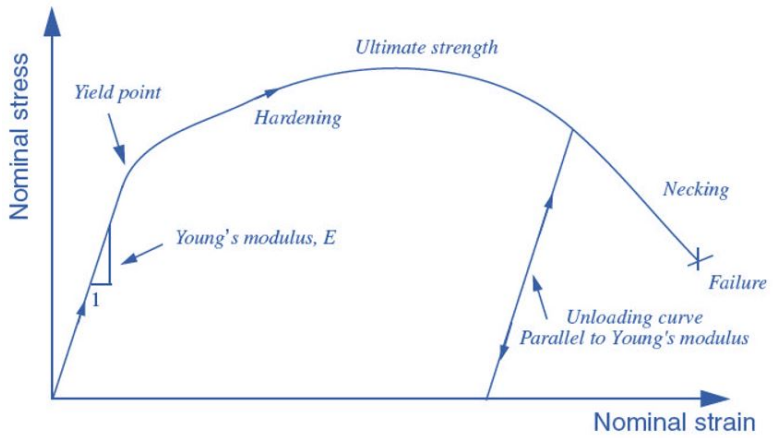

Figure 4.1: Stress-strain diagram for ductile material [5]

this is almost always the case if strains exceed 5 % [29]. An example for this case is a simulation where loads are rotating with the structure i.e. a part or assembly is loaded in bending initially, but the loading turns to tension after deformations start. Further discussion about inclusion of non-linearity in the context of this study will be presented in subsection of selecting the solver.

On the other hand, dynamic stress analysis is related to problems in which inertia effects must be considered. In Abaqus/Standard, implicit operators applies direct-integration of the equations of motion, while Abaqus/Explicit uses the central-difference operator [28]. In an implicit dynamic analysis in each time increment the integration operator matrix must be inverted and this results in a set of nonlinear equilibrium equations, while in an explicit dynamic analysis displacements and velocities are calculated in terms of quantities that are known at the beginning of an increment. Therefore, in explicit analysis the global mass and stiffness matrices need not be formed and inverted which leads to saving time, considerably. In an explicit dynamic analysis the size of time increment is quite important since central-difference operator is only conditionally stable, but in the implicit operator the size of the time increment is not a restriction and it is unconditionally stable.

4.2. Pre-processing

In this section, the procedure for modeling of the joint components in Abaqus is described in detail. This includes defining material characteristics, modeling EPS parts and assembly of them, defining contacts between surfaces of the parts and applying load and Boundary Conditions (BCs).

4.2.1. Material Definition

In order to model material features properly several initial runs in Abaqus/Standard using static solver were carried out and it was observed that due to occurrence of large displacements and strains in some regions of the joint, the runs were aborted. Therefore, material properties were modelled by considering nonlinearity.

Prior to reaching the yield point, the deformation of steel creates only elastic strains and these strains disappear when the applied load is removed. However, once the strains in steel exceed the yield point, permanent (inelastic) deformation begins to occur. These strains which are associated with the permanent deformation are called plastic strains. When steel deforms beyond the yield point both elastic and plastic strains accumulate in it.

Typically, the stiffness of steel decreases dramatically once the material yields. Generally, ductile metals like steel that have yielded will recover their initial elastic stiffness when the applied load is removed (see Figure 4.1). Often the plastic deformation of steel increases its yield stress for subsequent loadings: this behavior is called work hardening [5].

The material properties of the EPS components were provided in Section 3.1. In order to simulate a more realistic behaviour of EPS joint using FEA, it is often recommended to use the true stress and true plastic strain relationships. The true stress (σ_{true}) and the true strain (ϵ_{true}) can be determined based on material test results using the following equations [5]

$$\sigma_{true} = \sigma_{eng}(1+\epsilon_{eng}) \tag{4.1}$$

$$\epsilon_{true} = ln(1+\epsilon_{eng}) \tag{4.2}$$

where (σ_{eng}) and (ϵ_{eng}) are engineering stress and strains measured in tensile tests. True stress is the applied load divided by the actual cross-sectional area of material where the area changes with time while engineering stress is the applied load divided by the original cross-sectional area of material.

According to data from material certificate available for different parts of EPS which include yield strength (S_y), ultimate tensile strength (u_t) and final elongation ($A5$), the material modeling in Abaqus was performed. The data for strain corresponding to ultimate strength was not available, however based on stress-strain diagram available for S355 steel in the literature [30], it was assumed that the respective strain for ultimate strength is equal to one third of the strain value corresponding to the $A5$ where the rapture for test material occurs. $A5$ is permanent elongation for proportional specimens with length L_0 equal to 5 times of diameter [31]. In this way, a linear strain hardening has been introduced for different grades of S355 steel. The stress-strain diagram assumed for sleeve is shown in Figure 4.2 as an example. The elastic modulus and the material density are considered 210000 MPa and 7850 kg/m^3, respectively. Poisson's ratio of steel is set to 0.3.

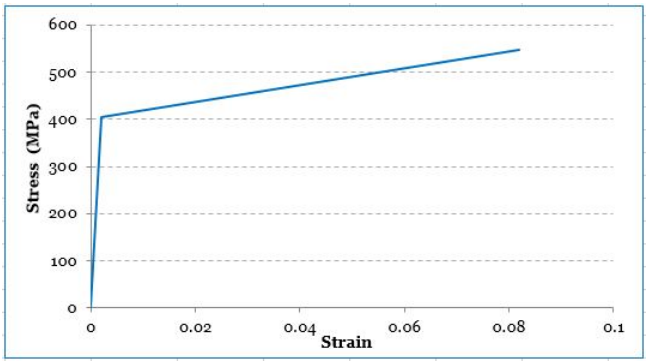

Figure 4.2: Sleeve bi-linear stress-strain diagram

Material characteristics of different parts of EPS are listed in Table 4.1. In Abaqus, post-yielding behaviour of the material can be defined in plasticity section. The plastic data define the true yield stress of the material as a function of the true plastic strain [5]. Table 4.2 shows as an instance the conversion from engineering to true material properties data for sleeve. The plastic strain is obtained by subtracting the elastic strain from the value of the total true strain as it is expressed in the following equation

$$\epsilon_{pl.true} = \epsilon_{true} - \epsilon_{elastic} = \epsilon_{true} - \frac{\sigma}{E} \tag{4.3}$$

At small values of strain, the differences between the engineering and true strains are negligible, but at larger strain values the differences become significant. Thus, providing the proper stress-strain data to Abaqus is extremely important especially when strains in the simulation are large.

4.2.2. Modeling EPS Parts and Assembly

The modeling of the joint system components has been done in Abaqus. The dimensions of the parts are available in Appendix A.3 - A.5. It is not possible to model only part of the system based on symmetric assumptions, because the sleeve is not symmetric. It has four slits and just one of them is a complete cut-through. Moreover, the end plate has three screws which are the locations for applying load. These have resulted in necessity to model the joint system thoroughly and therefore

Table 4.1: Material characteristics of EPS parts

Part	**Yield Strength** S_y (Mpa)	**Ultimate Strength** S_ut (MPa)	**Elongation, A5** %
End plate	404	547	25.6
Pin	962	1074	16.8
Sleeve	404	547	25.6
Test boss	420	583	21.2

Table 4.2: Sleeve stress and strain conversions

Eng Stress	**Eng Strain**	**True Stress**	**True Strain**	**Plastic Strain**
Yield Str. 404	0.0019	404.77	0.0019	0
Ultimate Str. 547	0.0853	593.66	0.0819	0.0800

Note: Stresses are in MPa.

there are increased number of nodal degrees of freedom and subsequently increased computational time in solving process.

The parts are modelled as a 3D homogeneous solid and assembly of the parts implemented according to manner conducted in experimental set-up. The cylindrical parts have been set in place by defining coaxial constraint and a face to face constraint has been defined for positioning the end-plate since it is in touch with face of the sleeve throughout the simulation time.

A simplification has been made to the EPS joint in order to make the model simpler and to decrease the simulation time. This has been done by omitting the fastening screws of the end plate and therefore equivalent axial load is defined instead of screw preload. In this way, the number of contact surfaces have decreased and complexity of the analysis is reduced since the main focus of this FEA is evaluation of stresses in the contact surfaces of pin-sleeve-test boss.

4.2.3. Defining Contact

The parts of the EPS are in contact with each other and two forces act on these parts; one is normal force to the contact surfaces and the other one is shear force which originates from friction between the surfaces and resists the tangential motion (sliding) of the bodies.

The distance separating two surfaces is called the clearance and contact constraint is defined when the clearance between two surfaces becomes zero [5]. Obviously this means as long as there is a clearance between surface, there is no contact pressure.

Surfaces usually transmit shear as well as normal forces across their interface when they are in contact with each other. Thus, it is needed to take into account frictional forces which resist the relative sliding of the surfaces. One of the common frictional model used to describe the interaction of contacting surfaces is *Coulomb friction*. The model characterizes the frictional behavior between the surfaces using a coefficient of friction, μ. In this analysis, friction coefficient is considered 0.2, similar to the value considered in theoretical part for metal-metal contact. As it is illustrated in Figure 4.3, the tangential motion is zero until the surface traction reaches a critical shear stress value, which depends on the normal contact pressure, according to the following equation [5]:

$$\tau_{crit} = \mu p \tag{4.4}$$

where p is the contact pressure between the two surfaces. This equation gives the limiting frictional shear stress for the contacting surfaces. When the shear stress equals or exceeds the limiting frictional shear stress, μp, the contacting surfaces will start to slip (slide relative to each other) across

their interface.

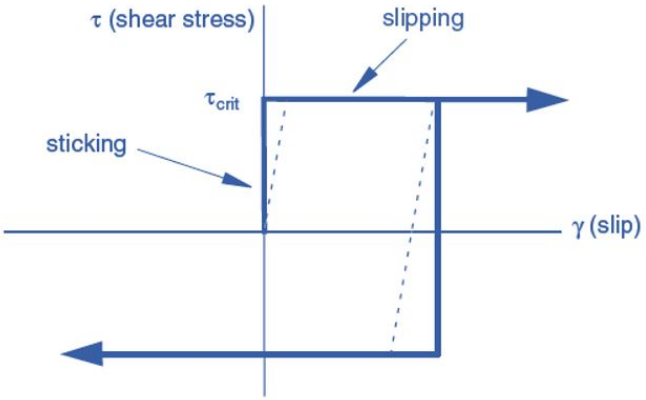

Figure 4.3: Frictional behavior [5]

Another important parameter while modeling a contact is definition of master and slave surfaces. There are two types of contact discritizations in Abacus including node-to-surface and surface-to-surface [32]. In node-to-surface, the nodes on slave surface contact the discretized segments of the master surface. Nodes of the slave cannot penetrate to the discretized segments on the master although the vice versa is possible. For this reason, the selection of master and slave is important. As a rule, the slave should be the more finely meshed surface. If the mesh densities are similar the slave surface should be the one with the softer material. For surface-to-surface, contact condition is formulated based on the shape of both the master and slave surfaces. The region of contact is distributed in an average sense over regions near the slave nodes rather than on individual slave nodes and therefore large penetrations of master nodes into the slave surface do not occur [33] which prevents stress or pressure spike in some nodes and provides a more realistic stress distribution.

In this FEA, surface-to-surface discretization has been used and the pairs of master-slave include; pin-test boss, pin-sleeve, test boss-sleeve and sleeve-end plate.

4.2.4. Loading and Boundary Conditions

The boundary conditions (BCs) of the EPS are modeled according to the test setup implemented during experimentation. In the conducted tests, one of the ends of the pin was constrained inside the support of the test jig which resembles a clamped BC. The modeling of this constraint is defined by an encastre BC in Abaqus with all translational and rotational degrees of freedom restricted. The other end of the pin is exposed to an axial load calculated according to Eq. (2.15) based on the applied torque to the joint system. The FEA is carried out for applied torque of 200 Nm which is the largest torque applied to EPS during the tests. This creates an axial load equal to 62.5 kN to each M16 screw. This load is exerted to the end plate in the form of pressure to a surface equal to cross sectional area of the screw. The insertion of load to the EPS is defined by a linear amplitude function.

The other BC which has been considered in FE modeling is related to the test boss which is restricted to move axially during the tests and it has been modeled by keeping its movement equal to zero in z-direction. An illustration of the loading and BCs are shown in Figure 4.4.

4.3. Processing

This section contains a brief description of mesh type and how it is applied to EPS parts and also about selecting the solver to run the FEA.

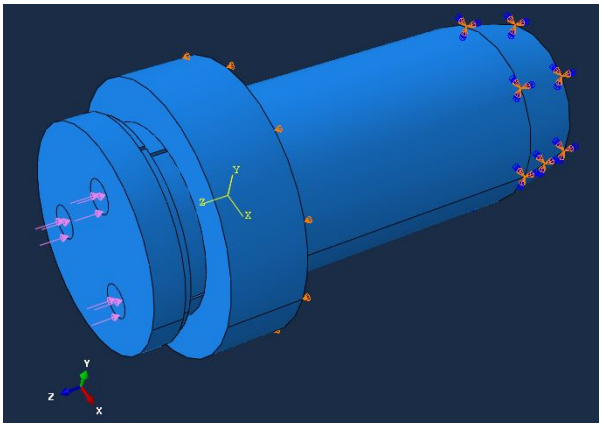

Figure 4.4: Loading and boundary conditions

4.3.1. Meshing

The quality of the element determines the accuracy of the solution in a FE simulation [34]. In FE meshing, element shape is mostly determined based on geometry of part. Meshing a complex shape with triangles or tetrahedra elements is very convenient and these elements are used in Abaqus automatic meshing algorithms and are suitable for general usage [35]. Other useful element shapes are quadrilaterals and hexahedra which have a better convergence rate than triangles and tetrahedra, and their sensitivity to mesh orientation is not an issue [35]. Even though triangles and tetrahedra are less sensitive to initial element shape, but a good mesh of hexahedral elements usually provides a solution of equivalent accuracy at less cost.

Another important parameter in meshing is mesh structure. Compared with structured meshes, unstructured meshes have the following advantages [36]:

(i) It is more adaptable to complex geometric configurations, especially when triangular elements are used,

(ii) The mesh model can be generated automatically.

Although unstructured meshes such as triangular and tetrahedral elements can be fitted suitably to complex geometries, however their calculation accuracy is low. Quadrilateral and hexahedral elements are more common in engineering analysis and have higher accuracy [36]. Therefore, hexahedral element has been selected to mesh EPS parts in this study.

The *sweep* technique is selected in order to apply unstructured mesh to the parts. *Medial axis* algorithm is the chosen solving algorithm in this analysis. This algorithm first decomposes the meshed region into a group of simpler regions and then it uses structured meshing techniques to fill each simple region with elements [33]. For relatively simple regions which contain a large number of elements, the medial axis algorithm generates a mesh faster than the other algorithm in Abaqus which is advancing front.

The element selected to mesh EPS parts is **C3D8R**, a continuous 3-dimensional, 8-node linear brick, reduced integration, hourglass controlled element. Due to the reduced integration, the locking phenomena that is a problem with some element types like C3D8 element did not appear [37]. This element is not stiff and is appropriate for bending problems.

Basically, stresses and strains are most accurate in the integration points. Since the integration point of the C3D8R element is located in the middle of the element, for this reason it is required to have small elements or a finer mesh. This can improve to capture stress concentrations at the boundary of the model [37].

The mesh size is identical for sleeve, test boss and end plate and it is half of the mesh size for pin since after running several primary simulation jobs, it was observed that pin is exposed to lower stress level and therefore its mesh size has been considered coarser to reduce simulation time. Fig-

ure 4.5 shows applied mesh to EPS. It is visible that mesh distribution is not uniform on end plate and the reason is partions defined on the surface of this part in order to apply load. Since a region that is meshed finer is usually less stiff [29], it should be noted that the transition between regions of different element sizes is smooth. This prevents occurrence of spurious stresses in this regions which can lead to false result.

Another effective parameter in mesh selection is hourglassing. In practice, the C3D8R element is not very useful without hourglass control. In the Abaqus version used for this analysis, starting with hourglass control is automatically activated for this element [37].

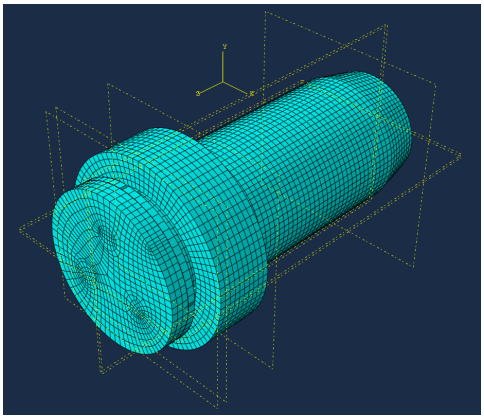

Figure 4.5: EPS mesh system

4.3.2. Selection of Solver

Selection of a suitable solver depends on the type of the problem and the way the model is loaded. In this FE study, through running several simulations a comprehensive investigation for selection of solver has been conducted and the three tested solvers including implicit static (static general), implicit dynamic and explicit dynamic are discussed in this subsection.

Implicit Static. Implicit static solver is generally known to be more accurate and efficient than explicit dynamic solver for simple 2D problems. However, for complex 3D problems with large deformations, the implicit static procedures encounter a number of inherent difficulties especially in incremental forming processes [38]. Implicit static finite element formulations require a very long computational time and several solution techniques have been developed to reduce the computational time, namely the dual mesh technique, Arbitrary Lagrangian Eulerian (ALE) technique, etc.

Loading of EPS is initially done through a slow process in practice and at the beginning of this FEA, it was assumed that the model is loaded statically equivalent to load of fastening torque. But the simulation process using implicit static was aborted and the solver was not able to complete the job.

Although the modeling of EPS is simplified and actually screws are omitted from the model, but still the complexity of problem led to unsuccessful attempts. From beginning of the implicit static analysis, *large displacement* warning appeared which is related to large displacements and deformations in the parts that causes non-linearity. It can be concluded that large strain rate makes implicit static an inappropriate option for this analysis.

Furthermore, it is expressed in the literature [39] that dramatic change in contact pressure may sometimes make it difficult to complete contact simulations in Abaqus static analysis.

Implicit Dynamic. This solver uses direct-integration method and in Abaqus/Standard it is called the Hilber-Hughes-Taylor operator which is an extension of the trapezoidal rule [27]. The Hilber-Hughes-Taylor operator inverts the integration operator matrix and then solves a set of simultaneous nonlinear dynamic equilibrium equations at each time increment. This solution is

done iteratively using Newton's method.

One of the methods to overcome drawbacks of a static simulation is switching to an implicit dynamic simulation because the inertial forces act as natural stabilizers [39]. This can increase simulation time considerably, but it is assured that a converged solution would be found.

The implicit dynamic is unconditionally stable for linear systems and it is a great advantage. The size of the time increment that can be used to integrate a linear system does not impose a limit. However, establishing stability results for integration operators in the context of nonlinear equations is difficult. For practical purposes the linear stability results can be used as an adequate indication for properties of the integration method for nonlinear systems [40].

Since the focus of this FEA is a final static response, a quasi-static method has been selected. This has introduced inertia effects to the problem, but since the loading process of EPS is not completely static, it can simulate real case scenario better. By applying very small time increments the accuracy of modeling increased and it reached to convergence by spending extra computational time.

Explicit Dynamic. Explicit methods are inherently dynamic. Explicit solvers can be used successfully for quasi-static problems to avoid convergence problems as long as the kinetic energy of the system is kept low. It is not easy to predict at what level the effect of kinetic energy in respected problem is low but an acceptable rule of thumb might be to set the limit on the kinetic energy to be less than 5 % of the strain energy. This goes some way to ensuring that the problem is still essentially quasi-static [39].

Using mass scaling technique in explicit quasi-static analysis may affect solution by changing magnitude of kinetic energy [39]. Therefore, in this FEA no mass scaling is considered for explicit solver.

The dynamic explicit method appears to be very effective in analyzing complex incremental contact problems [38]. While in implicit dynamic effect of strain rate is minimum and it is suitable for easy or moderate contact conditions, in explicit dynamic strain rate has significant effect and it makes the solver efficient in dealing with complex contact conditions.

Explicit analyses offer a substantial required-computational-time-reduction with comparable outcomes with implicit [41]. This matter was observed during running simulations fed with implicit and explicit algorithms.

Size of the stable time increment determines the applicability of explicit solver to quasi-static problems. The program must perform N increments each of t seconds duration, where t is given by [39]

$$t = \frac{2}{\omega_{max}} \tag{4.5}$$

and ω_{max} is the highest eigenvalue in the system. The total number of increments, N, required to complete the analysis is therefore given by T/t. Reduction of the cpu analysis time for a given mesh is achievable either by increasing the time increment, t, or reducing the total time, T. Therefore in this study a total time of 0.5 seconds is considered for explicit analysis.

4.4. Post-processing

In this section, a comparison between results from implicit dynamic and explicit dynamic is presented and the purpose is to evaluate and then select the most suitable solver for the rest of this study to implement optimization analysis. Simulations are carried out in a computer with characteristics of Core (TM) i7- 6700 cpu @ 3.4 GHz and RAM capacity of 16 Gb.

The results of simulation for implicit dynamic and explicit dynamic are shown in Figures 4.6 and 4.7. The mesh size for parts including test boss, sleeve and end plate is equal to 5 mm, but the mesh size for pin is 10 mm since the size of pin is larger than the other parts and the main reason was to

decrease simulation time.

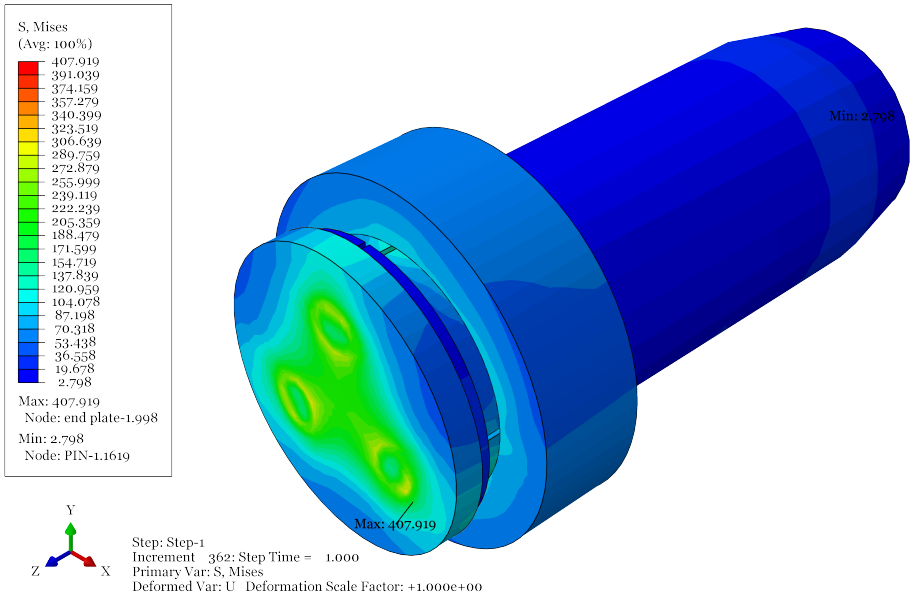

Figure 4.6: von Mises stress distribution for EPS obtained from implicit dynamic analysis

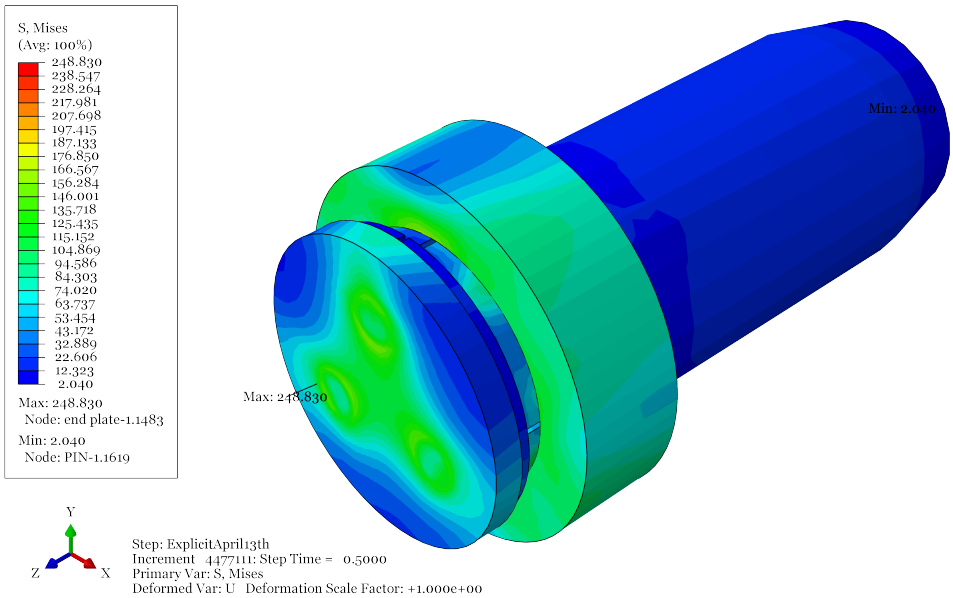

Figure 4.7: von Mises stress distribution for EPS obtained from explicit dynamic analysis

The load applied to EPS through each of the three circular partitions on the end plate is 310.85 MPa which is equivalent to 200 Nm torque to each screw. Based on Eq. (2.15), the preload of M16 screw exposed to 200 Nm torque is

$$F_i = \frac{200}{0.2 * 0.016} = 62.5KN \tag{4.6}$$

and since the radius of each partition is considered 8 mm in FE modeling, the resultant pressure of the preload according to the relation F_i/A is 310.85 MPa.

By comparing the maximum amount of von Mises stress from the two analysis, it is obvious that implicit dynamic gives higher value for this parameter. Both of the solvers have captured the maximum von Mises stress in the end plate pointing out to the back face of it, but besides the magnitude, the location of maximum stress is also different.

In order to make this comparison more clear, stress states for test boss obtained from the two different solvers are provide too. Figures 4.8 and 4.9 show stress distributions for the test boss. The unit of stress is in MPa. Since the experimental job was performed with focus on test boss and experimental results for this component are available, FE results are given here to evaluate which solver is more successful in providing reliable results.

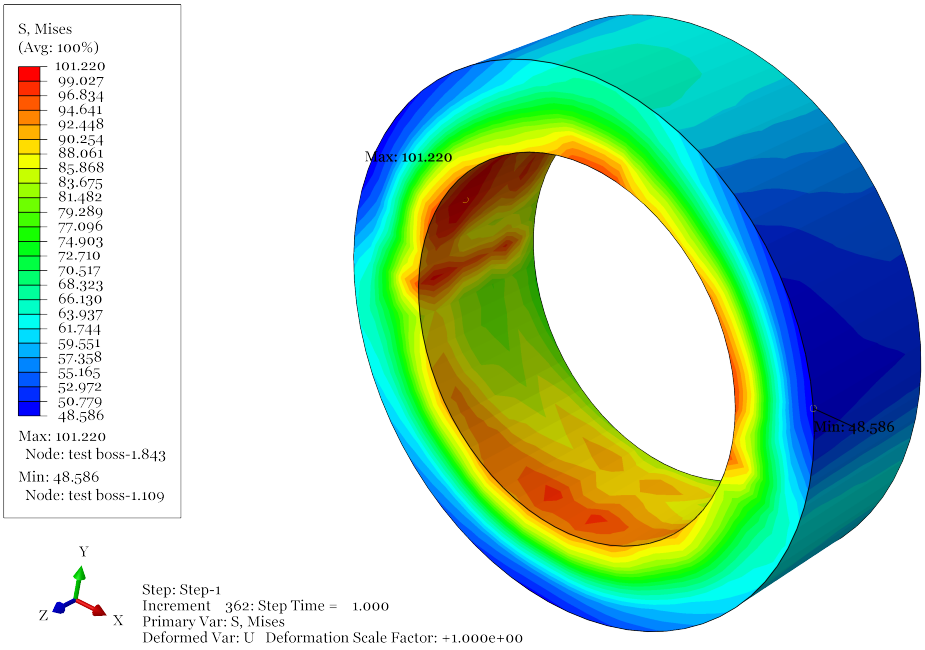

Figure 4.8: von Mises stress distribution for test boss obtained from implicit dynamic analysis

By referring to Table 3.3 which gives von Mises stress of the test boss for maximum measured strain in non-lubricated sleeve condition, it is concluded that implicit dynamic provides better results than explicit. The drawback of the explicit method is that it is conditionally stable [42]. The stability limit for an explicit solver depends on maximum time increment given in Eq. (4.5) and it must be less than the smallest transition times for a dilatational wave to cross any element in the mesh. Secondly, the explicit method is naturally limited to the analysis of short transient problems.

One of the important items in FE simulation is to apply sufficiently refined mesh to parts. The level of refinement has direct impact on accuracy and convergence of the results. Regardless of solver type, coarse meshes can yield inaccurate results in analyses. The numerical solution tend towards a specific value when the mesh density increases. When further mesh refinement produces a negligible change in the solution, the mesh is said to be converged. This creates confidence that for the FEM, the simulations will produce mathematically accurate and reliable results.

The mesh convergence study is usually performed by monitoring any parameter in the analysis such as temperature, pressure, stresses, strains, energies, etc. The most important parameter for a particular simulation can be selected to check for convergence. In this thesis, the primary parameter of concern, is the stress induced in the EPS parts. Therefore the maximum value of von Mises stress and maximum magnitude of displacement of the test boss are considered for evaluating of mesh convergence study. Table 4.3 contains the corresponding values. The first simulation with coarse mesh size of 10 mm for each joint component was unsuccessful to complete the analysis. After 77 %

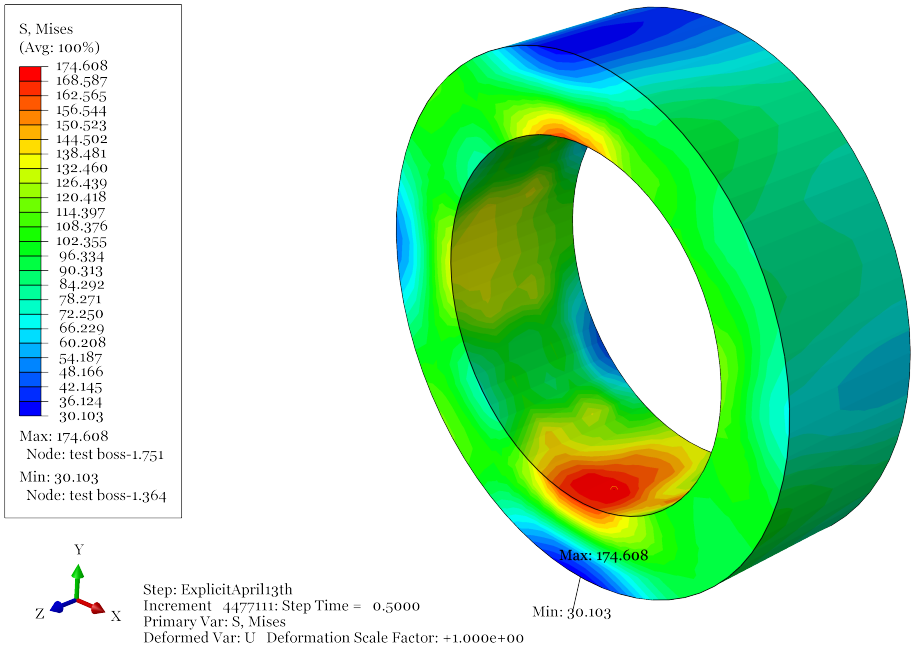

Figure 4.9: von Mises stress distribution for test boss obtained from explicit dynamic analysis

progress, the simulation job stopped and the main reason is in fact Abaqus was not able to evaluate parameters on the integration points because of large mesh size. Joint component like sleeve has a low thickness on its end section and therefore it is needed to have finer mesh at edges.

Table 4.3: Mesh convergence study

Simulation No.	Mesh Size	von Mises	Displacement
1*	10	-	-
2	7	161.27	0.061
3	6	95.18	0.025
4	5	100.51	0.024
5	4	106.86	0.025
6**	2	-	-

Note: * Incomplete job; 77 % progress
** Incomplete job; 32 % progress

Simulation number 2 with approximately coarse mesh size was not computationally suitable and besides considerable simulation time of 9.5 hours its results are not accurate and reliable. Simulation number 5 provides good results close to experimental results and by comparing it results with simulation number 4 there is no big difference between them. In order to carry out a more accurate analysis, simulation 6 was performed, but this simulation job was interrupted. The reason for that is related to CPU and RAM capacity of the system the simulation were conducted by it. Conducting such a simulation requires using a stronger computer with greater CPU and higher RAM capacity which is not the focus point in this thesis.

Further discussion about results of FEA is provided in next chapter. The results which will be discussed are obtained from simulation 5 that not only provides values in good agreement with experimental results and moreover it is efficient in computational time aspect. The number of elements produced by this mesh size for end plate, pin, sleeve and test boss include 2516, 15847, 2552

and 4100, respectively.

4.5. Summary

The methodology and steps of modeling EPS joint in ABAQUS was presented in this chapter. Through investigation of different solvers available in Abaqus/Standard and Abaqus/Explicit it is concluded that implicit dynamic algorithm provides better and more reliable results. The adopted mesh size of 4 mm for EPS components is assumed fine enough for the rest of the study which was selected after mesh convergence study. In the next chapter, results of FEA will be provided and they will be compared with results of theoretical part presented in Chapter 2 and experimental results of Chapter 3. This is followed by an optimization study in Chapter 6.

5

Comparative Discussion of Results

Results of the stress analysis of the EPS will be presented in this chapter. FEA provides an insight into the stress distributions in the different components of the joint. The pre-processing and processing steps of the FE simulations are performed according to the methodology described in Chapter 4 and here, post-processing results are center of focus. As mentioned in Chapter 4, the load applied to EPS during FE modeling was 200 Nm and the FE results are corresponded to that load. The results are presented separately for each joint component and they are compared with available analytical and experimental results.

5.1. End Plate

End plate is a part of EPS which has the function of transferring the axial load to expanding sleeve which leads to clamping force in the joint system. As mentioned in Chapter 4, the modeling of EPS was simplified to reduce simulation time by omitting of fastening screws and consequently their contact surfaces. The results of FEA for this part are provided in this section.

The axial stress in the end plate can be determined by S33 in Abaqus. The maximum axial stress is equal to 318.42 MPa which resulted from pressure of 310.85 MPa applied to each circular partition on the front face of the end plate. The characteristic of this stress is compressive. The modeling of end plate is simplified and it does not represent real case scenario, because in real application the end plate has three holes instead of the circular partitions.

In Figure 5.1, von Mises stress distribution is illustrated and it shows that the maximum von Mises with magnitude of 405.67 MPa exceeds end plate material true yield strength which is 404.77 MPa. In addition, Tresca stress which is a more conservative yield criteria gives a maximum value of 451.97 MPa and emphasizes the fact that in some regions of the end plate plasticity has occurred. In order to have a better understanding of what happens in reality on the test boss a more precise modeling is investigated.

The end plate in EPS does not have important functional role and even happening of plastic deformations in parts of it will not affect its functionality. More over, the recommended torque for tightnening of end plate screws is less than the one considered in FE simulation and in fact lower stress would be produced in the end plate by applying the recommended torque. However, it is of interest to know that what would occur when end plate has holes.

In order to evaluate the stress state in the end plate more precisely, a model of it containing three holes is analysed separately in Abaqus by following the same parameters considered for modeling EPS. The end plate equipped with three screws has been exposed to axial load of screws and the back side of the end plate which actually is in contact with face of the sleeve is restricted to have displacement in z-direction. The illustration of end plate exposed to axial load of screws is shown

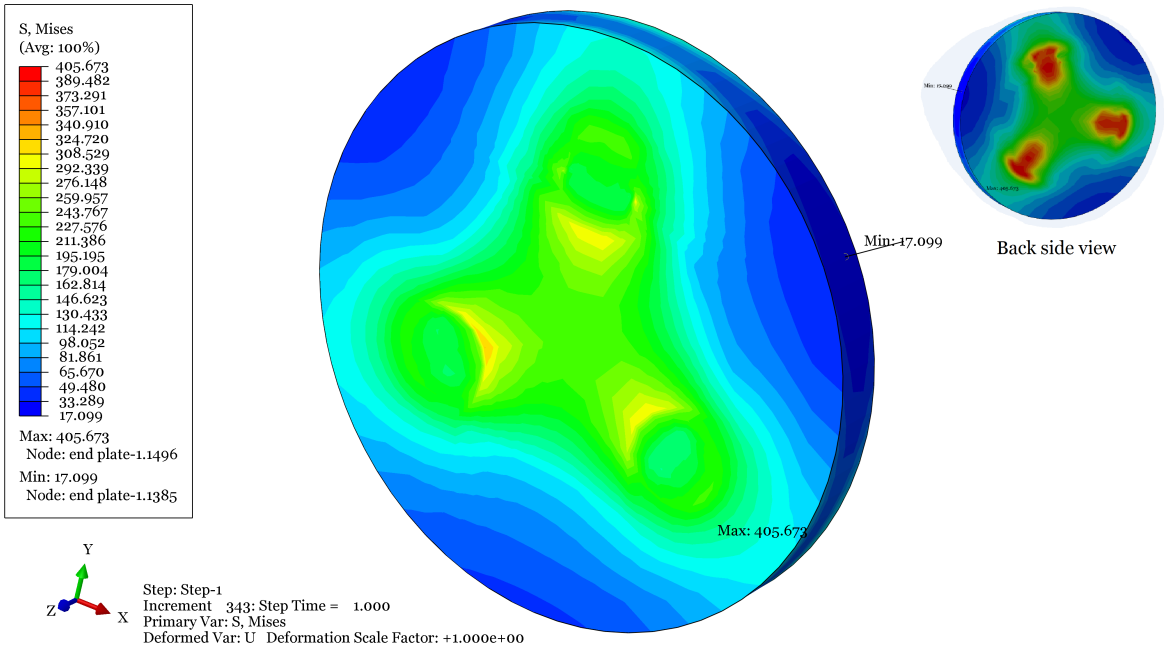

Figure 5.1: von Mises stress in the end plate

in Figure 5.2a. The reaction force on the back side of the end plate is shown in Figure 5.2b and it resembles contact force between the end plate and sleeve since the area of applying this simply support condition has exactly the same cross sectional area of the sleeve. The maximum reaction force is 6.605 kN.

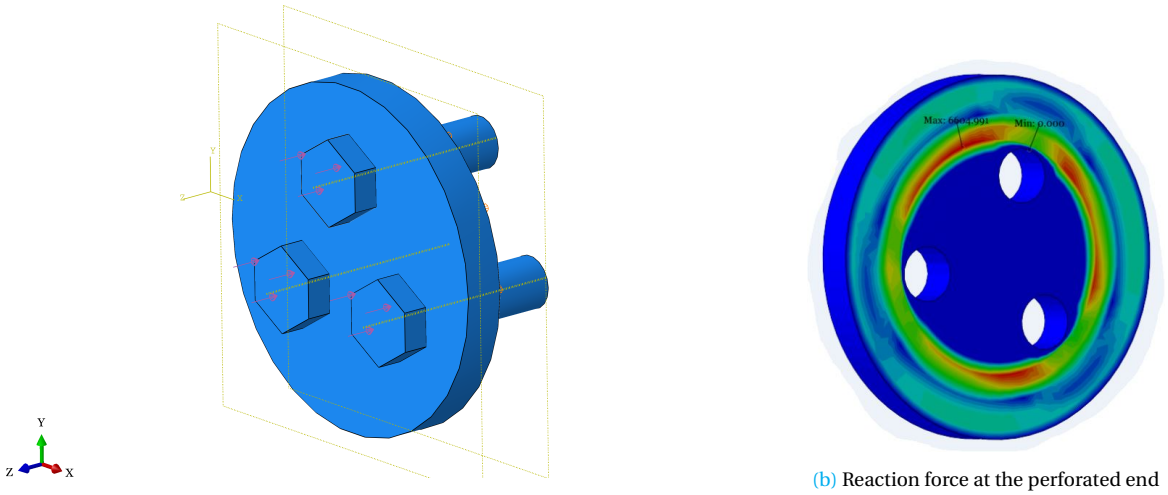

(a) End plate model representing actual condition

(b) Reaction force at the perforated end plate

Figure 5.2: Actaul model of end plate

The maximum principle stress in the perforated end plate with the three holes is 622 MPa which is much higher than material yield strength. The location of the maximum stress is at the edge of the holes exactly under collar of the tightening screws and the reason is the sharp edge which has resulted in stress concentration. The von Mises stress state in the perforated end plate is similarly showing the maximum stress at the edges of the holes with a value higher than yield as is shown in Figure 5.3. The maximum Tresca stress happens at the same location as maximum von Mises has

happened with value of 506.47 MPa.

There are no experimental result for end plate to compare it with the FE result. Up to knowledge of author, there is also no direct formula for a circular perforated plate subjected to pressure loading. Therefore FE tool is a useful and reliable tool to perform a stress analysis on such a part.

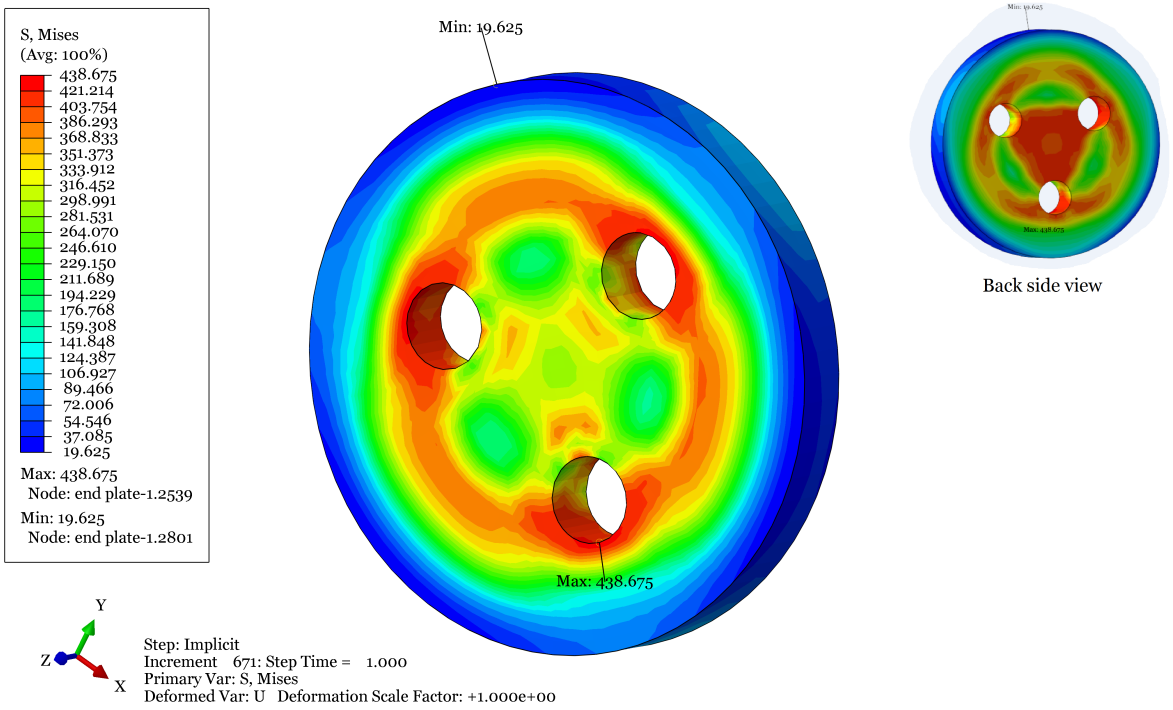

Figure 5.3: von Mises stress in the perforated end plate

5.2. Sleeve

In this section, FE results of sleeve is provided. Sleeve plays the most important role in EPS joint, because its expansion leads to creation of clamping force. Figure 5.4 shows von Mises stress distribution in the sleeve. The level of this stress is in elastic region in different parts of the sleeve. The maximum value is 337.7 MPa which has happened in the collar edge near the contact surface between the end plate and sleeve. The characteristics of this stress is tension which is related to expansion of the sleeve. As it was expected, the back side of the sleeve collar has experienced a low level of stress since it does not have any contact with other parts and the stress of this region is resulted from Poisson's effect. Tresca stress state is similar to von Mises stress and it points out the maximum stress at the same region as von Mises criteria with difference in magnitude with a value of 384.1 MPa, around 14 % higher than maximum von Mises stress.

There has been no experimental study in this thesis in order to obtain results for strains and stresses in sleeve. However, the accuracy of formulas presented in Section 2.2 can be evaluated here. Those formulas are derived for a perfect sleeve without any slits while the sleeve in Bondura EPS has four slits which one of them is a cut-through (complete cut). It can be useful to investigate to which extent those formulas are valid or whether they can be used in practice for a split sleeve.

Eq. (2.32) provides radial stress for sleeve in its contact surface. In order to be able to find radial stress along the tapered length of the sleeve, it is required to calculate stress derivative through Eq. (2.52) since both the radial stresses of sleeve and pin vary along the tapered length and they are dependent on the rate of change in stress. The simplified form of Eq. (2.32) after finding stress derivative is

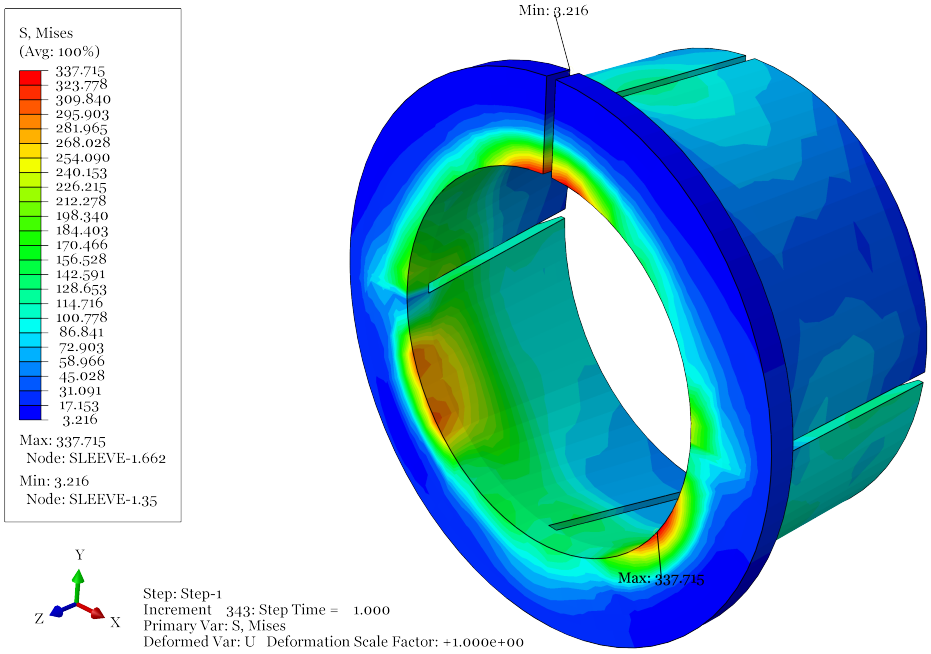

Figure 5.4: von Mises stress state in sleeve

$$\sigma_{2r} = \frac{p(R - x\tan(\beta))^2 \cos(\beta)(1 - \mu\tan(\beta))}{(R - x\tan(\beta))^2 - (r_{z0})^2}(1 - \frac{r_{z0}^2}{r^2}) \tag{5.1}$$

By substituting sleeve geometrical characteristics including; R = 43.4 mm, r_{z0} = 44.45 mm, β = 12°, and friction coefficient μ = 0.2, the above equation yields

$$\sigma_{2r} = \frac{0.9366215516p(0.0434 - 0.2124107526x)^2}{(0.0434 - 0.2124107526x)^2 - 0.0019758025}(1 - \frac{0.0019758025}{r^2}) \tag{5.2}$$

It is clear that Eq. (5.2) is a function of both x and r due to taper and by finding pressure, p, thorough Eq. (2.19), the radial stress for sleeve could be achieved.

The corresponding stress for sleeve in FE simulation is S11 (the maximum principle stress) when it is in horizontal plane, because other planes will add stress components which requires further calculation to find out radial stress. This is valid as if the effect of shear stresses are ignored. Therefore, a path is defined in the horizontal plane across the tapered length of the sleeve equal to the contact length. This path is shown in Figure 5.5. It is along one of the sleeve cuts (it could also be defined on the other side due to symmetry). The radial stress on this path is compared with the result of Eq. (5.2) in Figure 5.6a. Figure 5.6b shows the contact length between the sleeve and pin which is approximately 35 mm.

Figure 5.6a shows that both theoretical and FE results predict an increase in the magnitude of radial stress as it moves from the edge of the sleeve towards its collar which is equivalent to move from approximately beginning of pin taper towards its end. However, FE curve has some unusual jumps which could be related to inaccuracy of FE calculations on the integration points due to mesh size. This matter needs more study. The dash line is a linear trend line for FE curve which highlights the stress increase at the end of the pin. Furthermore, it could be expressed that the prediction of Eq. (2.32) for maximum radial stress is in good agreement with FE results even though it is for a perfect sleeve.

There are no theoretical formula to derive hoop stress for sleeve, thus presenting FE results for sleeve are ignored. Another parameter with great importance that can be studied in this section is

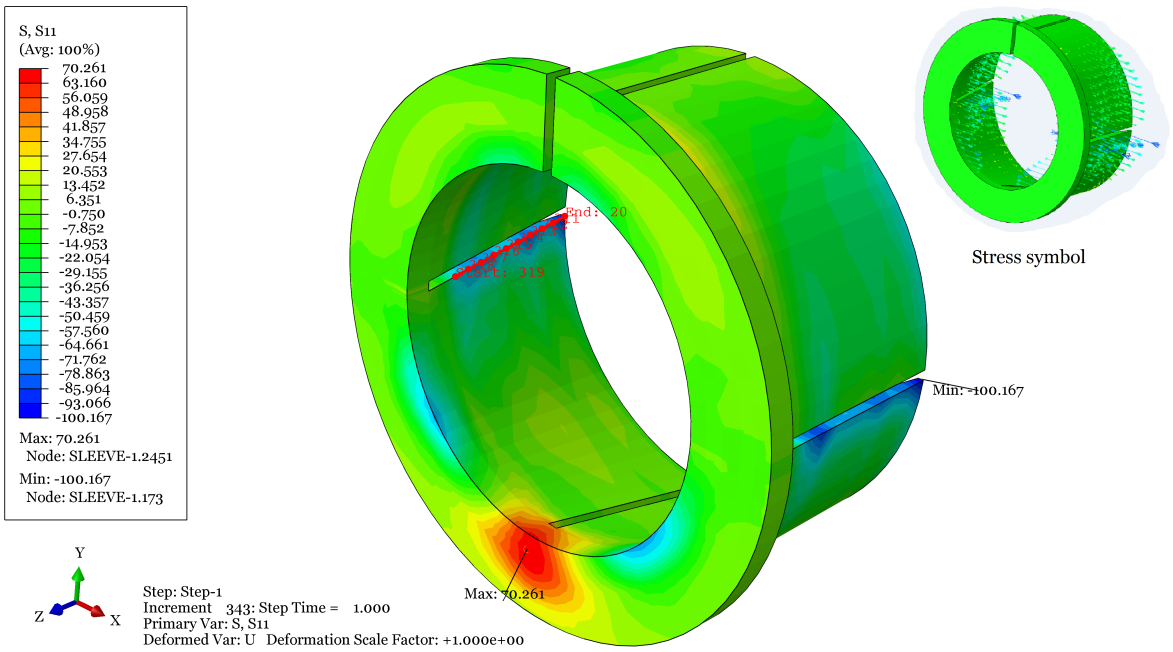

Figure 5.5: Radial stress state in sleeve

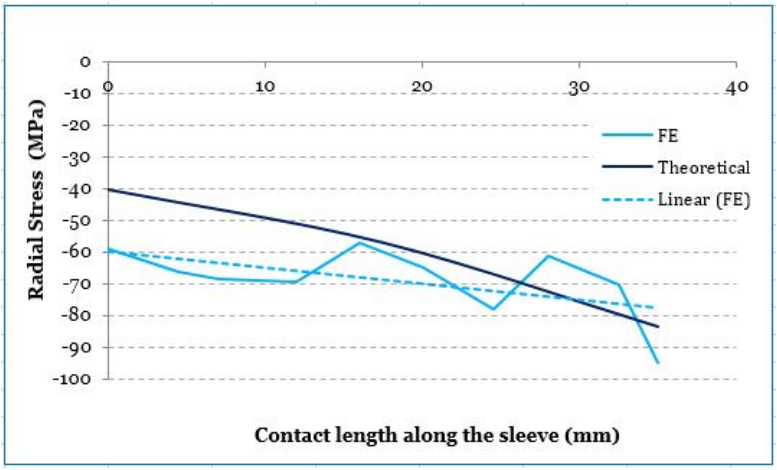

(a) Sleeve radial stress along contact length

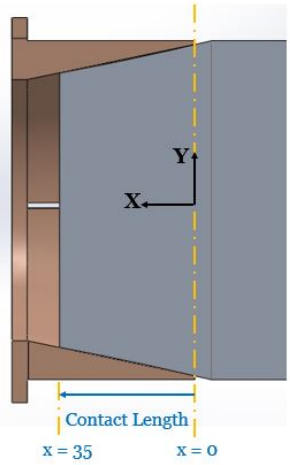

(b) Illustration of contact length

Figure 5.6: Sleeve radial stress

contact pressure between sleeve and pin. Eq. (2.19) gives contact pressure between pin and a perfect sleeve. Using this equation and regarding the material and geometrical characteristics of sleeve, the contact pressure is derived along contact length and it is depicted in Figure 5.7a. The contact pressure increases from sleeve edge towards its collar. The contact pressure obtained from FEA is given in the same graph for both sleeve and pin. The contact pressure of the sleeve obtained from FE is in good agreement with the graph of theoretical formula even though it is not completely uniform and has some dramatic peaks and troughs. It was expected that FE results for both sleeve and pin would have the same value, but they are different. This matter is related to definition of master-slave surfaces. The surface of pin is defined as master which experiences less deformation during contact while the surface of sleeve is defined as slave and since it undergoes larger deformation it has higher contact pressure. Based on the comparison between the theoretical and FE results it can

be concluded that Eq. (2.19) is appropriate for prediction of contact pressure of the sleeve-pin.

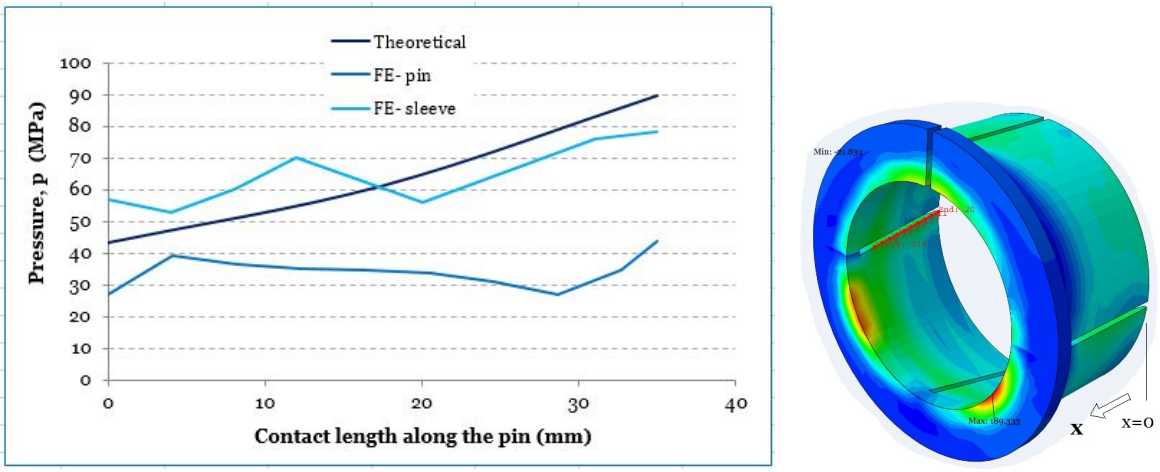

(a) Contact pressure along the contact length

(b) Sleeve pressure distribution, FE

Figure 5.7: Comparison of contact pressure

5.3. Pin

In this section, theoretical and analytical results for pin are subject of investigation. Similar to the case indicated for sleeve, S11 stress in Abaqus which is the maximum principle stress at horizontal plane resembles pin radial stress. Distribution of S11 and a path parallel to the one used for presenting radial stress for sleeve are shown in Figure 5.8.

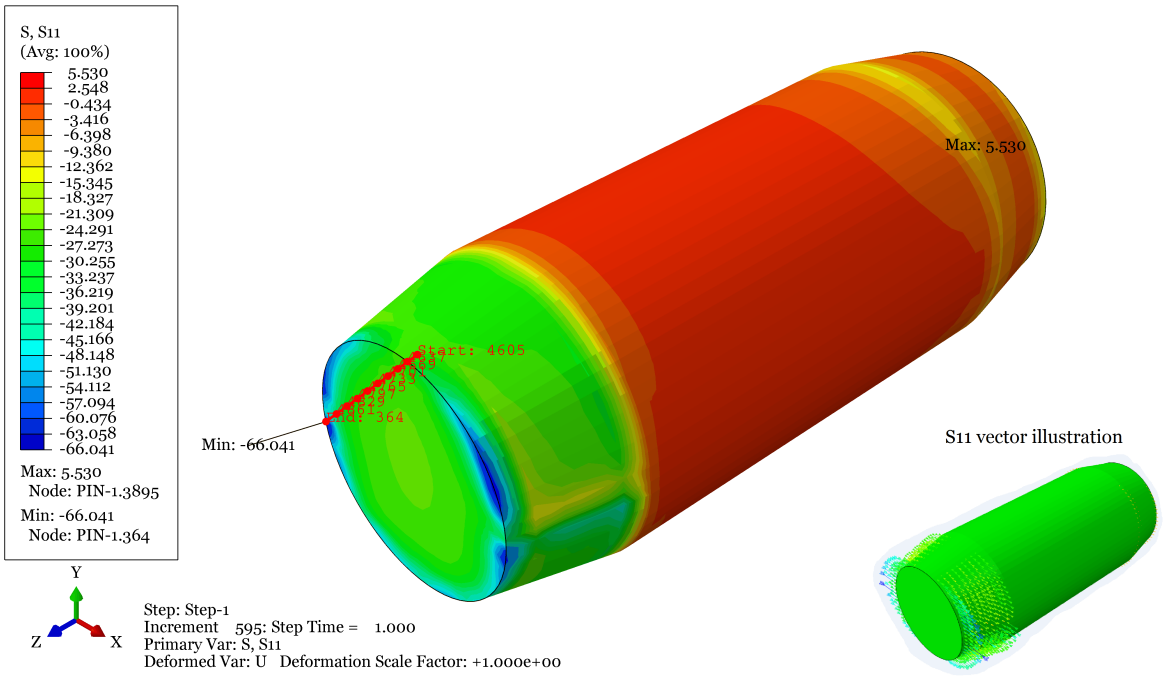

Figure 5.8: Radial stress state in pin

Eq. (2.21) from theoretical chapter gives radial stress for pin. This equation is dependent on stress derivative similar to Eq. (2.32) which is valid for sleeve. Variations of radial stress along the corresponding path for both theoretical formula, Eq (2.21), and the FE results are shown Figure 5.9.

By comparing the two graphs it is visible that FE and theoretical results are not in good agreement with each other. In different regions along the contact length discrepancies exist between the two curves. FE method calculates the stress value for each element and since the sleeve has four slits which one of them is a complete cut the induced pressure of sleeve to pin is not symmetric and it is actually non-uniform. Therefore existence of non-uniformity in radial stress of the pin is not strange. FEM shows this matter and local differences are visible in the FE graph. Both FE and theoretical methods show increase in the magnitude of radial stress along the contact length.

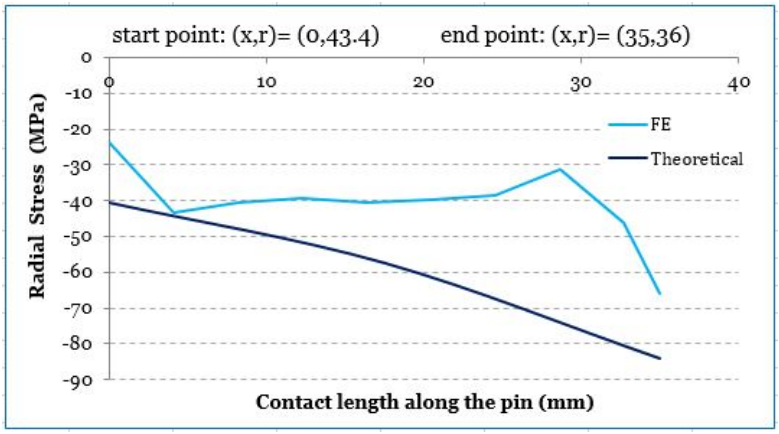

Figure 5.9: Pin radial stress along contact length

FE results show that the maximum von Mises and Tresca stresses happen at the same point that maximum principle stress, S11, has occurred and their values are 57.62 MPa and 66.31 MPa, respectively.

Pin axial stress is another parameter that can be investigated here. Figure 5.10 shows axial stress distribution along the pin length. The FEM has predicted the maximum axial stress at the other end of the pin where it was completely restricted to move as a clamped support. In addition, on the other side which is in contact with the sleeve, stress distribution is different from analytical method. The analytical method considers maximum axial stress at the end of pin taper and assumes its minimum value equal with zero at the beginning of the taper (x=0 at Figure 5.6b). But the FE results are in contradiction to theoretical results and they show that at the end of pin taper the axial stress is less than at the beginning of taper. Furthermore it shows that the center of the pin experiences lower stress than the outer parts of the pin which can be considered reasonable since the axial force affecting on the pin is created due to axial load on sleeve and the sleeve is hollow.

The theoretical expression for axial stress of pin was shown in Figure 3.9 and it is provided here again in Figure 5.11 in order to make a comparison between the theoretical and FE results with this difference that here it is drawn for applied torque of 200 Nm. Because of compressive nature of the axial stress a negative sign is added to the theoretical stress to represent its nature. The theoretical method shows an increase from beginning of pin taper towards its end i.e. from $x=0$ to $x=35$ mm while FE results shows an opposite behavior. The theoretical method predicts pin maximum axial stress equal to 46.38 MPa and the corresponding FE value is 41.9 MPa. This difference in prediction of longitudinal stress distribution highlights the need for applying a finer mesh, but unfortunately running a simulation with finer mesh interrupted due to RAM capacity. However, it looks like that assumption for theoretical stress distribution on BC expressed in Eq. (2.47) that considers zero stress at the beginning of taper is not valid enough and requires further investigation.

Pin hoop stress can be determined by evaluating S22 at horizontal plane. The maximum observed value for pin hoop stress is nearly identical to its radial stress which is around 69.69 MPa. Tresca and von Mises stress distributions along the tapered end are higher at the end of the pin (x = 35 mm) and decrease towards the beginning of the taper.

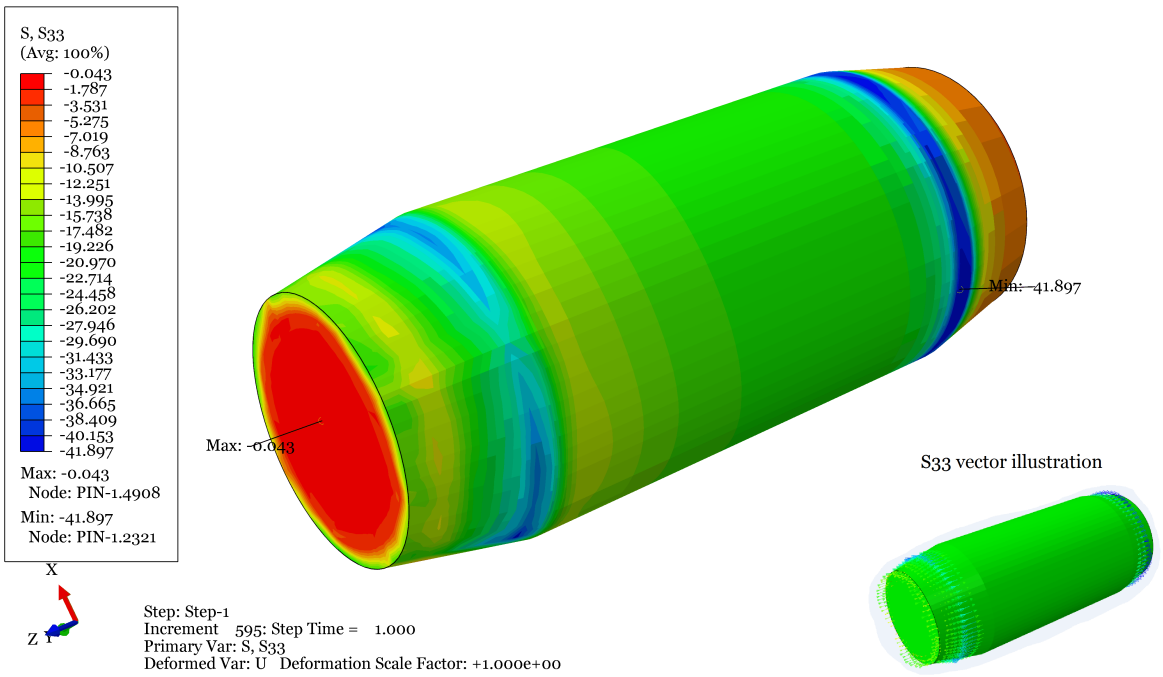

Figure 5.10: Axial stress state in pin

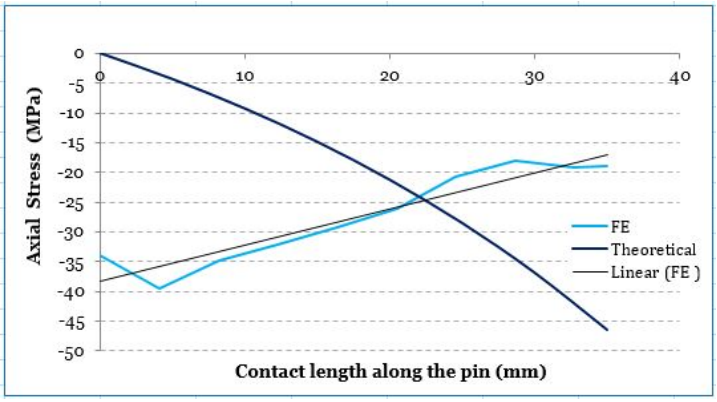

Figure 5.11: Comparison of axial stress between FE and analytical along contact length

5.4. Test Boss

FE results of the test boss are presented in this section and they are compared with experimental results of Chapter 3. The von Mises stress state for the test boss produced in post-processing of Abaqus is shown in Figure 5.12. The magnitude of maximum von Mises stress in the test boss predicted by FEM is close to the value which was calculated before and present in Table 3.3 based on experimental measurements. The prediction of FEM for test boss maximum von Mises stress is 107.59 MPa while the corresponding experimental value is 124.07 MPa and it shows that FEM has good accuracy. However there is a difference between position of the maximum von Mises in the test boss predicted by FEM. Abaqus predicts the position of the maximum von Mises stress aroud angular position of 155°, while based on the experimental measurements performed by strain gauges installed at angular positions of 0°, 90°, 180° and 270°, the maximum von Mises has been found to occur at 90°. The FE predicted point was not placement for any strain gauge during experiments, therefore it could be concluded that further experimental research is required to investigate this subject.

Tresca stress is another criteria to be compared for the test boss. FEM gives maximum Tresca

stress at the same point that von Mises has occurred and its magnitude is 120.04 MPa which compared with experimental value of 131.2 MPa (Table 3.3) could be considered as a close result. It is believed that applying a finer mesh to EPS components can make the FE results closer to experimental results. The other reason for existence of difference between the results of these two methods is simplifications applied during FE modeling.

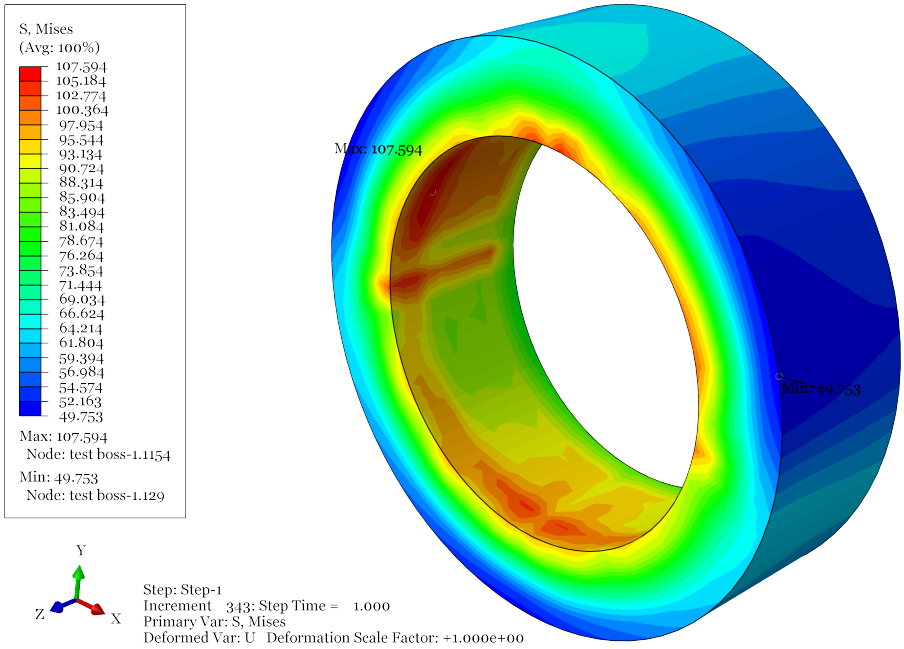

Figure 5.12: von Mises stress state in the test boss

Abaqus provides principle stresses for each joint component. These principle stresses at different planes can present hoop, radial and axial stresses. In order to extract hoop stress for the test boss two different cuts are applied to it as shown in Figure 5.13. By applying a cut using the vertical plane, hoop stress is obtained for the test boss by reading S11 and similarly S22 gives the hoop stress by cutting the test boss using a horizontal plane. Abaqus calculates S11 and S22 for each element and it shows a non uniform stress distribution along the cross sections of the cuts with higher values on inner surface of the test boss. In order to make a comparison with experimental results only the maximum value on each cross section is considered. The comparison of FE and experimental hoop stress on inner surface of the test boss is given in Table 5.1. The similar comparison for hoop stress on the outer surface of the test boss is provided in Table 5.2.

Table 5.1: Comparison of hoop stress in the test boss on its inner surface

Angular Position	**Experimental** (Mpa)	**FE** (MPa)	**FE Error** %
0°	55.93	85.9	53.58
90°	96.82	75.77	21.74
180°	57	84.85	48.86
270°	60.19	83.82	39.26

By comparing the results from Tables 5.1 and 5.2 it is concluded that accuracy of FEM to predict hoop stress is not exact and it has some considerable deviations from experimental values. In the case of hoop stress on inner surface of the test boss besides the difference in values between FE and experimental, FEM predicts the position of maximum hoop stress in the horizontal plane while

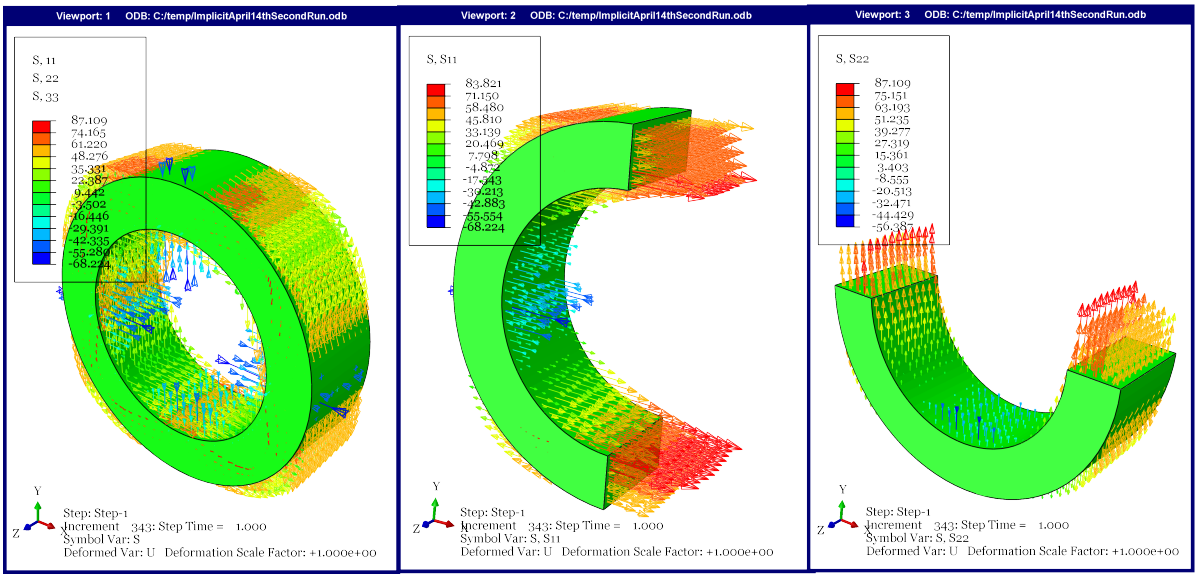

Figure 5.13: Hoop stress state in the test boss

Table 5.2: Comparison of hoop stress in the test boss on its outer surface

Angular Position	**Experimental** (Mpa)	**FE** (MPa)	**FE Error** %
0°	36.12	51.59	42.83
90°	62.37	50.97	18.28
180°	36.75	49.44	34.53
270°	38.83	48	23.62

experimental results indicate that the maximum hoop stress has happened on the top part of the test boss at 90°. FEM predictions for the hoop stress on outer surface of the test boss are better than previous case, but still the magnitude of error is significant.

Radial stress is another subject of study and comparison. Radial stress distribution along the test boss is shown in Figure 5.14. The radial stress values from FEM are compared with corresponding values from experimental measurements in Table 5.3. Compared to the hoop stress, FEM predictions for radial stress are closer to experimental measurements. Moreover, FEM predicts the position of maximum radial stress correctly, pointing out at top of the test boss at angular position of 90°, similar to test results.

Table 5.3: Comparison of radial stress in the test boss

Angular Position	**Experimental** (Mpa)	**FE** (MPa)	**FE Error** %
0°	-19.86	-19.07	4.14
90°	-34.37	-27.91	23.15
180°	-20.24	-18.65	8.53
270°	-21.37	-15.84	34.91

The principle stress S33 in Abaqus represents axial stress in the test boss. This stress originates from friction force between sleeve and test boss. Experimental results show a nonuniform axial stress along the circumference of the test boss since the radial stress which is the main component for creation of axial stress is not uniform (Table 5.3, second column).

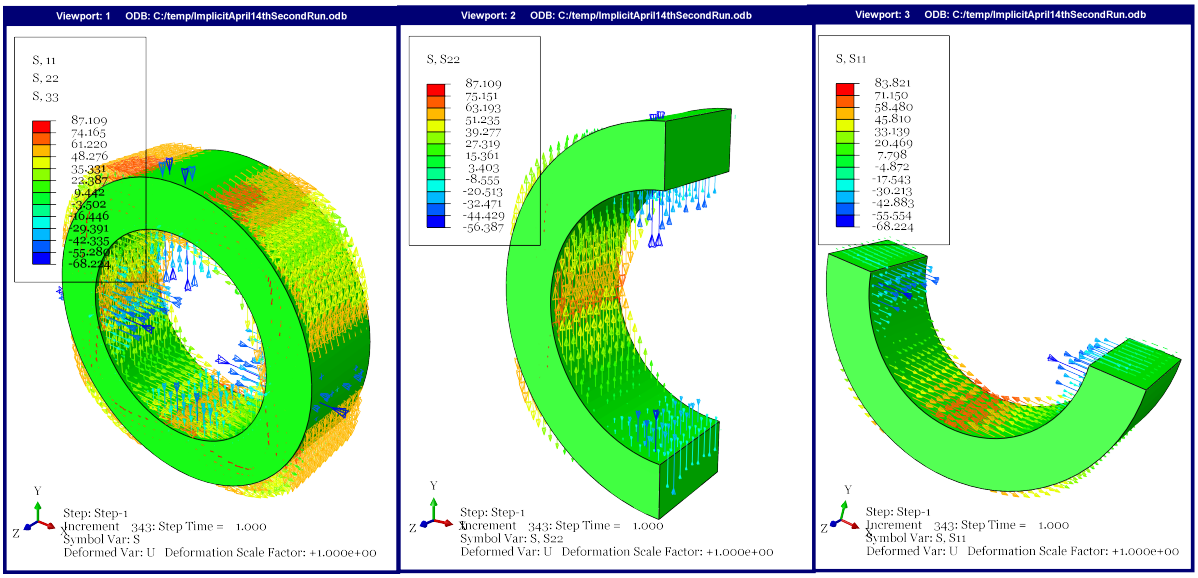

Figure 5.14: Radial stress state in the test boss

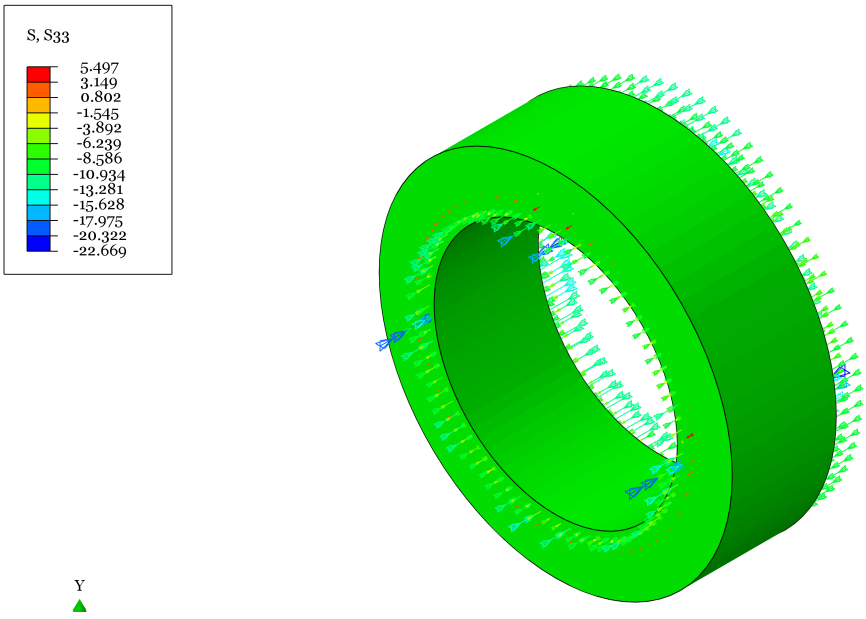

Figure 5.15: Test boss axial stress

The axial stress from experimental method can be calculated by Eq. (3.5). By assuming friction coefficient μ= 0.2, the equation is simplified to $0.277\sigma_{r(int)}$. Based on this assumption, the minimum and maximum experimental axial stress are -6.16 MPa and -10.65 MPa where the negative sign shows the compressive characteristic of this stress. The FEM predicts the axial stress of the test boss between the range of -22.67 MPa and +5.5 MPa indicating that both the compressive and tensile stresses have occurred in the test boss. Occurrence of tensile stress in some part of the test boss seems to be logical since compressive frictional force in inner side of the test boss pulls its surrounding materials. This can be considered one of the advantages of the FE that can capture material behavior locally and it is not restricted to present only an overall response as the theoretical method does. As the stress vectors show in Figure 5.15, most of the test boss experiences an axial stress in the range of -4 MPa to -13 MPa which is close to experimental range.

5.5. Parametric Study on Friction Coefficient

Friction Coefficient, μ, is the only parameter whose value is assumed during both theoretical and FE studies. The value of friction coefficient is assumed 0.2 based on the proposed values for steel-steel surface interaction [3]. Since in the experimental study of this thesis a series of tests were carried out on lubricated sleeve 3.2.2, a parametric FE study is carried out to evaluate the effect of this coefficient and compare the results to achieve a better view on this parameter. The effect of variation of μ is studied on pressure and stress in EPS joint components.

The variations of μ has direct effect on pressure and stress state of the joint components except the end plate. The parametric study shows that the stress state of the end plate is not affected by variations of μ. The other joint components experience change in pressure and stress as μ varies. Table 5.4 shows variations of pressure based on μ. The values of this table are the maximum pressure occurred in the joint components according to FEM. They indicate by decreasing μ the pressure experienced by EPS joint components increases. This is totally in agreement with experimental results provided in Figure 3.16 for the test boss which shows that lubrication has resulted in increase in the magnitude of radial stress and consequently pressure (since σ_{radial} = -p). The unit of pressure in the table is in MPa.

Table 5.4: Variation of pressure based on μ

Part	**μ=0.4**	**μ=0.3**	**μ=0.2**	**μ=0.1**
Sleeve	171.934	183.186	189.333	191.101
Pin	20.834	24.609	33.096	46.060
Test boss*	16.301	20.779	28.159	43.884

Note: * The pressures of the test boss are compressive.

When μ decreases between contact surfaces of the joint components, the level of wasted energy due to friction decreases and it results in higher stress state in the components. In order to evaluate the effect of μ on the stress state of the components von Mises stress has been the subject of concentration. Figure 5.16 illustrates variations of von Mises stress in the test boss and it is obvious in the images that as long as the μ decreases more regions in the internal surface of the test boss experience higher stress and in addition the stress distribution becomes more uniform. Accumulation of stress in the front side of the test boss distributes better throughout the test boss when μ decreases and this matter is observable for μ = 0.2 which is near to real case scenario.

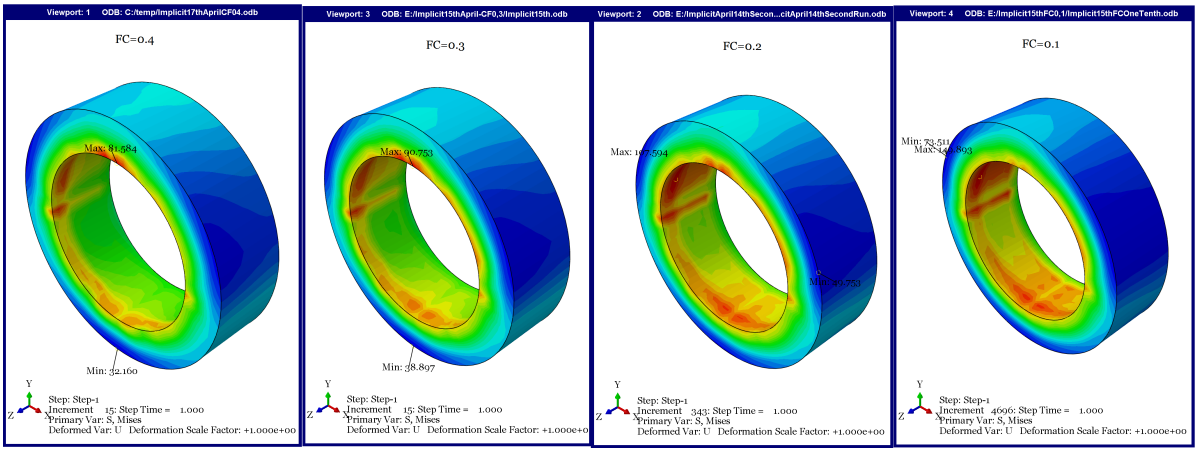

Figure 5.16: Variation of von Mises stress in the test boss based on μ (FC: Friction Coefficient)

The values of maximum von Mises for joint components with different μ values are provided

in Table 5.5. Except the different behavior of von Mises stress versus μ for sleeve, the other joint components follow the rule that as μ decreases the level of von Mises increases. The reason for the unusual behavior of sleeve could be related to larger deformations and displacements of it, because greater μ values mean more resistance against relative movements and consequently higher stress state.

Table 5.5: Variation of von Mises stress based on μ

Part	μ=0.4	μ=0.3	μ=0.2	μ=0.1
Sleeve	400.595	356.406	337.715	347.777
Pin	27.884	29.384	38.027	59.621
Test boss	81.584	90.753	107.594	149.893

The maximum von Mises stress calculated for the test boss in lubricated sleeve condition was 262.08 MPa (Table 3.3). This value is much higher than the maximum value of von Mises stress for the test boss in Table 5.5. This means in experimental tests for lubricated sleeve the value of μ was lower than 0.1.

The variations of von Mises stress with respect to μ for the test boss is shown in Figure 5.17. At μ = 0.2, FE von Mises stress is approximately 12% lower than the experimental value. By keeping this difference, μ can be extrapolated using the following equation

$$vonMises = -2964.3\mu^3 + 3051.5\mu^2 - 1130.9\mu + 235.44 \tag{5.3}$$

where the above equation is a cubic polynomial extracted from the trend line tangent to the FE curve. By reduction of 12% from the experimental value of 262.08 MPa, the corresponding μ for lubricated sleeve is found to be 0.0043. It means using Bondura lubrication paste has reduced μ to the mentioned value. These argument is valid for assumed value of μ = 0.2 for non-lubricated state, however more experimental study is required to find the exact value of μ.

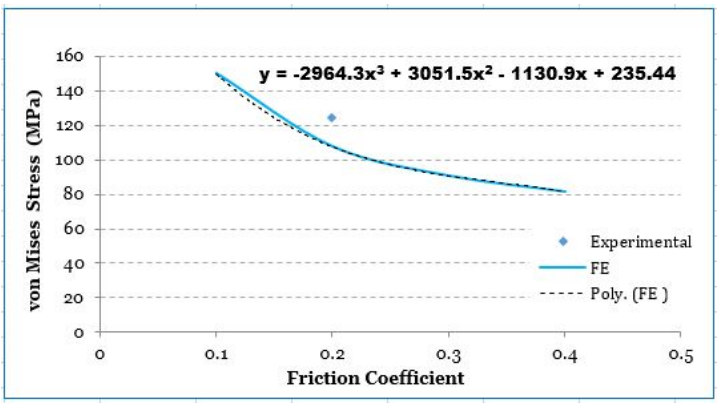

Figure 5.17: Variations of von Mises stress wrt μ for the test boss

It is possible to find the friction coefficient in the EPS according to the von Mises values in the test boss. If we trust the FE results and consider them as basis, by drawing a horizontal line which passes through the experimental value of 124.07 MPa, the intersection point on FE curve in figure above gives friction coefficient μ = 0.16 in the joint system. This value is not conservative and finding a more precise value for friction coefficient in the Bondura EPS needs more experimental research.

5.6. Summary

In this chapter, the finite element results extracted from post-processing part of Chapter 4 were presented and compared with the theoretical and experimental results. Every component of the EPS joint were investigated separately and their stress state were discussed in details.

The FE results of end plate showed local plasticity in regions subjected to axial load, therefore a simulation close to its real geometry containing holes for inserting fastening screws were carried out and a better stress illustration were achieved for this component.

The FE results for sleeve including radial stress and contact pressure were very close to proposed values of theoretical formulas of Chapter 2. Therefore it is concluded that Eq. (2.19) and Eq. (2.32) can be used to estimate pin-sleeve contact pressure and radial stress, respectively, even though they are derived for a perfect sleeve without any slits.

The FE results for pin were not in good agreement with theoretical formulas of Chapter 2 including Eq. (2.19) and Eq. (2.21) specially axial stress distribution along pin taper. This difference maybe related to mesh size since applying finer mesh requires having a stronger computer with higher CPU and RAM capacity. Moreover, it can be expressed that assumptions taken in theoretical method are not completely precise and this matter requires experimental method to find where the positions of the maximum and minimum are located in the pin considering that the load exerted on the pin is through the tapered part, not the end of the taper.

The FE results for test boss were in good agreement with experimental results. Although FE hoop stress predictions for the test boss were not so precise, other stress components like von Mises, Tresca and radial stresses were close to experimental results.

The parametric study on friction coefficient shows that when friction decreases the magnitude of pressure and stress in joint components increase except for sleeve where it showed an opposite behavior. This matter is compatible with experimental results for the test boss. Moreover an approximation formula for relation between von Mises stress versus friction coefficient in the test boss was derived based on the results of the FE parametric study.

6

Optimization

To produce sustainable and competitive products parameters like selection of parts material and geometric design are very important in industry. Optimization is a useful tool to create an appropriate component in early stages of design process or even to promote the design of an existing component.

The concept of structural optimization is divided into three categories including size, shape and topology optimizations [43]. Based on the definitions for these categories it is concluded that size optimization is not related to optimization problem of this study because this type of optimization often deals with issues related to truss-like structures mostly bridges, support frames and etc. In size optimization a nonsupporting member could be fully removed if its radius or height is included in the variable groups and moreover it is also concerned with changing the thickness of plates [44].

Topology and shape optimizations are useful tools to provide an optimal component design in early phases of the design process while preserving strength and endurance requirements of components. A topology optimization in a finite element context modifies the connection between elements in association with pre-defined objectives and constraints [43]. In other words it is reduction in the amount of material while the stiffness of the structure or component is preserved at a level to endure or resist applied loads with respect to predetermined design safety factor. Since this reduction of material needs more machining process on the pin and it means more time and cost due to machining operations, topology optimization is put aside in this study. It is worth mentioning that topology optimization could be a subject of study if the production method of pin was molding or 3D printing where mass reduction means reduction of production time and consequently costs.

In shape optimization process on a structure or component, shape in the terms of thickness and radius undergoes changes. As there is always a need to reduce mass of a final product in order to cut the production cost while preserving the aspect of manufacture-ability, it is becoming more usual to include shape optimizations in early phases of the component development process. There are some parameters like angle of taper for the ends of the pin and pin strength (shear capacity vs contact stresses on inner side of support) which are very important and are considered in shape optimization process of the pin.

During the previous chapters by investigating the analytical, experimental and FEM a thorough understanding of loads and stresses impacting on expanding joint mechanism is achieved and the obtained results are used in optimization process through this chapter.

The optimization process of this chapter is carried out for Bondura EPS Φ88.9 exposed to recommend torque of 160 Nm. An extra FEA was run to obtain input data for the intended optimization. The results of this simulation show that all of the components of the EPS experience deformations in elastic region while as mentioned in Chapter 5, end plate had some local plasticity when the joint was loaded with a load equivalent to 200 Nm torque.

6.1. Shape Optimization

The objective of this section is to perform a structural shape optimization and determine the optimal shape which improves the stress distribution in the test boss (actually equipment support) and to reduce the stress level in this part. The shape optimization process is carried out in *Abaqus Topology Optimization Module* (ATOM). Conducting the optimization process for whole the assembly was not possible since Abaqus shape optimization is only viable for General Static and Perturbation algorithms and due to using Dynamic/Implicit for analysis of EPS joint in this study, considering all joint components was impossible. Therefore, just pin component is considered in shape optimization process with objective to improve its shape. In practice, the diameter of the pin is determined based on diameter of the equipment bore, but the taper angle of pin at its ends is a variable parameter which can be optimized.

In order to carry out a shape optimization, it is necessary to define a loading scenario for the joint assembly. Bondura EPS is used in different heavy industrial machines and in this study a loading scenario which is common in lifting operation of a crane is considered as a case study (shown in Figure 6.1).

Even though the pin is considered as a single part in optimization process, but the effect of contact pressure imposed from sleeve cannot be ignored. Thus, based on the magnitude of von Mises obtained in FEA and the form of stress distribution along the pin, a preload is defined for it. This preload could be achieved by applying either a pressure on the tapered ends of the pin which in fact were in contact with sleeve or by applying a surface traction force. Considering pressure as a preload is more acceptable since it creates a similar stress distribution in the pin with just this difference that the position of maximum von Mises stress is changed.

Figure 6.1: Bondura® EPS application in crane [1]

The loading of pin is in fact divided into two steps, the first step as mentioned for load imposed from sleeve which is produced by applying 63 MPa pressure to the pin tapers and the second step for lifting a weight of 20 tones which is modelled by applying a pressure of 10.04 MPa to the upper surface of the pin. In both loading steps, the load increases linearly from zero up to the maximum value.

The boundary conditions of the pin are modeled in a way to provide pin stress distribution similar to its state in joint. One end of the pin with shorter taper length (right side) is constrained in all three translational movements and moreover it is restricted to have rotational movement around z-axis. The other side of the pin is restricted in x and y directions.

In order to carry out the optimization task mesh smoothing capability of the Abaqus has been used. The left taper of the pin is considered as the design area and it is actually the region of the pin that will be modified during the optimization process. Determination of the maximum von Mises in the design area is done by creating design response setup. The objective function is defined to minimize the maximum von Mises stress throughout the design response area. Another parameter in optimization process is defining constraints. It is set by keeping the volume of the design response unchanged during the optimization process.

Geometry restriction imposes more constraints. Through this process, two geometry restrictions are defined; one rotational symmetric restriction which is applied to tapered part in order to preserve the roundness of optimized shape and the other one is a fixed area which is applied to the middle part of the pin since the diameter of this part should be unchanged.

In first step of the loading to the pin which resembles the sleeve contact load to pin, the maximum von Mises in pin is 45.946 MPA and in second step related to the lifting operation load the

resultant von Mises is 71.68 MPa occurring in the right side of pin midpart near to its taper. Therefore, the shape optimization is done in a way to minimize maximum von Mises in the midpart of the pin. The BCs and von Mises stress distribution of pin while it is under operational condition is shown in Figure 6.2.

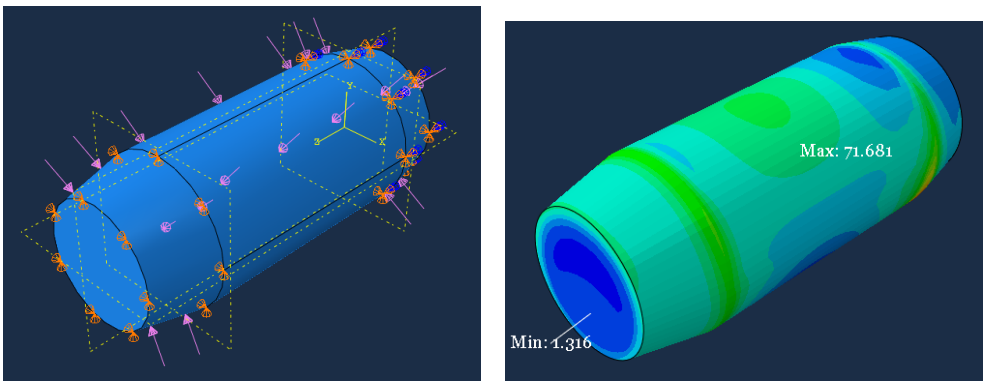

(a) Boundary conditions and loading to pin in operation

(b) Pin von Mises stress distribution in operation

Figure 6.2: Pin in Operation

After running the optimizing simulation, the final shape of the pin with new configuration on the left taper is achieved. The steps of ATOM optimization, the new shape and also the magnitude of von Mises after optimization job is shown in Figure 6.3.

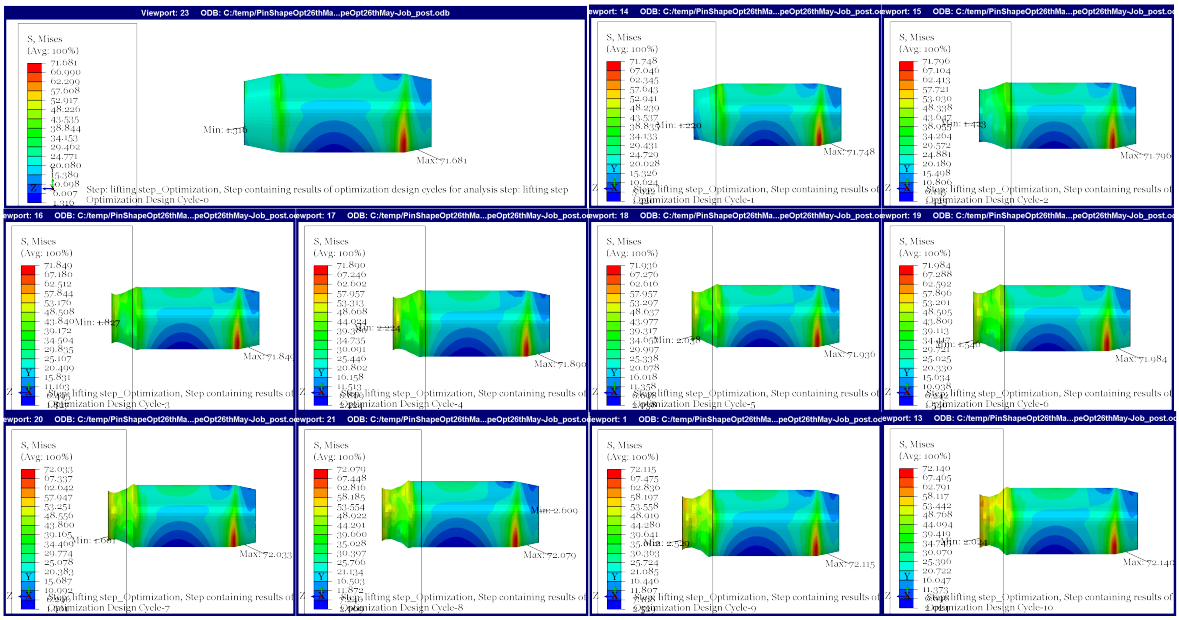

Figure 6.3: The steps of shape optimization for pin

The optimized shape does not follow a linear shape and the profile is approximately a hyperbolic curve. Basically, it is necessary to carry out an extra analysis to examine the distribution and magnitude of von Mises in EPS joint to evaluate the effect of optimized shape. This can be done after applying modifications to the final optimized shape produced by Abaqus [45, 46].

By looking at image of cycle 10 in Figure 6.3, two main drawbacks with the final optimised shape are visible. The first one is related to the protrusion produced at the beginning of taper. This bulge will prevent insertion of pin inside the support bore. The second drawback is due to existence of

dent near the end of the taper. This will cause problem for mating of pin-sleeve. Thus, the profile of tapered section is modified and it is shown in Figure 6.4a. The taper of the sleeve is modified to provide a perfect mating while it is mounted on the pin (Figure 6.4b).

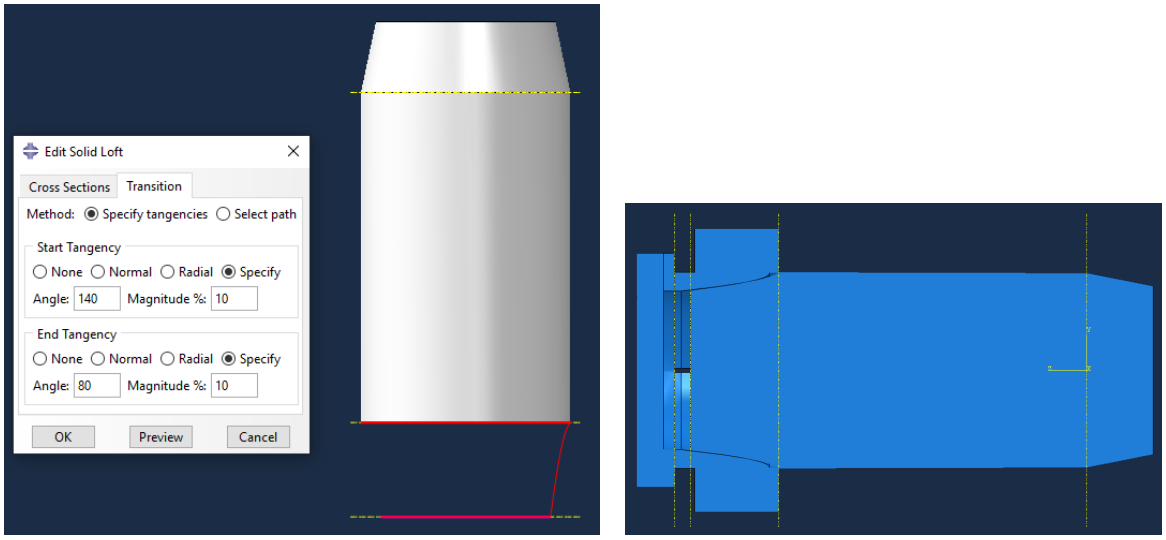

(a) New profile for pin (b) New profile for sleeve

Figure 6.4: Modified profile of pin-sleeve taper after optimization

Von Mises stress distributions in EPS components are illustrated in Figure 6.5a after running FE simulation. In order to provide possibility for making comparison between stress state of optimised shape with current Bondura EPS joint which has angle of taper equal to 12°, von Mises stress distribution of the latter is provided in Figure 6.5b. It is worth to emphasize that the FEA is conducted for applied torque of 160 Nm which is proposed by Bundora Technolgy AS.

Starting the comparison from the end plate, it is observable that distribution of von Mises is similar in both cases of optimised shape and current shape. The only difference is related to magnitude of von Mises stress which can be justified based on relative movements or displacements of end plate. Due to curved profile of pin-sleeve taper in optimised shape, the advancement of sleeve on pin is reduced and therefore the relative displacement affects stress level. During assembly of components in Abaqus model, two assembly constrains were defined for end plate and sleeve attachment including coaxial and face-to-face contact. Therefore movements of sleeve has direct effect on displacements of end plate and thus its stresses.

The sleeve with new profile of optimised shape experiences a better stress distribution along its length and in addition, the magnitude of maximum von Mises stress occurring in sleeve is decreased from 275.25 MPa to 203.93 MPa. Furthermore, in optimised shape, the location of maximum von Mises stress has change from collar to beginning of the sleeve taper.

By comparing the von Mises stress state in optimized shape and current design of pin, it is obvious that the stress distribution in optimized shape is localized to beginning of the taper. The magnitude of von Mises stress has increased considerably by factor of 3. This amount of stress may affect the lifetime of the pin considering in the FE simulation, EPS was only subjected to screws preload. It is clear that in real operation that joint system is exposed to external load, the magnitude of stress in pin will increase.

Test boss which resembles equipment support is definitely the most important joint component. Therefore, the level of stress in test boss is very important since it has direct impact on wear characteristics and rigidity of the joint. The optimized shape of the taper leads to creation of more stress in the test boss and the values show an increase from 85.49 MPa to 128.62 MPa which indicates 50% increase. Based on this fact, it can be concluded that the magnitude of torque applied to

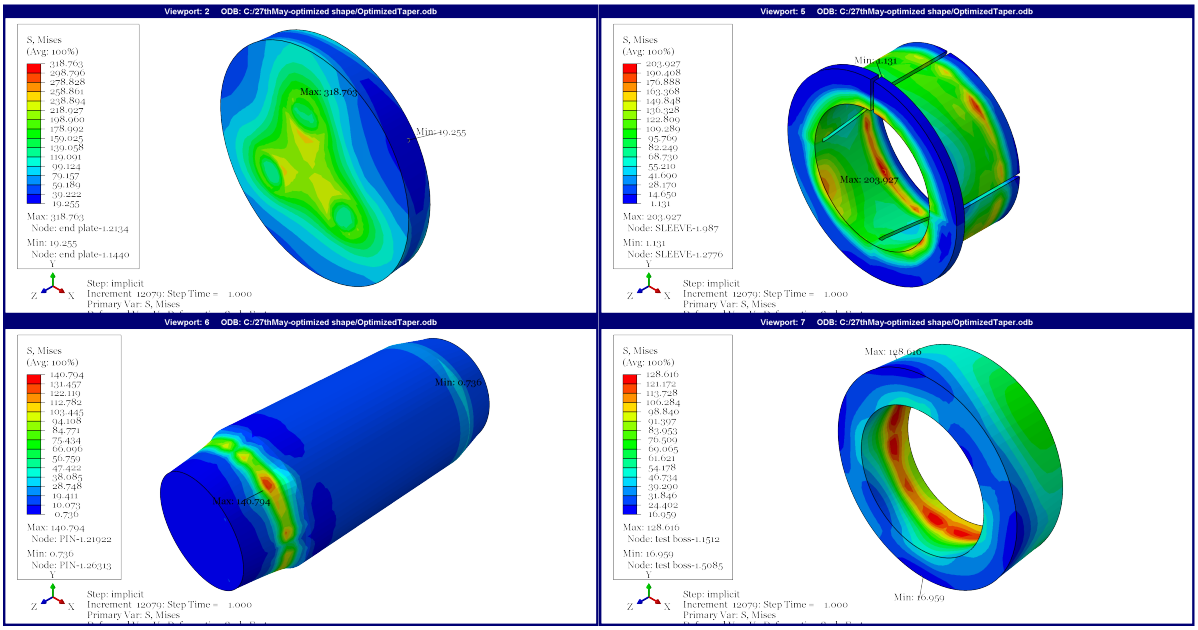

(a) Optimised shape

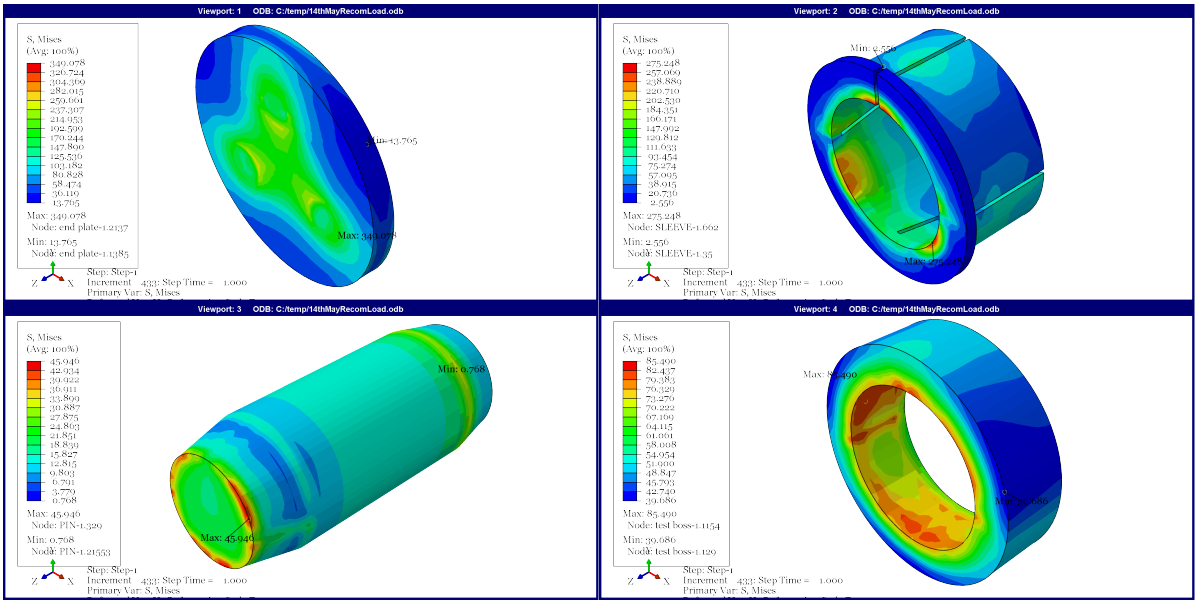

(b) Current design

Figure 6.5: Von Mises stress distribution in EPS components

EPS screws can be decreased in order to have the same level of stress.

However, one of the critical aspects of this optimised shape is that it causes localization of stress to a specific region of the test boss, while the current design shows relatively a uniform stress distribution. This issue may affect the wear phenomena in equipment support and can have negative effect on the lifetime of the equipment, but it is not a serious problem, since by increasing the applied torque to EPS screws it is possible to expand sleeve to higher extent regarding the fact that the optimised shape requires lower torque for the same value of clamping force. Further investigation about stress state and capabilities of the achieved optimised shape needs more experimental research.

6.2. Parametric Study of Pin-Sleeve Angle of Taper

In order to analyse the effect of pin-sleeve taper on stress distribution of the EPS joint, a parametric study was conducted to provide a better understanding about this feature. The analysis was performed for five different angles of taper for pin-sleeve mating surface including 8°, 10°, 12°, 14° and 16°. Thickness of end part of the sleeve in all cases was preserved equal to 1 mm to represent a manufaturable sleeve.

The corresponding maximum value of von Mises stress and pressure are given in Tables 6.1 and 6.2. The simulations related to angles of taper 8° and 10° were unsuccessful to be completed and the appeared error code was related to RAM capacity. Therefore, the mesh size of pin was changed from 4 to 8 to reduce the number of elements and volume of calculations. Even applying this coarser mesh did not lead to completion of the jobs and as it is indicated in the note section of Table 6.1, the jobs partially ended. However, the results are acceptable since they follow the pattern observed for the other three angles. It is believed that stress values for taper angles of 8° and 10° are a little bit more than given values in the following tables, specially for the pin since it has coarser mesh it definitely becomes more rigid and due to lower deformations, it experiences lower stress level. This matter is clear when comparing the values of von Mises and pressure for the pin.

Table 6.1: Maximum von Mises stress in EPS components vs pin-sleeve angle of taper

Part	**8°**	**10°**	**12°**	**14° ***	**16° ****
End plate	320.53	297.67	349.08	283.51	286.96
sleeve	253.35	187.03	275.25	230.74	192.35
Pin	23.85	24.62	45.95	44.65	43.32
Test boss	99.11	92.44	85.49	77.53	71.67

Note: * Incomplete job; 94.84 % progress
** Incomplete job; 93.27 % progress

Table 6.2: Maximum pressure in EPS components vs pin-sleeve angle of taper

Part	**8°**	**10°**	**12°**	**14°**	**16°**
End plate	293.47	284.03	299.01	262.91	245.91
sleeve	94.28	96.937	153.47	105.51	97.47
Pin	27.00	25.22	37.378	38.62	42.28
Test boss	26.01	23.83	22.52	18.84	17.11

To assess the results better, the values of the previous tables are illustrated in Figure 6.6. Both maximum von Mises stress and pressure in the test boss increase linearly as the angle of taper decreases. The reason is related to the thickness of the sleeve. When the angle of taper in sleeve decreases the thickness of sleeve along the taper length will decrease. Therefore for the same axial preload, the deformation of sleeve and consequently experienced stress will increase. In addition, it can be concluded that both von Mises and pressure in pin behave independently from variations of angle of taper according to discussion indicated about mesh size and partial completion of analysis for taper angles of 8° and 10°.

The optimal angle of taper is an angle which creates the maximum radial stress or pressure in the equipment support, here the test boss, while keeping the total stress in the joint components as low as possible. By looking at Figure 6.6b it is clear that taper angle of 12° creates the maximum pressure in the sleeve with significant difference compared to other angles. However, this angle creates high level of stress in the sleeve. Other angles like 10° and 16° result in lower stress level in the sleeve, but

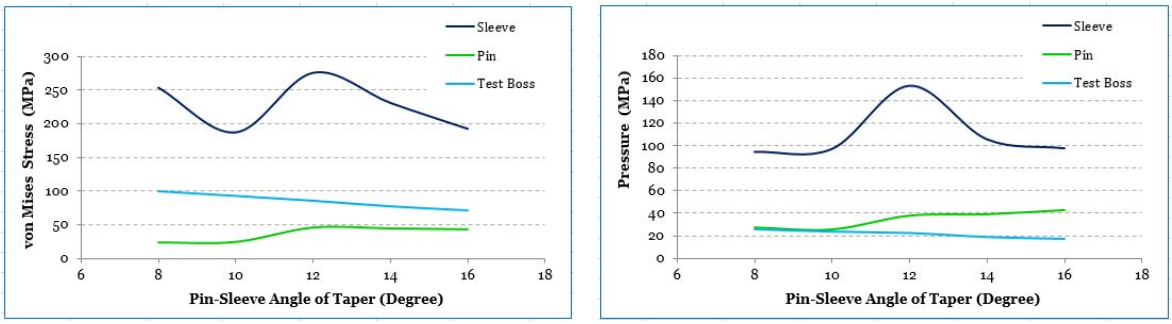

(a) von Mises vs angle of taper

(b) Pressure vs angle of taper

Figure 6.6: Effect of angle of taper on stress state of EPS parts

they do not create radial stress as high as 12° that may lead to slack in the joint. Therefore, 12° has advantage over these two angles.

Considering the fact that rigidity of the joint and prevention of slack are the most important parameters in the joint system, and also noting that stress level in the sleeve (and other components) are in elastic region, it can be concluded that angle of taper of 12° gives the most appropriate result ensuring a rigid and reliable joint.

6.3. Summary

In this chapter, based on results of FEA which were compared and validated with respect to experimental results, a shape optimisation analysis was carried out using Abaqus optimization module, ATOM. The optimization process resulted in a profile which needed modifications. After applying modifications to the produced profile for pin-sleeve taper, a FEA were implemented. The results show that the optimized shape creates higher stress and consequently clamping force for the same magnitude of applied torque to the EPS. This means by adopting the optimised shape, lower amount of torque is required for the same clamping force compared to the current design which has angle of taper equal to 12°.

A parametric study were carried out in order to assess the effect of pin-sleeve angle of taper in more details. The results of this study show that angle of taper of 12° creates the maximum pressure and radial stress in the test boss which means higher magnitude of clamping force in EPS compared to other angles in the range of 8° to 16°.

7

Conclusion and Recommendations

7.1. Conclusions

This thesis has attempted to address the aims and objectives set out in Chapter 1, Section 1.3. of the thesis. The experimental part of this thesis which was prepared for three different test layouts including non-lubricated sleeve, lubricated sleeve and lubricated cut sleeve has provided detailed information about stress distribution and magnitude in the test boss that resembles equipment support. The experimental results clarify that stress concentrations happen in regions near sleeve cut-through and in regions next to it (with 180° angular distance from sleeve cut-through).

Measured results by CMM show that at the beginning of screw tightening, expanding sleeve moves forward along the pin taper, but after reaching to a level of torque (around 80 Nm), sleeve advancement stops and pin undergoes tension and elongates.

Other findings of the experimental study is related to dissipation of energy applied to EPS via torque. Around 63% of the applied torque dissipates in the form of elastic hysteresis and expanding the sleeve and only 37% of it is effectively used to expand the test boss. A part of dissipated torque which is around 33% is used to deform the sleeve elastically and about 30% of it is wasted in the form of elastic hysteresis deformation in different joint components to overcome friction.

The FE results for sleeve including radial stress and contact pressure are very close to proposed values of theoretical formulas of Ref. [2]. Therefore it is concluded that those formulas can be used to estimate pin-sleeve contact pressure and radial stress, even though they are derived for a perfect sleeve without any cuts. However, FE results for pin are not in agreement with the corresponding theoretical formulas. One of the reasons maybe related to mesh size since mesh size can affect results of FEA. The FE results for test boss were in good agreement with experimental results. FE results for von Mises, Tresca and radial stresses are very close to experimental results and the partial differences are probably related to assumptions and simplifications.

FE parametric study on friction coefficient shows that when friction decreases the magnitude of pressure and stress in joint components increase except for sleeve where it showed an opposite behavior. This matter is compatible with experimental results for the test boss. Moreover an approximation formula for prediction of von Mises stress in the test boss was derived based on the FE parametric study results.

The shape optimisation analysis in this thesis was carried out using Abaqus optimization module, ATOM. The optimization process resulted in a profile which needed some modifications. After applying modifications to the produced profile for pin-sleeve taper, a FE analysis were implemented. The results show that the optimized shape creates higher stress and consequently clamping force for the same magnitude of applied torque to the EPS. This means by adopting the optimised shape, lower amount of torque is required for the same clamping force compared to the current design with angle of taper equal to 12°.

FE parametric study on pin-sleeve angle of taper show that angle of taper of 12° creates the maximum pressure and radial stress in the test boss which means higher magnitude of clamping force in EPS compared to other angles in the range of 8° to 16°.

7.2. Recommendations for Future Works

Some recommendations for further research about EPS and the results obtained in this thesis are suggested as follows:

1. The experimental study in this research is carried out on a test boss with the shape of a thick cylinder, while in practice the equipment support that EPS is installed in has other shapes like eye pad, thick plate etc. Therefore it is recommended to conduct experimental or FE studies regarding these different shapes of the support.

2. Modelling the whole EPS containing fastening screws will provide a better presentation about real stress state in the joint. Abaqus has the ability to apply bolt preload. Conducting this analysis is highly recommended.

3. The purpose of this thesis was to find out the stress distribution and magnitude in the equipment support, but other aspects like functioning of the pin under different types of loading can be proposed since EPS is used in different type of heavy machines.

4. The optimization process implemented in this study was performed based on von Mises stress in the pin. However in practice, pin undergoes dynamic loads during operation. Therefore implementing an optimization process based on fatigue characteristics is recommended for further study.

5. The optimization job in this thesis has provided a new profile for pin-sleeve taper which has made it possible to reach to the same amount of clamping force with lower torque to EPS. Further investigation of this feature through experimental research is recommended.

6. Another shape for pin-sleeve taper similar to profile shown in Figure 7.1 seems to be interesting to evaluate in order to assess its capabilities and advantages.

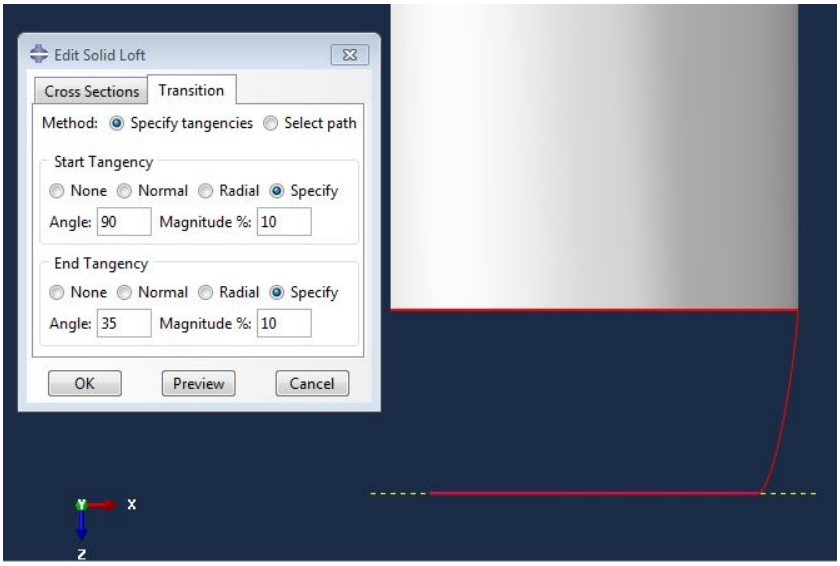

Figure 7.1: Proposed profile for pin-sleeve taper

Bibliography

[1] Bondura. bondura pivot pin technology, cranes. https://www.youtube.com/watch?v=TXw_JTck_Mc&list=WL&index=43&t=209s, 2012. In comment section, accessed on 2021/01/10.

[2] Andrzej Andrzejuk, Zbigniew Skup, and Robert Zalewski. Analysis of a conical sleeve with pivot joint loading of axial force. *Journal of Theoretical and Applied Mechanics*, 52(2):345–358, 2014.

[3] Richard G Budynas, J Keith Nisbett, and Kiatfa Tangchaichit. *Shigley's mechanical engineering design*. McGraw Hill New York, 2005.

[4] Internet Web Page kernel description. https://www.bestech.com.au/blogs/understanding-a-wheatstone-bridge-strain-gauge-circuit/. Accessed: 2021-03-05.

[5] Abaqus 2016. *Getting Staerted with Abaqus/CAe*. Dassault Systems.

[6] Zhang Dongliang, Wang Binwu, and Liu Fei. The contact stress analysis about the conical expansion sleeve connection. In *2013 Fifth International Conference on Measuring Technology and Mechatronics Automation*, pages 1157–1159. IEEE, 2013.

[7] Imad Berkani, Øyvind Karlsen, and Hirpa G Lemu. Experimental and numerical study of bondura® 6.6 pin joints. In *IOP Conference Series: Materials Science and Engineering*, volume 276, page 012028. IOP Publishing, 2017.

[8] Muhammad Maaz Akhtar. Expanding pin system – combined radial and axial locking system, master thesis, university of stavanger, norway, 2020.

[9] N Motosh. Development of design charts for bolts preloaded up to the plastic range. *ASME Journal of Engineering for Industry*, pages 849–851, 1976.

[10] Arthur Peter Boresi, Richard Joseph Schmidt, Omar M Sidebottom, et al. *Advanced mechanics of materials*. Wiley New York, 6 edition, 2003.

[11] Richard L Hannah and Stuart E Reed. *Strain gage users' handbook*. Springer Science & Business Media, 1992.

[12] Karl Hoffmann. *Applying the Wheatstone bridge circuit*. HBM Germany, 1974.

[13] Internet Web Page kernel description. https://www.hbm.com/en/7164/how-to-find-the-right-strain-gauge/. Accessed: 2021-03-05.

[14] Internet Web Page kernel description. https://www.electronicshub.org/wheatstone-bridge/. Accessed: 2021-03-05.

[15] Q Zou, TS Sun, SA Nassar, GC Barber, and AK Gumul. Effect of lubrication on friction and torque-tension relationship in threaded fasteners. In *International Joint Tribology Conference*, volume 42592, pages 591–602, 2006.

[16] Ying Hong, Xuesheng Wang, Yan Wang, and Zhao Zhang. Study on reducing the risk of stress corrosion cracking of austenitic stainless steel hydraulically expanded joints. *Engineering Failure Analysis*, 113:104560, 2020.

[17] José María Mínguez and Jeffrey Vogwell. Effect of torque tightening on the fatigue strength of bolted joints. *Engineering Failure Analysis*, 13(8):1410–1421, 2006.

[18] A.-E. Jiménez and M.-D. Bermúdez. 2 - friction and wear. In J. Paulo Davim, editor, *Tribology for Engineers*, pages 33–63. Woodhead Publishing, 2011.

[19] Wenjie Qin, Min Wang, Wei Sun, Philip Shipway, and Xudong Li. Modeling the effectiveness of oil lubrication in reducing both friction and wear in a fretting contact. *Wear*, 426:770–777, 2019.

[20] M Al-Chalabi and CL Huang. Stress distribution within circular cylinders in compression. In *International Journal of Rock Mechanics and Mining Sciences and Geomechanics Abstracts*, volume 11, pages 45–56. Elsevier, 1974.

[21] Internet Web Page kernel description. `https://www.instron.us/en-us/our-company/library/glossary/e/elastic-hysteresis#`. Accessed: 2021-03-12.

[22] Bertram Hopkinson and Trevor G Williams. The elastic hysteresis of steel. *Proceedings of the Royal Society of London. Series A, Containing Papers of a Mathematical and Physical Character*, 87(598):502–511, 1912.

[23] Internet Web Page kernel description. `http://www.harrisonep.com/electropolishing-ra.html`. Accessed: 2021-03-05.

[24] Mohsen Hamedi. Intelligent fixture design through a hybrid system of artificial neural network and genetic algorithm. *Artificial Intelligence Review*, 23(3):295–311, 2005.

[25] Weifang Chen, Lijun Ni, and Jianbin Xue. Deformation control through fixture layout design and clamping force optimization. *The International Journal of Advanced Manufacturing Technology*, 38(9-10):860, 2008.

[26] Kyung-Young Jhang, Hai-Hua Quan, Job Ha, and Noh-Yu Kim. Estimation of clamping force in high-tension bolts through ultrasonic velocity measurement. *Ultrasonics*, 44:e1339–e1342, 2006.

[27] Abaqus 2016. *Analysis User's Guide: Volume I: Introduction, Spatial Modeling, Execution Output*. Dassault Systems.

[28] Abaqus 2016. *Analysis User's Guide: Volume II: Analysis*. Dassault Systems.

[29] Martin Bäker. How to get meaningful and correct results from your finite element model. *arXiv preprint arXiv:1811.05753*, 2018.

[30] Daniele Forni, Bernardino Chiaia, and Ezio Cadoni. Strain rate behaviour in tension of s355 steel: Base for progressive collapse analysis. *Engineering Structures*, 119:164–173, 2016.

[31] Internet Web Page kernel description. `https://www.rodacciai.com/UPLOAD/paginemultiple/mechanicaltests_ENG.pdf`. Accessed: 2021-04-06.

[32] Abaqus 2016. *Analysis User's Guide: Volume V: Prescribed conditions, Constrains Interactions*. Dassault Systems.

[33] Internet Web Page kernel description. https://abaqus-docs.mit.edu/2017/English/SIMACAECAERefMap/simacae-t-itnhelpsurftosurfstd.htm. Accessed: 2021-04-08.

[34] Nam-Sua Lee and Klaus-Jurgen Bathe. Effects of element distortions on the performance of isoparametric elements. *International Journal for numerical Methods in engineering*, 36(20):3553–3576, 1993.

[35] Abaqus 2016. *Analysis User's Guide: Volume IV: Elements*. Dassault Systems.

[36] Hao Tian, She Li, and Xiangyang Cui. Development of element model subroutines for implicit and explicit analysis considering large deformations. *Advances in Engineering Software*, 148:102805, 2020.

[37] Internet Web Page kernel description. https://web.mit.edu/calculix_v2.7/CalculiX/ccx_2.7/doc/ccx/node27.html#int1. Accessed: 2021-04-15.

[38] PM Pauskar, K Sawamiphakdi, and DQ Jin. Static implicit vs. dynamic explicit finite element analysis for ring rolling process modeling. In *AIP Conference Proceedings*, volume 712, pages 412–417. American Institute of Physics, 2004.

[39] AM Prior. Applications of implicit and explicit finite element techniques to metal forming. *Journal of Materials Processing Technology*, 45(1-4):649–656, 1994.

[40] Internet Web Page kernel description. https://abaqus.uclouvain.be/English/SIMACAECAERefMap/simacae-t-simconfiguredynamicimplicit.htm. Accessed: 2021-04-16.

[41] Hamid Naghibi Beidokhti, Dennis Janssen, Mehdi Khoshgoftar, Andre Sprengers, Emin Semih Perdahcioglu, Ton Van den Boogaard, and Nico Verdonschot. A comparison between dynamic implicit and explicit finite element simulations of the native knee joint. *Medical engineering & physics*, 38(10):1123–1130, 2016.

[42] JS Sun, KH Lee, and HP Lee. Comparison of implicit and explicit finite element methods for dynamic problems. *Journal of materials processing technology*, 105(1-2):110–118, 2000.

[43] Kuang-Hua Chang. *Design theory and methods using CAD/CAE: The computer aided engineering design series*. Academic Press, 2014.

[44] Peter W Christensen and Anders Klarbring. *An introduction to structural optimization*, volume 153. Springer Science & Business Media, 2008.

[45] Pravardhan S Shenoy and Ali Fatemi. Connecting rod optimization for weight and cost reduction. *SAE transactions*, pages 523–530, 2005.

[46] Necmettin Kaya, Idris Karen, and Ferruh Öztürk. Re-design of a failed clutch fork using topology and shape optimisation by the response surface method. *Materials & Design*, 31(6):3008–3014, 2010.

Appendices

A

Appendix

A.1. HBM Strain Gauge

HBM

Dehnungsmessstreifen
Strain gages
Jauges d'extensométrie

Bestellnummer Order No. No. de référence	**K-LY4-1-05-120-3-3**
Typ Type Type	3/120 LY41-3L-3M
Widerstand Resistance Résistance	120 Ω ±0.35 %
Stückzahl Contents Quantité	10
k-Faktor Gage factor Facteur k	2.00 ±1.0 %
Temperaturkoeffizient des k-Faktors Temperature coefficient of gage factor Coefficient de température du facteur k	93 ±10 [10^{-6} / K] (-10°C ... +45°C)
Querempfindlichkeit Transverse sensitivity Sensibilité transverse	0.2 %
Folienlos Foil lot Lot de la feuille	A417/41
Herstellungslos Production batch Lot de fabrication	812067502
Temperaturkompensation: Ferritischer Stahl mit Temperature compensation: steel with Compensation de température: acier avec	α = 10.8 [10^{-6} / K]
Maximale Brückenspeisespannung maximal bridge excitation voltage tension d'alimentation de pont maxi	3.5 V

Daten / Data / Données

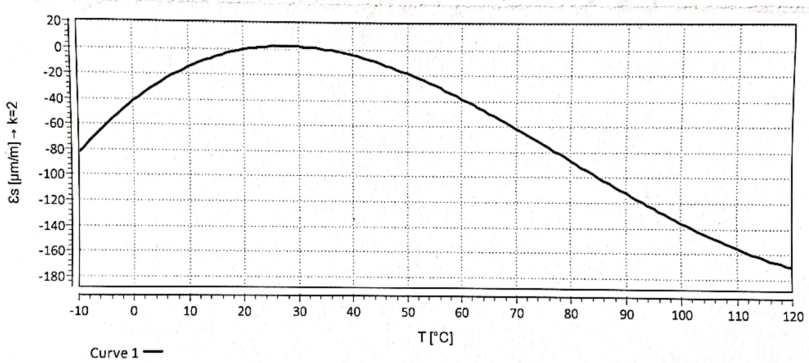

$\varepsilon_S(T) = -28.75 + 2.77 * T - 7.43E-02 * T^2 + 3.08E-04 * T^3 \pm (T-20) * 0.30\ [\mu m/m] + 0.639 * (T-20)\ [\mu m/m]$

Alle technischen Daten nach VDI/VDE 2635. Geben Sie bei Rückfragen bitte Bestellnummer und Herstellungslos an.

All specifications in accordance with VDI/VDE 2635. In case of further inquiries please indicate order no. and production batch number.

Toutes les caractéristiques techniques selon la norme VDI/VDE 2635. Dans toutes communications, prière d'indiquer le numéro de commande et le numéro du lot de production.

Temperaturgang der Dehnungsmessstreifen bei Applikationen mit oben angegebenen Wärmeausdehnungskoeffizienten α. Gemessen bei kontinuierlicher Temperaturänderung.

Kennlinie 1: DMS mit PVC Kabel.
T = Temperatur in °C
(dimensionslos)

Réponse en température des jauges d'extensométrie appliquées sur des matériaux dont des coefficients de dilatation termique α sont indiqués. Mesurée à variation continue de la température.

Courbe 1: Jauges avec câble en PVC.
T = température en °C
(sans dimension)

The **temperature response** refers to strain gages bonded to materials with specified coefficients of thermal expansion α. Values are measured with continuous temperature variation.

Curve 1: Strain gages with PVC cable.
T = temperature in °C
(dimensionless)

Kopfdaten / Header / Titre

A point (".") is used as decimal separator in data; the separator needs to be configured accordingly for import into Excel.

A.2. Test setup

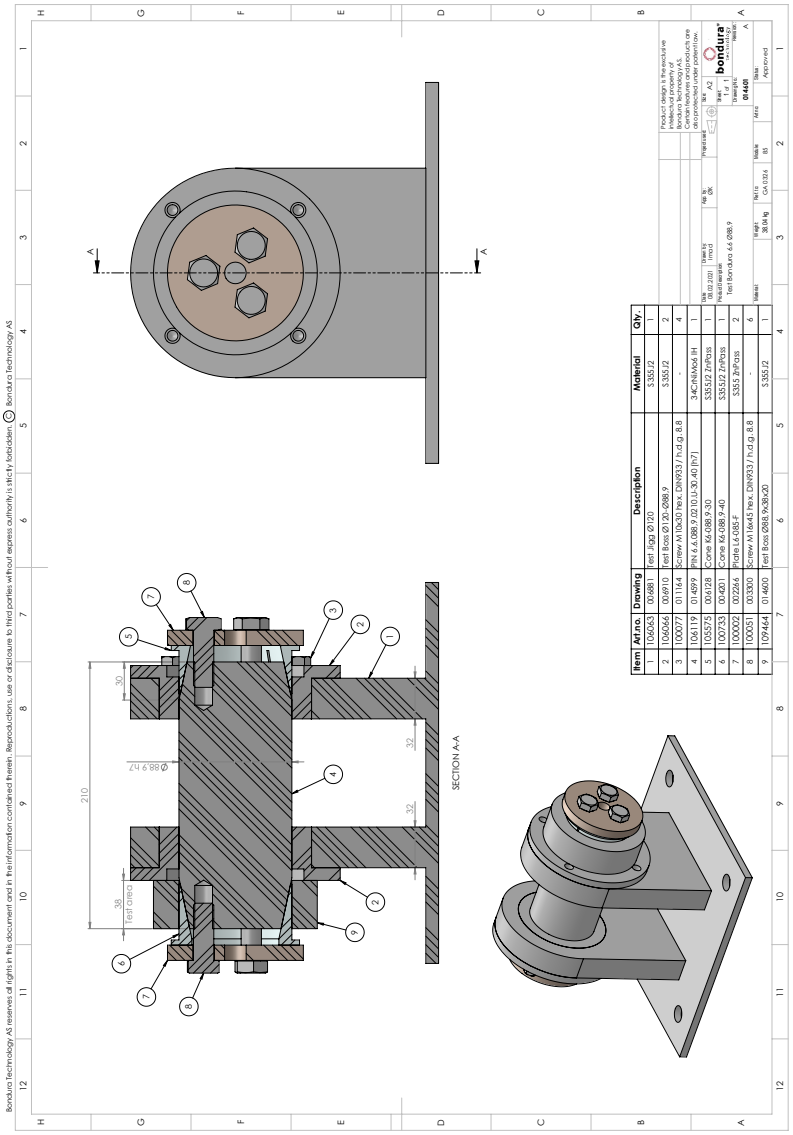

Item	Art.no.	Drawing	Description	Material	Qty.
1	106063	01.6881	Test Jiga Ø120	S355J2	1
2	106066	01.6910	Test Boss Ø120-Ø88.9	S355J2	2
3	100077	01.1164	Screw M10x30 Hex. DIN933 / h.d.g. 8.8	-	4
4	106119	01.6899	Pin L4.6.088.9-Ø10.0-L30.40 (h7)	34CrNiMo6 IH	1
5	105575	01.6128	Cone K4.088.9-30	S355J2 ZnPass	1
6	100733	01.4001	Cone K4.088.9-40	S355J2 ZnPass	1
7	100002	01.2264	Plate L4.6.085-F	S355 ZnPass	2
8	100051	01.3300	Screw M16x45 Hex. DIN933 / h.d.g. 8.8	-	6
9	109464	01.4600	Test Boss Ø88.9x38x20	S355J2	1

A.3. Pin

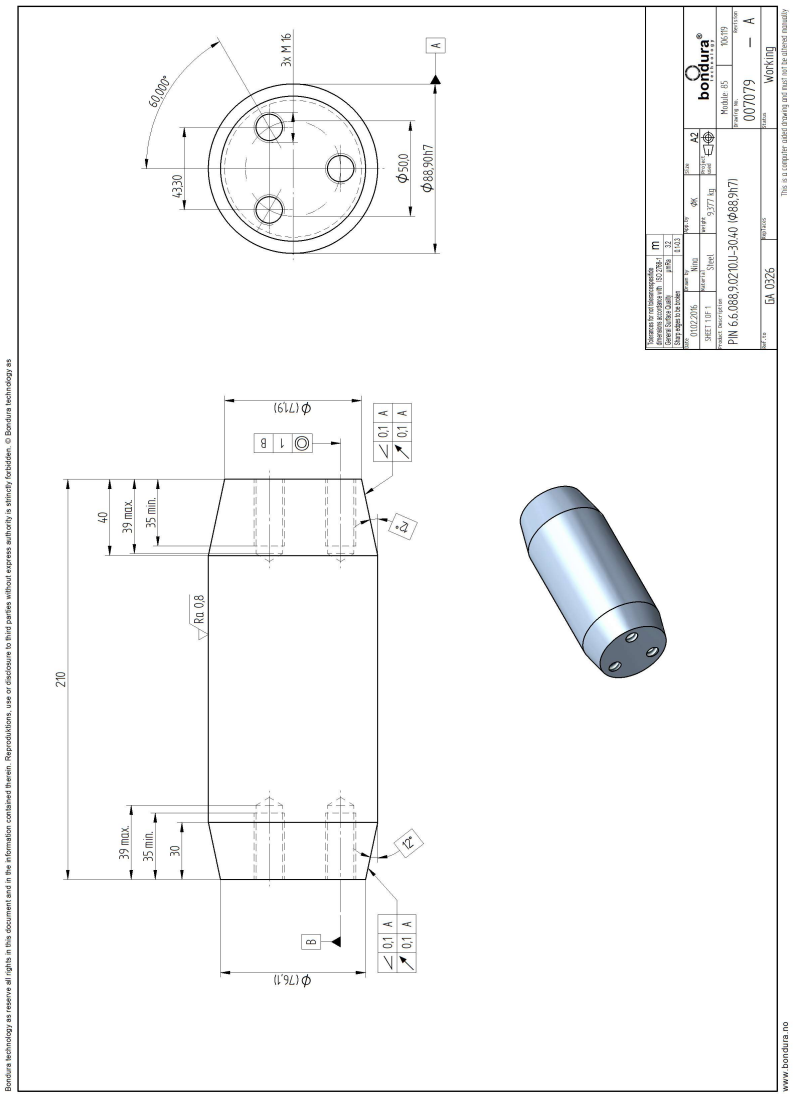
3x M 16
60,000°
43,30
ϕ50,0
ϕ88,9h17
A
ϕ(71,9)
B 1
0,1 A
0,1 A
40
39 max.
35 min.
2x
Ra 0,8
210
39 max.
35 min.
30
2x
B
ϕ(76,1)
0,1 A
0,1 A
bondura
Module 65
106189
007079
A
Working
PIN 6.6.088.9.0210U-30.40 (ϕ88,9h7)
GA 0326
Weight: 9,577 kg
Sheet
SHEET 1 OF 1
07.07.2015
Bondura technology as reserve all rights in this document and in the information contained therein. Reproductions, use or disclosure to third parties without express authority is strictly forbidden. © Bondura technology as
This is a computer aided drawing and must not be altered manually
www.bondura.no

A.4. Sleeve

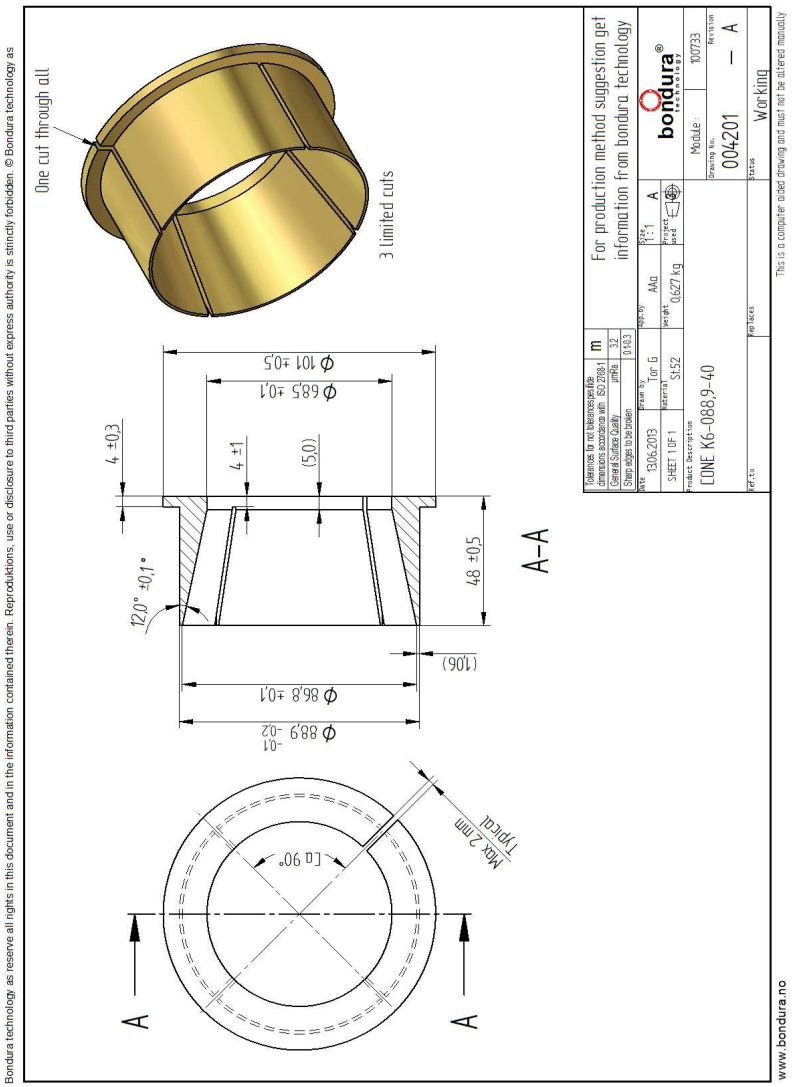
One cut through all
3 limited cuts
A–A
Max 2 mm
Typical
For production method suggestion get information from bondura technology
bondura
CONE K6-088,9-40
004201
A
Working
Bondura technology as reserve all rights in this document and in the information contained therein. Reproduktions, use or disclosure to third parties without express authority is strictly forbidden. © Bondura technology as
This is a computer aided drawing and must not be altered manually
www.bondura.no

A.5. Test Boss

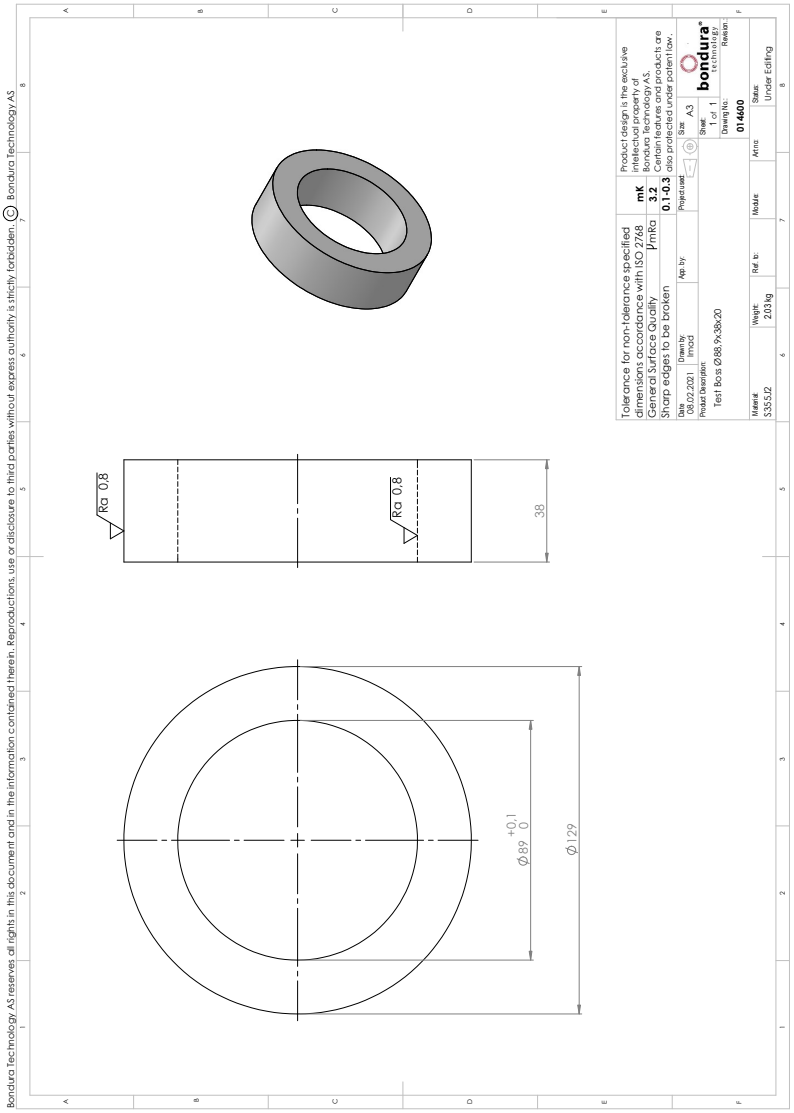
Ra 0,8
Ra 0,8
38
Ø89 +0,1 0
Ø129
Tolerance for non-tolerance specified dimensions accordance with ISO 2768
General Surface Quality
Sharp edges to be broken
Product design is the exclusive intellectual property of Bondura Technology AS. Construction and products are also protected under patent law.
Test Boss Ø88,9x38x20
S355J2
2,03 kg
01 4400
Under Editing
Bondura Technology AS reserves all rights in this document and in the information contained therein. Reproductions, use or disclosure to third parties without express authority is strictly forbidden. © Bondura Technology AS

A.6. Changing the position of sleeve opening in non-lubricated sleeve tests

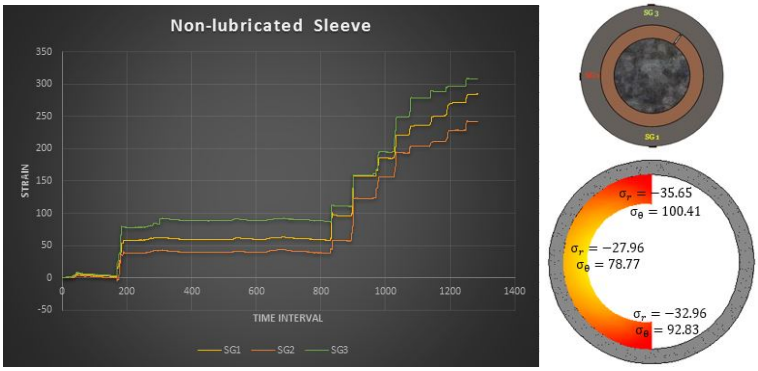

Figure A.1: Non-lubricated sleeve with sleeve complete notch at 45° and SGs at 270°, 180° and 90°

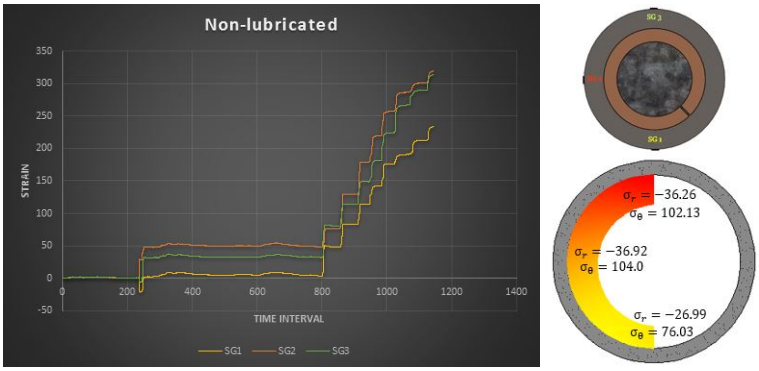

Figure A.2: Non-lubricated sleeve with sleeve complete notch at 315° and SGs at 270°, 180° and 90°

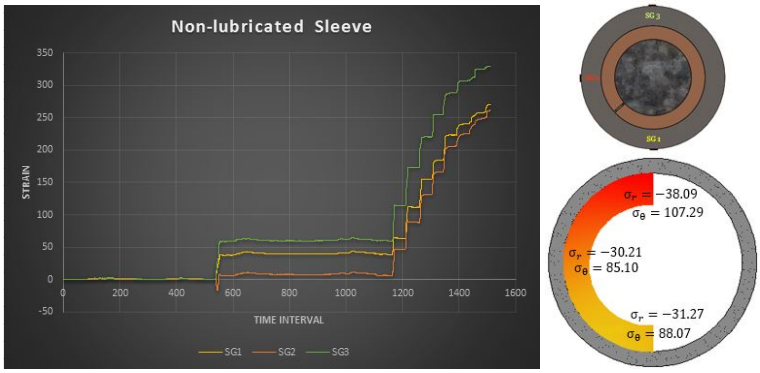

Figure A.3: Non-lubricated sleeve with sleeve complete notch at 225° and SGs at 270°, 180° and 90°

A.7. Changing the position of sleeve opening in lubricated sleeve tests

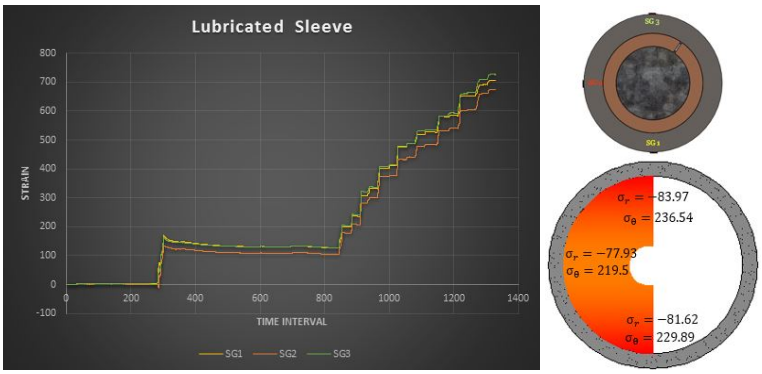

Figure A.4: Lubricated sleeve with sleeve complete notch at 45° and SGs at 270°, 180° and 90°

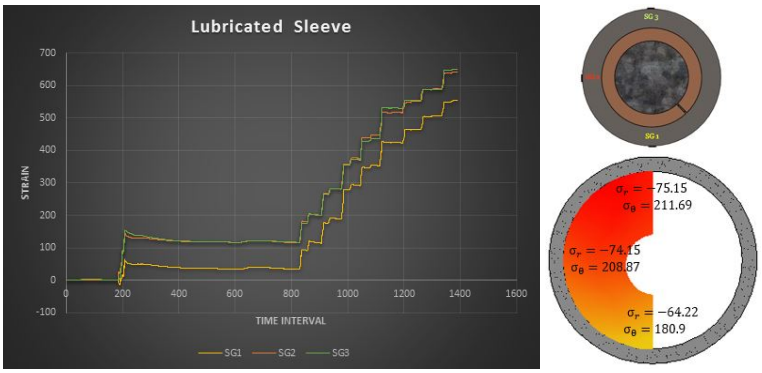

Figure A.5: Lubricated sleeve with sleeve complete notch at 315° and SGs at 270°, 180° and 90°

Figure A.6: Lubricated sleeve with sleeve complete notch at 225° and SGs at 270°, 180° and 90°

University of Stavanger

UNIVERSITY OF STAVANGER